



LEVEL *IX*

AD A 098 797

**CHEMICAL AND PHYSICAL ASPECTS OF MESOPHASE
FORMATION DURING CARBON-CARBON PROCESSING**

Contract No. F49620-78-C-0006

Air Force Office of Scientific Research (AFSC)
Bolling Air Force Base, DC 20332

DTIC
ELECT
MAY 12 1981

AFOSR Program Manager: Dr. D. R. Ulrich

Principal Investigator: Dr. J. J. Gebhardt
(215) 962-1227

SUMMARY REPORT

1 December 1977 through 31 January 1981

General Electric Company
Re-entry Systems Division
P.O. Box 8555
Philadelphia, PA 19101

DTIC FILE COPY

X

Approved for public release;
distribution unlimited.

81 5 12 064

UNCLASSIFIED

SECURITY CLASSIFICATION OF THIS PAGE (When Data Entered)

19 REPORT DOCUMENTATION PAGE		READ INSTRUCTIONS BEFORE COMPLETING FORM	
1. REPORT NUMBER 18 AFOSR/TR-81-0409	2. GOVT ACCESSION NO. AD-A098797	3. RECIPIENT'S CATALOG NUMBER	
4. TITLE (and Subtitle) Chemical and Physical Aspects of Mesophase Formation During Carbon-Carbon Processing		5. TYPE OF REPORT & PERIOD COVERED 9 Final Report	
7. AUTHOR(s) 10 J. J. Gebhardt		6. PERFORMING ORG. REPORT NUMBER	
9. PERFORMING ORGANIZATION NAME AND ADDRESS General Electric Company/RSD 3198 Chestnut Street Philadelphia, Pennsylvania 19101		8. CONTRACT OR GRANT NUMBER(s) 15 F49620-78-C-0006	
11. CONTROLLING OFFICE NAME AND ADDRESS Air Force Office of Scientific Research/wc Bolling Air Force Base, D.C. 20332		10. PROGRAM ELEMENT, PROJECT, TASK AREA & WORK UNIT NUMBERS 16 61102F 2303/93 (1) AE	
14. MONITORING AGENCY NAME & ADDRESS (if different from Controlling Office)		12. REPORT DATE 71 31 Jan 81	
		13. NUMBER OF PAGES 115 (12) 115	
		15. SECURITY CLASS. (of this report) Unclassified	
		15a. DECLASSIFICATION DOWNGRADING SCHEDULE	
16. DISTRIBUTION STATEMENT (of this Report) Approved for Public Release; Distribution Unlimited			
17. DISTRIBUTION STATEMENT (of the abstract entered in Block 20, if different from Report)			
18. SUPPLEMENTARY NOTES			
19. KEY WORDS (Continue on reverse side if necessary and identify by block number) Carbon-Carbon Composites, Coal Tar Pitch, Pyrolysis, Mesophase Formation, Pressure Effects, Molecular Weight Distribution, Sound Velocity, Compressibility, Viscosity, Thermal Conductivity			
20. ABSTRACT (Continue on reverse side if necessary and identify by block number) Pyrolysis studies were carried out at 0.5, 3.5 and 6.2 MPa (50, 500 and 900 psig) and 723 and 748K (450 and 475°C) for 2, 4 and 7 hours on Allied 277-15V coal tar pitch and on two developmental Koppers Co. pitches, types A and B. Determination of quinoline insolubles and coking values showed a generally positive effect of pressure on conversion. The developmental pitches gave higher conversions to coke and less gas evolution than 277-15V. The greatest variation in kinetics appears to occur during the first two hours and at temperatures between about 698 and 748K. Examination of pyrolyzed products			

DD FORM 1 JAN 73 1473

UNCLASSIFIED

SECURITY CLASSIFICATION OF THIS PAGE (When Data Entered)

4100 114

570

UNCLASSIFIED

SECURITY CLASSIFICATION OF THIS PAGE(When Data Entered)

by optical and scanning microscopy indicated that smaller particles tend to be formed at elevated pressure and that coalesced mesophase areas are more uniform and less perturbed by gas formation and percolation.

Thermal diffusivity and conductivity measurements were made as a function of temperature on as-received as well as outgassed 277-15V pitch using a laser flash diffusivity technique. Similar measurements were also made at room temperature on partially pyrolyzed specimens of 277-15V and the two Koppers Co. developmental pitches. Specific heats were determined by differential scanning calorimetry. Thermal conductivity of the partially pyrolyzed materials decreased during the first two hours of pyrolysis, then increased gradually thereafter. No sudden or large changes were noted; the presence of bubbles in both solid and liquid specimens probably accounts for the observed scatter.

Sound velocity was measured in liquid phenanthrene up to 101 MPa and in liquid 277-15V pitch at one atmosphere; adiabatic compressibilities at one atmosphere were computed for both materials.

Relative viscosities of naphthalene, phenanthrene and 277-15V pitch were measured up to 101 MPa; freezing point measurements were also made from observed temperature changes during freezing and melting. This permitted establishing an estimated freezing point of 393K for phenanthrene at 69.4 MPa and a full pressure-melting point curve for naphthalene up to 101 MPa and 390K. Viscosities increased by a factor of up to two for the two pure compounds at pressures up to 101 MPa and up to six for 277-15V pitch. Qualitative evidence of partial solidification at around 50-60 MPa was also observed for 277-15V pitch.

Accession For	
NTIS GRA&I	<input checked="" type="checkbox"/>
DTIC TAB	<input type="checkbox"/>
Unannounced	<input type="checkbox"/>
Justification	
By _____	
Distribution/	
Availability Codes	
Dist	Avail and/or Special
A	

UNCLASSIFIED

SECURITY CLASSIFICATION OF THIS PAGE(When Data Entered)

TABLE OF CONTENTS

	<u>PAGE</u>
SUMMARY	vii
1.0 INTRODUCTION	1
2.0 PYROLYSIS STUDIES	4
2.1 ANALYTICAL STUDIES	6
2.2 MICROSTRUCTURAL FEATURES	8
3.0 THERMOPHYSICAL STUDIES	12
3.1 SOUND VELOCITY MEASUREMENTS	12
3.2 COMPRESSIBILITY	14
3.3 THERMAL PROPERTIES	16
4.0 VISCOSITY MEASUREMENTS	21
4.1 MEASUREMENTS ON PHENANTHRENE AND NAPHTHALENE	27
4.2 MEASUREMENTS ON ALLIED 277-15V PITCH	30
5.0 DISCUSSION	33
5.1 PYROLYSIS UNDER PRESSURE	33
5.2 VISCOSITY MEASUREMENTS	34
5.3 THERMAL CONDUCTIVITY	35
6.0 REFERENCES	103
7.0 ACKNOWLEDGEMENTS	105

AIR FORCE OFFICE OF SCIENTIFIC RESEARCH (AFSC)
NOTICE OF TRANSMITTAL TO DDC
This technical report has been reviewed and is
approved for public release IAW AFR 190-12 (7b).
Distribution is unlimited.
A. D. BLOSE
Technical Information Officer

LIST OF FIGURES

	<u>PAGE</u>
1. Gel Permeation Chromatograms of Three As-Received Pitches (Top) and Partially Pyrolyzed Koppers Type A (KA) Pitch (Bottom)	37
2. Gel Permeation Chromatograms of Partially Pyrolyzed Koppers Type B (KB) Pitch (Top) and Allied 277-15V Pitch (Bottom)	38
3. Koppers Pitch, Type A, After Pyrolysis at 748K for 2, 4 and 7 Hours at 6.2 MPa (Top) and 3.4 MPa (Bottom)	39
4. Koppers Pitches After Pyrolysis at 748K for 2, 4 and 7 Hours. Top - Type A at 0.5 MPa, Bottom - Type B at 6.2 MPa	40
5. Koppers Pitch, Type B, After Pyrolysis at 748K for 2, 4, and 7 Hours. Top at 3.4 MPa, Bottom at 0.5 MPa	41
6. Allied 277 Pitch After Pyrolysis at 748K for 2, 4 and 7 Hours. Top at 6.2 MPa, Bottom at 3.4 MPa	42
7. Allied 277 Pitch After Pyrolysis at 748K for 2, 4 and 7 Hours at 0.5 MPa	43
8. Coalesced Mesophase in Koppers Type A Pitch After Pyrolysis at 6.2 and 0.5 MPa, 7 Hours 748K Showing Effect of Pressure in Reducing Turbulence	44
9. Coalesced Mesophase in Koppers Type B Pitch After Pyrolysis for 7 Hours at 6.2 and 0.5 MPa, 748K	45
10. Coalesced Mesophase in Allied 277 Pitch After Pyrolysis for 7 Hours at 6.2 and 0.5 MPa at 748K	46
11. Insoluble Particles Around Mesophase Droplets in Allied 277-15V Pitch	47
12. Appearance of Immiscible Phase in Koppers Type B and Allied 277-15V Pitches	48
13. Immiscible Phase in Coalesced Mesophase in Koppers Type B Pitch After Pyrolysis for 7-Hours at 6.2 and 0.5 MPa	49
14. Immiscible Layers in Bubbles in Unconverted Pitch Regions. Type A Left and Center, 277 Right. 100X	50
15. Connected Bubbles at Container Wall in Koppers Type A Pitch Pyrolyzed 7 Hours, 6.2 MPa (100X)	51
16. Surface Layers on Partially Pyrolyzed Koppers Type A Pitch - 3.4 MPa, 723K, 7 Hours	52

LIST OF FIGURES

(continued)

	<u>PAGE</u>
17. Surface Layers on Partially Pyrolyzed Koppers Type A Pitch - 6.2 MPa, 748K, 7 Hours Showing Smooth Glassy-Like Structure Beneath Surface Layer of Loose Particles	53
18. SEM Views of Larger Mesophase Droplets, Formed by Pyrolysis at 3.4 MPa, 7 Hours, 748K. Top Koppers Type A Exhibits Less Surface Debris Than 277-15 Pitch at Bottom	54
19. SEM Views of Koppers Type A Pitch After Pyrolysis for 2 Hours at 6.2 MPa and 748K - Note Small Spherical Particles on Particle Surface	55
20. SEM Views of Koppers Type A Pitch Pyrolyzed 7 Hours at 3.4 MPa and 748K	56
21. SEM Views of Koppers Type B Pitch After Pyrolysis for 4 Hours at 6.2 MPa and 748 - Fine Particles Appear to be More Coherent Than Those in Type A (Figure 19)	57
22. Schematic of High Pressure Sound Velocity Cell	58
23. Exploded and Assembled Views of High Pressure Sound Velocity Cell	59
24. Loading and Operating Views of High Pressure Sound Velocity Cell	60
25. Calibration Curve-Sound Velocity at 6.5 MHz in Water vs. Pressure at 303K	61
26. (Sound Velocity) ³ at 6.5 MHz vs. Pressure in Phenanthrene at Various Temperatures	62
27. (Sound Velocity) ³ at 6.5 MHz vs. Pressure in Phenanthrene at 393.3K	63
28. (Sound Velocity) ³ at 6.5 MHz vs. Pressure in Phenanthrene at 414.4K	64
29. (Sound Velocity) ³ at 6.5 MHz vs. Pressure in Phenanthrene at 440.0K	65
30. (Sound Velocity) ³ at 6.5 MHz vs. Pressure in Phenanthrene at 465.0K	66
31. (Sound Velocity) ³ at 6.5 MHz vs. Pressure in Phenanthrene at 490.6K	67

LIST OF FIGURES

(continued)

	<u>PAGE</u>
32. (Sound Velocity) ³ at 6.5 MHz vs. Pressure in Phenanthrene at 513.9K	68
33. (Sound Velocity) ³ at 6.5 MHz vs. Pressure in Phenanthrene at 537.8K	69
34. (Sound Velocity) ³ at 6.5 MHz vs. Pressure in Phenanthrene at 562.2K	70
35. Sound Velocity vs. Temperature in Phenanthrene at 6.5 MHz and Allied 277-15V Pitch at 2 MHz, Atmospheric Pressure	71
36. Adiabatic Compressibility of 277-15V Pitch and Phenanthrene at Atmospheric Pressure	72
37. Schematic of Specimen Container for Flash Diffusivity Measurements	73
38. Laser Flash Diffusivity Data Form	74
39. Measured and Calculated Specific Heats of 277-15V Pitch	75
40. Thermal Conductivity of As-Received and Outgassed 277-15V Pitch vs. Temperature	76
41. Schematic of High Pressure Viscometer with Friction Seal	77
42. Calibration of Viscometer with Water-Typical Data Form	78
43. Calibration of Viscometer Using Castor Oil.....	79
44. Modified High Pressure Viscometer with Seal Bellows	80
45. Drop Time of Needle in Phenanthrene at Various Temperatures vs. Pressure	81
46. Effect of Pressure on Melting Point of Naphthalene	82
47. Drop Time of Needle in Naphthalene at Various Temperatures vs. Pressure	83
48. Viscosity of Naphthalene at 0.1 and 101 MPa vs. Temperature	84
49. Positive Print of Radiograph Showing Needle within Viscometer	85
50. Drop Time of Needle in Allied 277-15V Pitch at Various Temperatures vs. Pressure	86

LIST OF FIGURES

(continued)

	<u>PAGE</u>
51. Increase in Drop Time in Pitch with Time at 629.3K and 101 MPa. Drop Time at 101 MPa vs. Temperature	87

LIST OF TABLES

	<u>PAGE</u>
1. Properties of Pitches Used in Pyrolysis Studies	88
2. Analytical Data on Partially Pyrolyzed Pitches	89
3. Molecular Weight Distribution and Composition of Partially Pyrolyzed Pitches	90
4. Sound Velocity-Pressure Data for Water at 6 MHz	91
5. Sound Velocity in Phenanthrene at 6.5 MHz at Pressures up to 101 MPa	92
6. Sound Velocity in Allied 277-15V Pitch at 2 MHz	93
7. Specific Heat of 277-15V Pitch	94
8. Thermal Conductivity/Diffusivity of 277-15V Coal Tar Pitch	95
9. Thermal Diffusivities of Three Partially Pyrolyzed Pitches	96
10. Thermal Conductivity Partially Pyrolyzed Pitches	97
11. Cell Constant Determination for Viscometer	98
12. Viscosity of Castor Oil	98
13. Viscometer Data (Drop Time) for Phenanthrene	99
14. Viscometer Data (Drop Time and Viscosity) for Naphthalene	100
15. Viscometer Data (Drop Time and Viscosity) for Allied 277-15V Pitch	101
16. Drop Time in Allied 277-15V Pitch vs. Time at Temperature at 101 MPa	102

SUMMARY

Experimental studies were carried out to elucidate some of the effects of pressure on properties of coal tar pitch materials and simpler fused ring compounds. Sound velocity measurements were made on phenanthrene up to 562K and 101 MPa and on Allied 277-15V pitch up to 541K at 0.1 MPa. The latter deviated markedly from the nearly linear relationship between sound velocity and temperature found for phenanthrene. Adiabatic compressibilities at 0.1 MPa were calculated.

A high pressure falling needle viscometer was constructed and calibrated. Relative viscosities of naphthalene, phenanthrene and Allied 277-15V pitch were measured at pressures up to 101 MPa and at temperatures up to 373, 573 and 608K respectively. Naphthalene and phenanthrene showed a two fold increase between 0.1 and 101 MPa, while a six fold increase was measured for the pitch specimen.

A melting point - pressure curve was established for naphthalene based on observed temperature variations during pressure changes. The pitch specimen gave qualitative evidence of partial solidification around 50 MPa and 533K.

Thermal diffusivity and conductivity were measured on as-received and partially pyrolyzed specimens of 277-15V pitch and two developmental Koppers Co. pitches, using a laser flash technique. Minor trends to lower conductivity were noted for short pyrolysis times; the conductivity then rose slightly on further pyrolysis.

Pyrolysis analytical results and optical and scanning microscopy observations showed a positive effect of pressure on rate of conversion and noticeable repression of turbulence and percolation at 6.2 MPa. All three pitch materials, appear to contain or to form an immiscible phase during pyrolysis, which collects inside gas bubbles and cracks in the unconverted regions of the specimen.

1.0 INTRODUCTION

The manufacture of polycrystalline graphites of various grades has been a widely practiced industrial process for a sufficiently long time for the general relationships among raw materials, processing parameters and properties to be relatively well understood (1). Brooks and Taylor (2), White (3), and others have described the overall mechanisms by which polynuclear aromatic mixtures of relatively low molecular weight such as coal-tar pitches polymerize to a metastable liquid crystal-like intermediate state (mesophase) from which they progress to carbon char and eventually graphite crystallites by heat treatment. The wide variation in properties of the raw materials, principally coal tar and petroleum pitches, together with a long period of process development to achieve acceptable properties within reasonable costs have led to a host of finished graphites with varying properties, usually tailored to meet specific requirements of strength, electrical conductivity, porosity, thermal expansion, purity etc. (4).

The advent of carbon-carbon (C/C) composites, actually graphite fiber reinforced graphite, has brought about a need for more rapid, precise and controlled graphite formation from liquid precursors within the voids and interstices of arrays of preassembled fiber bundles than has heretofore been required. Simultaneously, variations in pitch raw stocks, not unusual for an industrial 'natural' product, have made it more difficult to predict composite fabrication and performance on the basis of the properties of 'typical' available raw materials. A further requirement for shortened production schedules has led to impregnation and coking of the pitch within the preforms at elevated pressures while at the same time expanded use of C/C composites has increased not only the volume to be processed, i.e. densified, but also preform sizes and geometries.

As a consequence there has arisen a need to know more precisely some of the physical and chemical responses of polynuclear molecules and mixtures such as coal tar pitch at elevated pressures and temperatures. This is particularly so of transport property data such as viscosity and thermal diffusivity and conductivity needed to permit prediction of processing parameters and rates of change to be used in impregnation and pyrolysis within relatively fragile and expensive preforms. Rates of heating, pressure application, impregnation and penetration, gas formation and percolation, liquid exudation and finally coke yield and distribution within the preform can be expected to be influenced by changes in pitch properties with time at temperature and pressure. Preform strength and integrity can also be compromised by unexpected internal stress buildup due to imbalances in the pressure-temperature response of the impregnated, reacting pitch.

Progress has been made recently in understanding the nature and composition of coal tar and petroleum with respect to mesophase and graphite formation at atmospheric (5) as well as elevated pressure (6). The purpose of the work described in this report has been to add to this knowledge by direct determination of selected transport properties of an accepted coal tar pitch standard as well as observations of its behavior during the early phases of mesophase formation under pressure. In view of the aforementioned variations in properties with the ultimate origin of natural pitches, two experimental reproducible and 'tailored' pitches were included in some of the measurements to assess how their 'typical' properties vary with pressure and time at temperature relative to the 'natural' product. In addition, phenanthrene and naphthalene were studied as pure, polynuclear aromatics, related to pitches, but free of the side chains, suspended particulates and molecular weight distribution typical of pitch mixtures.



Experimental work performed and to be discussed in this report includes

- a) studies of mesophase formation in three coal tar pitches at near atmospheric and moderately high pressure, which included determination of molecular weight distribution, quinoline insoluble measurement and microscopic examination;
- b) measurement of sound velocity of phenanthrene up to 101 MPa (15,000 psi) and coal tar pitch at one atmosphere and calculation of adiabatic compressibilities;
- c) measurement of viscosity of naphthalene, phenanthrene and 277-15V pitch up to 101 MPa using a falling needle viscometer;
- d) measurement of thermal diffusivity and conductivity of coal tar pitches in the as-received as well as partially pyrolyzed condition.



2.0 PYROLYSIS STUDIES

Partial pyrolysis of coal tar pitches was carried out under nitrogen in a laboratory autoclave at 0.50 MPa (50 psig), 3.5 MPa (500 psig) and 6.2 MPa (900 psig) at 748K (475°C) for periods of two, four and seven hours. Pitches used were Allied Chemical Corporation CP277-15V, Batch 501, and Koppers Co. Inc. developmental grades designated as type A and type B. The latter two grades are processed by the manufacturer so as to provide higher coke yields and improved impregnation properties respectively. In the subsequent discussion these will be referred to as "277" "KA" and "KB" for convenience. Typical properties are listed in Table 1.

Each pyrolysis experiment included three beakers containing about 150 gm of each pitch as well as three graphite crucibles 10 cm long, 1.27 cm i.d containing 3-5 gms of each material. Loosely fitting aluminum foil covers and glass wool plugs were used to prevent cross contamination and to repress excessive foaming. The graphite crucibles had previously been infiltrated with pyrolytic carbon at 1373K to prevent penetration of the structure by the molten pitch and to provide a uniform contact surface throughout. Additional specimens consisted of samples of graphite fiber (Union Carbide T-50, Hercules HM-PAN and Union Carbide VS 0032 pitch fiber as well as pyrolytic carbon coated T-50) attached to graphite rods with Union Carbide C-34 graphite cement. Volume constraints of the autoclave permitted the use of only one pitch in this case; 277 was selected.

In the pyrolysis, the autoclave was evacuated, back-filled to the experimental pressure with nitrogen, and heated to the experimental temperature, venting excess pressure as necessary. This required four hours. After holding at 748K for the required time, the autoclave was cooled under pressure by

natural conduction (four hours). A single experiment was conducted at 723K (4500C) and 6.2 MPa to evaluate the effect of temperature. The large sample of each pitch was used for weight loss measurements and for determination of physical characteristics (quinoline insolubles, coking value, softening point and scanning microscopy) by Koppers Co. The graphite test tubes were split to permit visual and metallographic examination of vertical cross sections of the as-settled samples as well as to provide readily comminuted specimens for molecular weight distribution, density, specific heat and thermal conductivity measurements. These results will be presented in the following sections.

2.1 ANALYTICAL STUDIES

Table 2 lists the results of quinoline insoluble (QI), coking value (CVC), softening point and weight loss measurements made on the pyrolyzed pitch samples. Included are data from one experiment carried out at 3.4 MPa (500 psig) and 723 K (450°C) to compare the effect of temperature. Examination of the results shows several distinctions among the three materials with respect to all of the variables - time and pressure as well as temperature. All for example, show a positive effect of pressure on percent QI at four hours and after, whereas KA and KB pitches appear to be slower to start than 277. This may reflect the higher initial content of QI in the latter, which may serve as a 'starter' as it were. Between 2 and 4 hours KA shows a much higher response to pressure than KB and 277 and by 7 hours has the highest conversion. KB on the other hand is more similar to 277 after 7 hours but responds to pressure increase more noticeably. The effect of temperature on all three materials is quite significant indicating a fairly narrow range within which kinetic studies of the early phases of mesophase formation might be usefully conducted.

Weight loss results indicate that KA is much less sensitive to temperature in this respect than either KB or 277, with the latter showing a considerably greater loss than either KA or KB. Softening point measurements follow the trend shown by QI measurements with both KA and 277 having values above 573K at 4 hours while KB still flows at 498K (225°C). Coking values are higher for KA, prepared as it was for this purpose, although at 0.5 MPa (50 psig), 277 gives a similar result. However, in view of the greater weight loss from the latter particularly in the first two hours, the overall gain in carbon in an impregnated body would be less.

Molecular weight distribution and weight and number averages were determined by gel permeation chromatography on samples of as-received as well as partially pyrolyzed pitches. Results are given in Figures 1 and 2 and Table 3. These were determined on the fraction extractable with chloroform, using μ -Styragel columns of 1000, 500 and 100 \AA particle size. A Waters Associates High Pressure Liquid Chromatograph was used, which was calibrated with naphthalene, anthracene, 2, 3 benzanthracene and pentacene. Specimens were taken from one half of the graphite test tube samples described above, and were pulverized using a glass mortar and pestle. The chromatograms show little variation in molecular weight distribution between the as-received and pyrolyzed pitches except in the case of 277. Here, the high molecular weight fraction has been removed after two hours at 0.5 as well as 6.2 MPa. This is probably the result of side chain splitting before reaching reaction temperature, and accounts for its significantly greater weight loss referred to earlier. Part of the weight loss observed is also due to vaporization of low boiling components such as trimethyl benzene, xylene and benzene which were found in an analysis of off gases in evacuating molten 277 pitch.

The data also indicate little influence of pressure on molecular weight distribution of the chloroform soluble fraction of KA and KB, only that there is less of it as a function of time. There is a slight decrease for 277. There appears to be some effect of pressure on all of the pitches in that greater fractions of the specimens remain soluble after two hours at 0.5 MPa than at 6.2 MPa for KB and 277 and at 3.4 MPa for KA.

2.2 MICROSTRUCTURAL FEATURES

Figures 3 through 7 show the general appearance of vertical sections of the material pyrolyzed in the graphite tubes. Variations from pitch to pitch are noticeable as well as within the same pitch, pyrolyzed at different pressures and for different times. As would be expected, bubbles are smaller at higher pressure and the volumes of coalesced mesophase higher at longer times. The latter are identifiable by the difference in reflectance between the bottom (coalesced region) and top (unconverted pitch) regions.

For metallographic examination, only the specimens from 7 hour runs at 0.5 MPa (50 psig) and 6.2 MPa (900 psig) were used. One half of the split graphite tube containing the as-settled specimen was mounted in Marasperse and sectioned along the tube axis, yielding a quarter section of the tube. This was remounted and polished for closer examination metallographically.

Specimens pyrolyzed at 6.2 MPa generally showed the effects of less turbulence than did those pyrolyzed at 0.5 MPa. The latter display a great deal more polarization over shorter distances due to turbulence and flow lines around bubbles, as shown in Figures 8-10. KA and KB were quite similar in terms of volume and location (at the bottom of the tube) of the coalesced phase, while the 277 specimen had a less well developed coalesced region. Finely divided quinoline insoluble particles and very small mesophase droplets also characterized the 277 specimen. The coalesced phase also appears to rest on a region of finely divided particles at the bottom of the tube. These particles could be resolved with some difficulty at high magnification, as small droplets surrounded by ejected solids as shown in Figure 11. The difference in hardness of these two components was evident by the different focus required

to resolve the particles and droplets separately. KA and KB showed little evidence in these views of such finely divided insolubles although at very high magnification they may be evident in SEM views as will be shown.

A characteristic common to all of the pyrolyzed specimens, was what appeared to have been an immiscible phase, confined mostly to the unconverted pitch region, at external surfaces as well as within large gas bubbles as shown in Figure 12. Small droplets of an immiscible material can also be seen in the coalesced region of the specimens pyrolyzed at higher pressure (6.2 MPa). These were nearly always spherical in the broad undisturbed areas shown in Figure 13, left, but were deformed where sufficient flow occurred, as in Figure 13 center. Because of the higher viscosity of the pitch and the lower tendency for gas evolution, these did not develop further into the streaks that appeared to occur in lower pressure pyrolyses (0.5 MPa), Figure 13 right, where gas evolved more rapidly and the pitch was somewhat more fluid. Distortions and layering of a separate phase occurred within large gas bubbles, usually in the unconverted pitch, possibly because of variations in solidification rates and thermal contraction. Typical examples are shown in Figure 14. They were usually absent in the coalesced regions.

In all cases the descent of mesophase droplets through the unconverted phase to the surface of the coalesced region was evident as in Figure 15 top, with the droplets tending to be larger in KA and KB than in 277. Droplet size also increased with descent and there was some tendency to cling to the walls. Gas bubbles also were found in connected strings at the walls where they were trapped as the coalesced region formed as seen in Figure 15.

Some of the characteristics of the partially pyrolyzed pitch mixtures observed in the metallographic studies can also be seen in scanning electron microscopy (SEM) views. Figure 16 for instance shows particles of KA apparently

coated with cracked outer layers containing some broken bubbles. At higher magnification the bubbles are seen to be connected and contain cracked material on the inner wall which may have arisen from the lamellar structures seen in Figures 13 and 14. Still higher magnification reveals the particulate nature of the cracked overlayer.

The particles are evidently 1000-2000 ⁰A in diameter and appear to be more or less spherical. It is possible that these are mesophase droplets before they grew to the extent that they were visible at relatively low magnification on coalescing into droplets such as are shown in Figure 12, left. Coalescence into larger droplets would be aided by the decrease in surface free energy, as well as by the mixing produced by turbulence or percolation.

At higher temperature (748K vs 723K) and conversion, the cracked outer layer seen in Figure 17 has a more continuous appearance, and less of a particulate structure. Whether the fine particles are representative of nascent Q.I. in KA which eventually coalesce or not is not readily discernible. However KA had virtually no QI initially whereas 277 contained about 6 percent. Contrasting SEM views of KA and 277 pitches pyrolyzed in the same experiment show considerably more solid particulates on the outer surfaces of the latter than appear on the former as is shown in Figure 18. Despite the low initial content of QI in the KA and KB pitches, significant amounts of very fine particulate material formed on even short pyrolysis times as is seen in Figures 19 and 20. These appear to be less fusible than those formed in KB pitch (Figure 21) which are less distinct as particles and appear to be more cohesive. The fine particles in 277 pitch appear to be more similar to those of KA rather than KB judging from limited observation.

The process of formation of the large and very visible mesophase spheres shown in Figures 15 and 18 for example evidently starts at considerably lower

temperatures than were used in these experiments. The appearance of distinct spheroids 1000-2000 ⁰ A in diameter in SEM views of partially pyrolyzed pitches seems to indicate that they were distinct and rigid enough to survive the cooling process. They evidently remained distinct until surface forces drew them together to much larger spheres as shown in Figure 18, where they did not yet lose their identity by complete coalescence.

2.3 FIBER BUNDLE RESULTS

Bundles of HM-PAN, VS0032 pitch and Thornel T-50 fibers which were immersed in 277 pitch during pyrolysis at 748K were examined by optical microscopy after mounting and polishing. In no instance were coalesced mesophase or droplets found among the filaments of the bundles. However the specimens examined were limited in number, making it difficult to generalize on this observation. A preferable approach would involve using small preforms, not subject to distortion by turbulence or gas release.

3.0 THERMOPHYSICAL STUDIES

3.1 SOUND VELOCITY MEASUREMENTS

Measurement of the velocity of sound materials can provide data of importance in determining other transport properties such as viscosity, and compressibility through relationships such as

$$\beta_{ad} = \frac{1}{v^2 \rho} \quad (1)$$

where β_{ad} is adiabatic compressibility, v is sound velocity and ρ is liquid density, and

$$\alpha = \frac{2}{3} \frac{\eta \omega^2}{\rho v^3} \quad (2)$$

where η is viscosity, ω is $2\pi\nu$, ν being frequency, and α is known as the sound absorption coefficient. In principle, direct measurement of sound velocity is experimentally simpler than other approaches. Thus, to begin a data base on relatively simple polynuclear aromatic compounds such as naphthalene and phenanthrene, to lead eventually to more complex mixtures such as coal tar pitch, sound velocity measurements were made at elevated pressure and temperature using a simple piston-cylinder measurement chamber pressurized by means of an Instron testing machine.

Figure 22 is a schematic of the cell designed and constructed on IRAD funds, which consists of: i) two, thick-walled cylinders made of Udimet-700 and 304 stainless steel for high (to 700°C) and low temperature use, respectively; ii) an Inconel liner for the working cavity; and iii) two stainless steel pistons which comprised the upper and lower containment walls and which transmitted pressure to the contents of the cavity. The pistons were fitted with compressible metal rings that deformed against the liner of the working chamber to effect the seal. Pressure on a fluid within the working cavity was achieved by compressing the pistons in a laboratory Instron testing machine. A piezoelectric

crystal and detector mounted on the upper and lower pistons were used to send an ultrasonic signal through the pistons and the fluid in the working cavity enabling sound velocity measurements to be used to monitor physical and chemical changes in the working fluid as a function of time, temperature and pressure. Figures 23 and 24 show the cell during assembly and in operation.

Accessories for the high pressure cell included a heater for achieving and maintaining temperature, a cell filling system with which the working cavity could be evacuated and filled with the molten experimental material kept under an inert atmosphere, and a piston alignment, insertion and removal device.

Although the pressure within the high pressure cell system as a whole can be computed from the Instron load cell, the measurement includes pressure applied to the experimental fluid plus the frictional drag of the seals against the cell liner. In order to calibrate the system, i.e., to determine pressure actually applied to the working fluid, the velocity of sound in de-ionized water was determined as a function of pressure at room temperature. Results are given in Table 4 and Figure 25. Measurements were made at both approach to and retreat from (i.e., increasing and decreasing) the pressure setting to evaluate the error associated with the seal frictional drag. The effect appears to be small. For example at 90.2 MPa (13,100 psig) sound velocity was measured as 1.649 km/sec on approach and 1.653 km/sec on retreat from pressure. Based on literature values for sound velocity in water at high pressure (7), this corresponds to a pressure error of about 1.2 MPa (178 psi).

Sound velocity measurements were made at 6.5 MHz in liquid phenanthrene, a model compound selected for baseline measurements between 394K (120°C) and 562K (289°C) and 0.1 MPa (1 atm) and 101 MPa (1000 atm). Table 5 shows the data

obtained. As was anticipated, velocity increases with pressure and decreases with increasing temperature, the former effect predominating as both parameters increase. The cube of sound velocity in liquids should be a linear function with respect to pressure (8) and this appears to be the case for phenanthrene at lower temperatures as is seen by Figures 26 through 34. Breaks in the curves at higher temperatures are probably indicative of lower pressure in the cell than indicated by the Instron cell load as a result of seal friction, particularly where velocity values are lower than anticipated. Where velocities appear to be higher than expected, one might postulate a phase change from liquid to solid. This was found to occur during viscosity measurements to be discussed later.

The velocity of sound was also determined in liquid coal tar pitch (Allied 277-15V) between 150° and 270°C at 0.1 MPa (1 atm); results are shown in Table 6 and Figure 35 compared to measurement in phenanthrene. Because of the higher acoustic losses in the pitch, measurements were made at 2 MHz.

3.2 COMPRESSIBILITY

Sonic velocity data can be related to adiabatic compressibility via the simple relationship

$$\beta = \frac{1}{c^2 \rho} \quad (3)$$

where β is compressibility, c is sound velocity and ρ is density, all at the temperature of interest.

Available density data for both phenanthrene (Reference 9) and coal tar pitch (Reference 10) were used with sonic velocity data to arrive at the compressibility factor curves for both materials at atmospheric pressure as shown in Figure 36.

Further work on measurement of sound velocity in 277 pitch at elevated pressure was undertaken. However increasing acoustic losses were encountered as well as difficulty in maintaining seal motion during compression and release. The losses are believed to be due to trapped gas bubbles which could not be released from the cell and which introduced numerous lossy interfaces between the crystal and receiver. Since the likelihood of obtaining reliable data was low, no further work on this aspect was attempted.

3.3 THERMAL PROPERTIES

One of the important characteristics of pitches which are being pyrolyzed in bulk, i.e., as in the interstices of large fiber preforms, is the rate at which heat is transported from the heat source to the most distant part of the reactor, which is the center in most cases. The work undertaken in this program in pyrolyzing pitches for varying times and at different pressures afforded an opportunity to evaluate thermal conductivity of these materials by means of diffusivity measurements using a laser flash diffusivity technique.

The standard flash technique is one of the simplest methods of measuring thermal diffusivity. A sample in the form of a small disk (1.27 cm Dia. and .25 cm or less thick) is brought to a desired steady uniform temperature in a furnace. A flash or pulse of thermal energy is then supplied to the front surface of the sample within a time interval which is short compared to the resulting thermal transient. The thermal diffusivity of the sample is then calculated from the temperature vs. time measurements at the back surface of the sample.

A neodymium glass laser is used (Apollo-model 35) to supply the required pulse of thermal energy. This particular laser has the desirable feature of a variable pulse width, 1.0 to 0.1 millisecond, which eliminates the need for pulse width corrections to the diffusivity calculation in most cases.

On the optical path just in front of the laser a piece of cover glass is positioned at 45° to the optical path to reflect a small amount of laser radiation to a photo cell. The output of the photocell is used to trigger the oscilloscope and this serves as a zero time reference for the measurement. Normally, solid samples would be mounted on a rotating holder in a tube furnace with optical windows. With the pitch, a special enclosed heater was built so the melted pitch could be held in a horizontal holder in a nitrogen atmosphere as shown in Figure 37. The laser beam is reflected down on the top of the pitch

sample. The holder for the pitch was made by bonding .001" thick stainless steel foil to the bottom of a ceramic ring. The temperature of the back face of the pitch was measured with a .003" diameter Chromel-Alumel thermocouple. To record the thermocouple output versus time, a dual beam oscilloscope was used. Both beams displayed the thermocouple voltage on the Y axis. The X axis sweep rates on the two beams were different by a factor of 10 to allow accurate measurement of the half time and at the same time also allow the long term temperature response to be recorded for the temperature loss correction. The scope traces were photographed for later computer aided data reduction.

A typical thermal response curve of the back face of the sample is shown in Figure 38. The equation for data reduction is given below,

$$\alpha = \frac{CL^2}{t_{1/2}} \quad (4)$$

where

α = thermal diffusivity

L = sample thickness

$t_{1/2}$ = time required for the back face of the sample to reach half of the eventual maximum excursion.

C is determined graphically using Cowan's correlations (11) from the ratio of $\Delta T_{(10t_{1/2})} / 1/2 \Delta T_{max}$. Both $\Delta T_{(10t_{1/2})}$ and ΔT_{max} are shown in Figure 38.

$$\text{Then } K = \alpha C_p \rho \quad (5)$$

Several specimen containment materials were tried in order to overcome the problem of meniscus formation, which prevents achievement of flat, parallel upper and lower surfaces of the specimen. Machinable ceramics were suitable except for entry of the pitch into the pores of the ceramic, rendering thickness measurements uncertain. A thin cover glass was also laid over the pitch surface

but gas bubble formation under the glass prevented good thermal contact from being made.

The most satisfactory material was a Teflon ring, used as a liner for the metal container. This did not completely eliminate meniscus formation but reduced it so that the specimen thickness through which the heat pulse passed was constant, or nearly so. Corrections for thermal expansion of the 277-15V specimen on heating to measurement temperature were made by using specific gravity vs. temperature data from the literature (10) and the known specimen weight and diameter. Specific heat values used to calculate thermal conductivity from the diffusivity data were determined in an earlier program using a Perkin-Elmer Differential Scanning Calorimeter and are given in Table 7 and Figure 39. Values calculated from an expression given in Ref. 12 were in considerable disagreement. An error in the referenced equation is suspected as indicated in Table 7.

Two series of measurements were made - the conductivity of 277 pitch as a function of temperature in the as received condition and after degassing for several minutes at about 373-383K, and conductivities at room temperature of partially pyrolyzed 277, KA and KB pitches after grinding a specimen and recasting a disc for measurement. Specimens were formed from the material in one vertical half of the graphite tube experiments discussed earlier. These were ground in a glass mortar and pestle and contained the coalesced mesophase as well as the unpyrolyzed portion of the sample to arrive at a more typical value for a bulk specimen.

Table 8 lists the thermal diffusivity and conductivity data for 277 pitch as a function of temperature while Figure 40 shows the trends with temperature. Also shown in Figure 40 is a steady state value obtained with a Dynatech differential scanning calorimeter. Computer aided analysis of the data yielded

the curve shown, indicating that for the short heating periods, thermal conductivity appears to be less sensitive to temperature than to other effects.

Measurements of thermal diffusivity were also made at room temperature (20°C) on two experimental pitches, Koppers KA and KB as well as Allied 277-15V after pyrolysis at 708K (475°C) for 2, 4 and 7 hours and 0.5 and 6.2 MPa. Thermal conductivities were calculated using specific heat data obtained on the specimens with a Perkin-Elmer Scanning Differential Calorimeter and densities determined by water immersion. The diffusivity values are listed in Table 9 together with specimen thickness and average values and standard deviations. Conductivity results are given in Table 10 as computed from average diffusivity values and specific heat and density values determined on the pyrolyzed pitch discs.

Values of thermal conductivity of as-received 277-15V pitch show a significantly greater variation with temperature than do those for the outgassed material. This can be attributed to the loss of volatiles having a higher hydrogen content, particularly above the softening point. Formation of bubbles and voids in this material reduce diffusivity and the thermal conductivity of the at the time of measurement. After outgassing, although the scatter is greater, perhaps due to variations in the rate of loss of volatiles, conductivities show much less variation with temperature over this relatively narrow range. In processes where vacuum impregnation is used conductivity values might be expected to fall between these curves depending on the volume of pitch involved and the extent of outgassing. For smaller amounts of material the values shown for outgassed material would probably be more reliable for heat transfer estimates.

Thermal conductivity differences among the three pitches studied, determined at room temperature on as-received as well as pyrolyzed material, do not

appear to be very large in view of the fairly significant standard deviations in diffusivity values in the pyrolyzed specimens. Diffusivity and conductivity values for as-received material are probably more reliable and appear to correlate with the softening points and specific gravities of the materials. This may in turn be related to their hydrogen contents.

Values for pyrolyzed specimens have significantly higher standard deviations indicative possibly of greater difficulty in selecting identical specimens. For the 277-15V and KB pitches there appears to be some variation with pyrolysis time at both 6.2 MPa and 0.5 MPa which could be related to loss of volatiles during the first two hours. After a noticeable decrease in conductivity during this time, a slight increase occurs with pyrolysis for longer times. This pattern is not followed by the KA pitch with which there was greater difficulty in casting the discs on which the measurements were made. Several values are suspect, especially since diffusivity was found to be related to specimen thickness, not a characteristic of the diffusivity technique. The technique however has a number of drawbacks particularly with respect to specimen homogeneity, i.e., the presence of varying amounts of solid material of different properties as well as of some frozen-in gas bubbles. Thus, thermal conductivity measurements, useful for following this property through the course of pyrolysis to relatively high conversions, would best be done by a more direct method if a feasible one can be developed.

On the whole, while the thermal data are not of diagnostic value relative to the chemistry of mesophase formation, they can be useful in deriving heating rate and heat flow estimates, especially for large amounts of material.

4.0 VISCOSITY MEASUREMENTS

The viscosity of liquid pitch exerts a strong influence on practical aspects of pyrolysis at elevated pressure. There are the change in viscosity below reaction temperature which influences penetration into the preforms, the rates of gas evolution and circulation effects as the pitch is warmed and convective currents are established. Further, there are unknown factors such as the possible solidification of the pitch or of some of its components as pressure is applied. Reaction rates, coalescence and turbulence during the early phases of pyrolysis can also be influenced, with probable effects on the graphite crystallites ultimately formed, for example, aspect ratio, size and defect content. Consequently, direct measurement of the viscosities of pure polynuclear aromatic compounds such as naphthalene and phenanthrene as well as that of a typical pitch became a principal goal of this effort. This required design, construction and calibration of a viscometer suitable for measurements up to at least 673K (400°C), preferably higher, although formation of mesophase droplets and gas release were expected to be troublesome at the higher temperature.

The viscometer originally designed for direct determination of model compound and pitch viscosity is shown in Figure 41. It is a falling needle type having a bore diameter of 0.4686 cm (0.1845 in.) and a total tube length of 60.96 cm (24 in.), constructed from heavy wall stainless steel tubing.^a Two electromagnetic coils are wound around the outside of the tube, separated by a distance of 30.48 cm (12 in.), to detect passage of the falling needle by interruption of the field generated by the coils. Friction seals are used and pressure achieved by an Instron test machine as discussed earlier.

The time, t , required by the needle to fall through the 35 cm distance between the coils is related to the viscosity of the fluid in the tube by the

(a) Autoclave Engineering Co., Erie, PA.

following equation

$$\eta = C_0 (\rho_N - \rho_L) t \quad (6)$$

where η is the fluid viscosity, ρ_N and ρ_L are the densities of the needle and liquid respectively. C_0 is a constant related to the geometry of the system, specifically the inner diameter of the tube and that of the needle. Figure 42 shows a trace of the field response as the needle falls through the coils.

Calibration of the viscometer is done by first approximating the most suitable needle diameter using the relation given in Ref. 13.

$$C_0 = \frac{g R^2 Z}{6L} \cdot \left(\frac{1 - Z}{1 + Z} \right)^3 \quad (7)$$

in which g is the gravitational constant, R is the inner diameter of the tube, L is the distance between coils and Z is the square of the ratio of the diameters of needle and the tube through which the needle falls.

Equation 7 is of value in two respects. First, it is helpful in choosing a needle diameter that will result in drop times that are not excessively long or short. Second, it provides a means to correct for any effects of dimensional changes in the apparatus that may occur due to temperature and pressure changes.

In the apparatus used, the tube was made of stainless steel with a bore diameter of 0.4686 cm. A thin tube of phosphor bronze was fitted over the outside diameter of the steel tube to support electrical pick-up coils which detected the passage of the needle as it fell. This technique is similar to that described in Ref. 13. Also, as with that work, an electromagnet was used to raise the needle to the top of the tube between measurements.

C_0 , which is a constant for a particular viscometer, is determined experimentally by measuring fall times in liquids of known viscosity and density. Since measurements on coal tar pitch were planned and a wide viscosity range was anticipated, determination of C_0 was made using both distilled water

($\eta \sim 1$ cp at 20°C) and castor oil ($\eta \sim 990$ cp at 20°C). Data from reference 14 were used for this purpose. It was found that for small needle diameters ($Z = 0.47$) the two liquids gave quite different values of C_0 . Increasing the needle diameter to $Z = 0.75$ almost eliminated this and a $Z = 0.83$ the same C_0 was obtained (within experimental accuracy) for both liquids.

Calibration measurements were made at room temperature using distilled water and castor oil as standards of known viscosity. Several needle diameters were used since the required clearance between the needle and capillary tube wall was not known. This separation controls the nature of the flow in the annulus which in turn produces the shear forces related to viscosity. Results of these preliminary measurements are given in Table 11 in terms of the values calculated for the constant C_0 .

It can be seen that as the needle diameter increased, closing the annular distance in the tube, the value of C approached constancy for liquids of different viscosities. A slightly larger needle (diam = 0.4262 cm) (0.1678 in) was then used to determine viscosity over a range of values to check these results. Water at various temperatures was used as the calibration liquid and yielded a value of 6.28×10^{-2} for C_0 . The viscosity of castor oil was then measured at various temperatures and compared to data given in Ref. 14, which were curve fitted to a cubic expression of the form

$$\ln \eta = F(T) \quad (8)$$

Figure 43 shows these results in which the squares represent handbook data, the points are calculated from the cubic polynomial and the circles represent the data shown in Table 12 obtained from measurements made on castor oil using the 0.4262 cm diameter needle and the value of C_0 determined from distilled water. These results are slightly low since density data for castor oil were not available and the room temperature value was used for calculating viscosity from equation (6). General agreement is considered satisfactory however.

Considering Eq. 7, the quantity Z is essentially unaffected by temperature as it is a ratio of two diameters and the thermal expansion coefficients are essentially the same for the two. However, both the needle diameter, d_n and tube length, L are affected and both increase with increasing temperature. The expansion coefficients are somewhat different as the coil separation (L) is determined by expansion of the phosphor bronze tube which supports the electrical pickup coils. However, the net effect in going from 20 to 75°C is to increase C_0 by only about 0.08%.

Turning to Eq. 6, the densities of the needle and the liquid are also affected by temperature rise. In going to 75°C, the needle density will decrease by only about 0.25% but the water density decreases by about 2.3%. Since the change in liquid density is significant, this density should be measured unless an accuracy of a few percent is not critical to the experiment. These densities are also affected by pressure, with the needle density increasing by about 0.07% at 101 MPa (15,000 psi) pressure and the water density increasing by about 3.6%. For the viscosity measurements on water, the water density was corrected for pressure by using compressibility data from reference 14.

Pressure will also tend to increase the tube diameter and decrease the needle diameter, thus affecting both d_n and Z in Eq. 7. The effect is to increase C_0 by about 2.8%, primarily due to the change in Z . It should be noted that this pressure effect on C_0 will increase at higher temperature due to the decrease in the elastic modulus of the steel.

Measurements on distilled water were initially made at one atmosphere pressure in order to determine C_0 from Eq. 6. This gave the following result (with viscosity expressed as centipoise):

<u>Temperature (°C)</u>	<u>No. of Measurements Averaged</u>	<u>C₀</u>
21.7	4	6.28 x 10 ⁻²
31.	3	6.40 x 10 ⁻²
75	3	6.08 x 10 ⁻²

The 75°C value for C₀ is the least accurate because of the shorter drop times. As noted above, the temperature correction for C₀ is negligible at these temperatures. If C₀ = 6.3 x 10⁻² at room temperature and one atmosphere is used to calculate viscosities, values are obtained which are high by 0.3% at 21.7°C, low by 1.5% at 31°C and high by 3.7% at 75°C, as compared to the data of reference 14. These errors are comparable to those of Bridgman, (Ref. 15) assuming that the data of reference 14 are the more accurate). Bridgman's data are given in the form of relative viscosities, taking the 0°C data as 1.00. If the handbook data are similarly expressed, the following results are obtained:

Relative Viscosities (1.0 Atmosphere) of Water

<u>Temp. (°C)</u>	<u>Handbook (14)</u>	<u>Bridgman (15)</u>	<u>% Difference</u>
0	1.000	1.000	0
10.3	0.7236	0.779	+7.6%
30.	0.4468	0.488	+9.2%
75.	0.2120	0.222	+4.7%

However, if the data are shifted to match at some intermediate temperature, then the difference would be about + 4.5%. Bridgman notes that he had considerable difficulty with water because the technique used to measure drop time was affected by the conductivity of the water. The technique used in the present work did not have this problem.

Measurements were next made at a pressure of 101 MPa (15,000 psi). The results, compared to Bridgman's data, were as follows:

% Change in Viscosity Due to 101 MPa (15,000 psi) Pressure (Water)

<u>Temperature (°C)</u>	<u>Present Work</u>	<u>Bridgman</u>
10.3	-	-4.6%
21.7	+ 0.3%	-
30.	+ 6.6%	+5.3%
75.	+ 6.5%	+7.7%

Note that Bridgman's data (and some earlier data he references) show a decrease in viscosity at this pressure at low temperatures and an increase at higher temperatures. From his data we expected to see very little change due to pressure at room temperature and this proved to be the case. At 30°C and 75°C the change due to pressure is comparable to that reported by Bridgman. In view of the above it was concluded that operation of the viscometer was satisfactory.

Efforts to measure the viscosity of 277 pitch were frustrated owing to the method of heating the tube (resistance winding) and difficulties in maintaining a sliding friction seal. With the higher temperatures required for measurements on pitch the gradient became severe although several attempts were made to gain experience. In all cases, the needle became stuck between the coils, necessitating redesign of the system. It should be noted that, with the same diameter tube and needle, recalibration was not required.

The improved viscometer design shown in Figure 44 consisted of a shorter tube with a bellows pressurizing system instead of the mechanical friction seals. The latter had proved troublesome because of a tendency for scoring and etching on the inner wall of the viscometer tube. High temperature coils were fabricated for measuring time of fall and the entire assembly was located in a radiant heated oven to permit thermal equilibrium to be achieved over the entire length of the tube.

4.1 MEASUREMENTS ON PHENANTHRENE AND NAPHTHALENE

Having demonstrated that the viscometer calibration held over a wide range of viscosities (e.g., water at 1.0 cp to castor oil at 990 cp) and that the change in the viscosity of water with pressure was in good agreement with Bridgman's data, measurements were made on phenanthrene.

Phenanthrene has a melting point of 101°C and a boiling point of 340°C. It was therefore decided to conduct measurements in the range of 120°C to 300°C. In conducting measurements at about 120°C, it was found that phenanthrene could be frozen by pressure. As Bridgman noted, freezing is readily detected by failure of the needle to fall. Therefore a series of measurements was made at 120°C to establish the freezing pressure.

It should be noted at this point that while the temperature in the body of the viscometer was uniform, the electromagnet used to raise the needle was located just outside the oven as was the needle. Thus the molten material at the top of the viscometer tube was about 30°C lower in temperature than in the center section of the tube (i.e., the measurement region). Thus it was possible to freeze the material at the top of the tube (preventing the needle from falling) at slightly lower pressure than in the center.

In conducting this series of pressure freezing experiments, it was noted that if the material was frozen and pressure was released to cause melting, the melting resulted in a drop in temperature in the main body tube (due to heat of fusion). Similarly, freezing by pressure increase caused a rise in temperature. This, of course, complicated fixing the freezing point since an increase in pressure sufficient to start freezing would result in a temperature rise that would favor melting. As a result, the freezing (or melting) point was not sharp. On several occasions it was noted that the velocity of the needle varied between the upper and lower pick-up coils. That is, if freezing

was in progress, the velocity through the lower coils would be slower, whereas the opposite was the case if melting was in progress. In this series of experiments at 120°C there appeared to be liquid at pressures as high as 10,500 psi and solid at pressures as low as 10,100 psi and it was concluded that the freezing pressure of phenanthrene at 120°C is about 10,300 psi.

The temperature changes on freezing (or melting) referred to above were on the order of 1.0 to 4.0°C. This was measured on the outside of the stainless steel viscometer tube and it is certain that the changes within the test material were much larger. It would not be difficult to locate a thermocouple within the liquid if a more accurate measurement were desired.

The results of the measurements on phenanthrene are given in Table 13. Although the density of phenanthrene as a function of temperature (at 1.0 atmosphere) had been measured no data on density as a function of pressure were available. Thus only drop times are listed in Table 13 and Figure 45. Since viscosity is proportional to drop time if other factors are constant, the drop times can be considered as relative viscosities if the changes in liquid density with pressure and temperature are small. Thus, the viscosity of liquid phenanthrene increases by a factor of about two between 0.5 and 101 MPa.

At the conclusion of this series of measurements it was discovered that the flexible diaphragm separating the test material and the hydraulic oil had ruptured and it is probable that the phenanthrene was contaminated by oil at the higher temperatures. This led to a change in the design of the diaphragm, but due to the pressure of time it was decided to examine naphthalene rather than to repeat the higher temperature measurements on phenanthrene.

Naphthalene is a smaller molecule than phenanthrene (2 fused rings instead of 3), has a melting point of 80.5°C and a boiling point of 218°C. It was

decided to make measurements in the 90°C to 180°C region. Care was taken not to get too close to the boiling point in any of these measurements in order to prevent boiling and an excessive pressure buildup which could cause equipment damage and delay data acquisition.

Through the prior experience with phenanthrene, freezing of naphthalene at elevated pressure was anticipated and it was possible to obtain a fairly good temperature-pressure freezing curve. This is shown in Figure 46. With the pressures available, freezing could be obtained at temperatures up to 112°C. Also because of the experience with phenanthrene, care was taken to note the sequence of the measurements rather than simply entering the results in a table. It was hoped that this would enable us to note any anomalies that might indicate problems with the diaphragm. The results are in excellent agreement with published data (16).

The results of the measurements on naphthalene are given in Table 14 and Figure 47. It will be noted that at Run #18 the temperature was dropped back to about 90°C and the fall time at 15 psi was measured. This appeared to be in good agreement with the first data and suggested that no diaphragm rupture had occurred. The measurements were continued and at run #33 a second check was made.

The experimental results shown in Table 14 in terms of drop time can be corrected for the effects of temperature and pressure on the density of naphthalene, since there are no published values. The correction for temperature is made through the bulk expansion coefficient

$$\beta = \frac{.04314}{(T_c - T)^{0.64T}}$$

where T_c is the critical temperature of naphthalene, 747.8K (17). Pressure has the opposite effect but to a lesser degree, amounting to only about 0.04 gm/cm³ at 101 MPa (18). Differences between viscosities calculated

from Equation (6) using the uncorrected density value of 0.9625 gm/cm³ (19) and those corrected for both temperature and pressure at measurement conditions are at most around 1.2% at 0.1 MPa and 0.6% at 101 MPa. These are also listed in Table 14. Thus the use of drop time and uncorrected density values over narrow temperature ranges appears to be satisfactory for most purposes, i.e.

$$\eta_{P_2} = \eta_{P_1} \left(\frac{t_2}{t_1} \right) \quad \text{where}$$

t is drop time and the subscripts 1, 2 relate to higher and lower pressures. Figure 48 shows these results compared to some published (20) and estimated values (21).

Although Run #33 in Table 14 does not appear to be significantly out of line, the drop time appeared to be a little long and it was expected that any oil contamination would result in a high viscosity. Therefore the apparatus was taken apart and it was found that the diaphragm had indeed ruptured and oil had contaminated the naphthalene. Again it is believed that this occurred at the higher temperatures.

As with phenanthrene, time did not permit rechecking of data. A sample of pitch was made available for test and it was decided that this had priority. Extensive changes were made in the diaphragm assembly and it appears that the rupture problem had been solved.

4.2 MEASUREMENTS ON ALLIED 277-15V PITCH

Several early efforts to measure the viscosity of 15V pitch at one atmosphere pressure failed as the needle would not fall. It was believed that because of the high "Z" (Z = 0.83) necessary for reliable measurements, the particulates in the pitch were causing the needle to bind as the clearance between the needle and tube wall was very small. A means was sought to remove the larger particulates and several pyrex tubes 1 m. long were filled with pitch

and held at 250°C for 5-7 days to permit the larger particles to sink to the bottom. The lower ends of the tubes were then cut off and the remaining material used to fill the viscometer.

The first attempts at measurement were made at 250°C but with no success. The needle appeared to be stuck somewhere in the tube and initially it was believed to be at the top. In an attempt to break it loose, the pressure was varied several times between 15 and 15000 psi. In this it was noted that a temperature change, indicating freezing, occurred at about 7200 psi. Therefore the temperature was increased to 325°C, but again with no success. Again pressure was varied and it appeared freezing occurred about 7800 psi. As subsequent tests show, it is probable that some components of the pitch freeze at these pressures, but the pitch as a whole does not.

After these unsuccessful attempts at measurement, the viscometer was cooled to room temperature and radiographed. The radiographs located the needle in the bottom of the tube as shown in Figure 49. The viscometer was again heated to about 325°C and attempts were made to raise the needle. It was found that it could be lifted through the lower pick-up coils but it would then break loose from the electromagnet and fall to the bottom of the tube. It became apparent at this point that some particulate matter must be stuck to the body tube wall in the region between the upper and lower detection (pick-up) coils.

To break this particulate matter loose, the magnetic pull of the electromagnet was increased several fold. This was eventually successful and the needle was raised and successfully dropped. On the second drop the needle stuck again between the pickup coils, but after being moved through the region several times with the electromagnet, the tube appeared to have been cleared and several satisfactory determinations were made.

The results of these measurements are given in Table 15 and Figure 50.

A minimum pressure of 200 to 500 psi was maintained at all times to suppress the tendency of the pitch to generate volatiles, preventing the needle from dropping.

Using the expansion data for pitch given in Ref. 10, density can be corrected for temperature and the results used to compute viscosity values from the experimental drop times and equation 6. These results are also given in Table 15. The value for viscosity at 609K, the highest temperature used, is about 2.5% higher than if no correction had been applied, i.e., if a density value of 1.290 g/cm³ (150C) had been used. The pressure correction is probably somewhat less, so that the viscosity values in Table 15 are probably within about one to two percent of a true value for this particular pitch.

Since viscosity measurements on 277-15 pitch made at the highest temperature (608K) in the first series appeared to indicate an increase in the time of the needle in the field of the lower coil, a series of measurements was made at a slightly higher temperature (628K) over a period of time. The data are given in Table 16 and show a small but progressive increase in drop time with time at temperature. Plotting these data to emphasize the rate of increase in Figure 51 (Left) suggests that the slope is not linear and that therefore a cumulative molecular change is occurring at this temperature which is somewhat lower than that at which many mesophase formation studies are performed. Plotted as in Figure 51 (Right) however over the entire temperature range in which measurements were made, the increase with time may seem insignificant with respect to the anticipated scatter, particularly in view of the times required to raise the needle, during which the temperature necessarily decreased in order to operate the electromagnet manually. Nevertheless, the trend with time is unmistakable and probably indicates that polymerization reactions are occurring, or that the quinoline insolubles in the pitch originally are growing.

5.0 DISCUSSION

5.1 PYROLYSIS UNDER PRESSURE

As has been observed by others (22-24), pyrolysis of coal tar pitch at even relatively moderate pressures, e.g. up to about 6 MPa (900-1000 psi) results in increased char yields. The same effect was observed in this work, with some differences among the three pitches, KA, KB and 277 being noticeable from the data in Table 2 particularly at short times. Between two and four hours, the effect of pressure on the rate of QI formation is greatest for KA and KB, which contained little or no QI initially compared to 277. As has been pointed out (23), the principal effect of pressure is to reduce the loss of lower boiling components such as naphthalene and anthracene although the early stages of the polymerization reactions themselves can also be affected by pressure. Increases in condensation polymerization rates at elevated pressures are common (25) and have been ascribed to repression of molecular translational and rotational modes, with a resulting increase in entropy. For such reactions in which the molecular volume of the transition species, V^\ddagger , is less than the volumes of the uncombined species, an increase in rate is also predicted (26). The increase in rate would also reduce loss of low boiling components by condensation before they evaporate, particularly when a viscosity increase due to pressure reduces bubbling and percolation. Thus the observed increases in yield of QI species under pressure can be attributed to effects on both the chemistry and the physics of the system.

The appearance of mesophase droplets is repressed by pressure to some degree since growth of the polymer species in the absence of percolation and bubbling, would be due principally to chemical processes. As the molecular weight increase progresses, solubility of the polymer decreases and further growth would depend principally on reactions at the periphery of the droplet.

Opportunities for growth, through collision, in which surface energies are lowered and solubility further decreased, would be limited to contact with other large molecules as the heavier particles sink. The dense coagulated mesophase or mosaic domains observed in these experiments at 6 MPa are similar to those described in other pressure pyrolysis experiments (5), with little evidence of flow or shear deformation of the mesophase. At 0.3 MPa of course, results are similar to observations made by other investigators (27). The advantage of pyrolysis at pressures of the order of 100 MPa is probably the retention of the reacting liquid in the smallest crevices and cracks through the effect of pressure on viscosity, gas solubility and gas bubble size, rather than on further increased reaction rates or reduced loss of reacting species.

5.2 VISCOSITY MEASUREMENTS

The behavior of naphthalene and phenanthrene with respect to increase in viscosity at elevated pressure is not unusual, judging from the similarity to the extensive work of Bridgman (14). Ratios of drop times at 101 and 0.1 MPa and various temperatures range from 1.97 to 2.2 for naphthalene and 1.84 to 1.99 for phenanthrene and can be considered constant within experimental error. In the case of pitch, this ratio decreases with increasing temperature from 7.24 at 543K to 4.49 at 608K, suggesting significantly increased mobility and less resistance to deformation. The increase in viscosity of pitch with time at 101 MPa and 628K is an interesting phenomenon in that it may indicate the beginning of polymerization. Under the experimental conditions used it is not possible to state definitely if any outgassing had occurred, i.e. if any hydrogen had been released, indicative of reaction. It does open the possibility that viscosity and possibly sound velocity measurements might be of some value in studying polymerization at low temperatures. Measurement of

viscosity vs time at other pressures, higher as well as lower might enable one to isolate the effect of pressure alone on reaction rates. Initial work with simpler systems such as anthracene would be somewhat easier to interpret.

5.3 THERMAL CONDUCTIVITY

Thermal conductivity measurements on 277 pitch vs temperature as well as on partially pyrolyzed KA, KB and 277 pitches did not show extreme variations, except in cases where bubble formation was noted. The influence of outgassing, percolation and turbulence is probably more significant than molecular changes. The effect of pressure on thermal conductivity in a pyrolyzing system would probably be more due to repression of these phenomena, bringing the thermal conductivity of the system closer to values for the undisturbed specimen. The influence of pressure per se on thermal conductivity does not appear to be more than about 10-15% for naphthalene at around 460K using the generalized equation

$$\frac{k_2}{k_1} = \frac{\epsilon_2}{\epsilon_1}$$

in which ϵ_2 and ϵ_1 are conductivity factors based on the reduced temperature and pressure of the liquid in question (29).

Considering the turbulent environment of the pyrolysis reaction, it is questionable if knowledge of the thermal conductivity of the pitch, even corrected for temperature and pressure, would be of significant help in evaluating rates of heat transfer in transient processing situations. Useful empirical factors could perhaps be derived by measuring at room temperature, the thermal conductivities of specimens removed from quenched, partially pyrolyzed specimens and relating the data to porosity, solids, mesophase content, and location in the pyrolysis chamber. Where pyrolysis is occurring within a relatively dense body such as a porous graphite or fibrous preform, the heat transfer process would probably be dominated by the properties of the solid phase.

Empirical corrections would be relatively simple to make, with pressure exerting a minor effect.

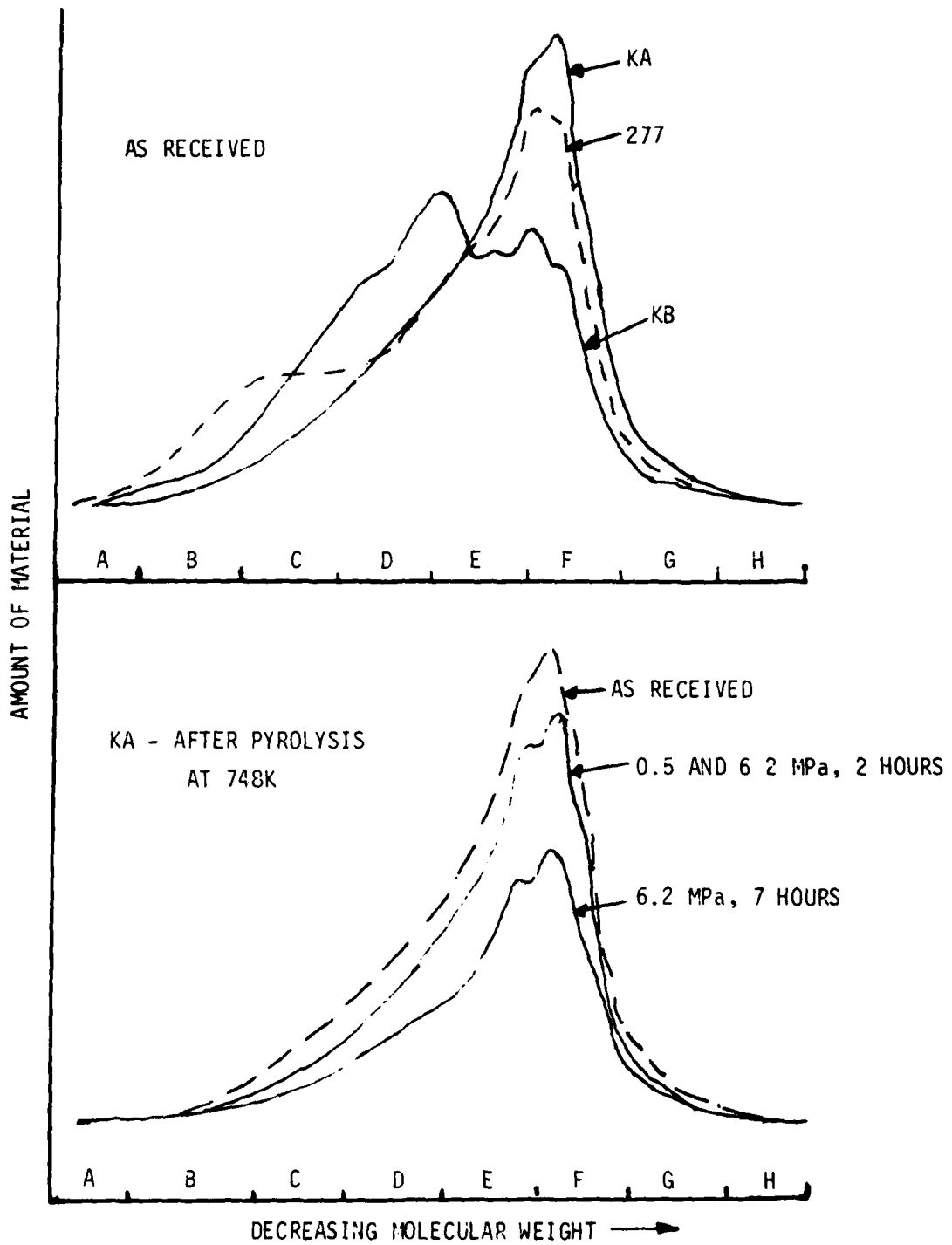


Figure 1. Gel Permeation Chromatograms of Three As-Received Pitches (Top) and Partially Pyrolyzed Koppers Type A (KA) Pitch (Bottom)

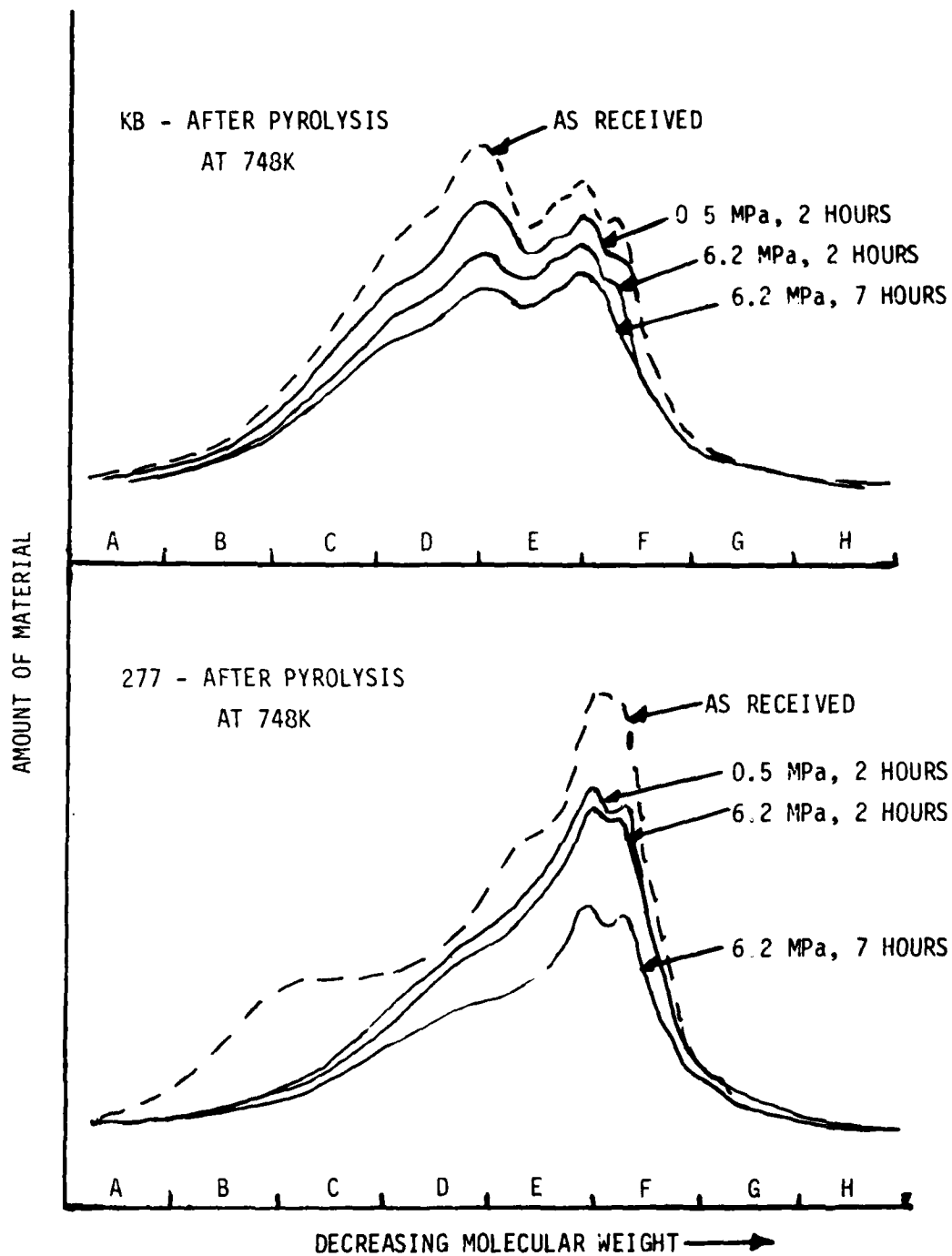


Figure 2. Gel Permeation Chromatograms of Partially Pyrolyzed Koppers Type B (KB) Pitch (Top) and Allied 277-15V Pitch (Bottom)



Figure 3. Koppers Pitch, Type A, After Pyrolysis at 748K for 2, 4 and 7 Hours at 6.2 MPa (Top) and 3.4 MPa (Bottom). 1.5X



Figure 4. Koppers Pitches After Pyrolysis at 748K for 2, 4 and 7 Hours. Top - A at 0.5 MPa, Bottom - Type B at 6.2 MPa. (1.5X)



Figure 5. Koppers Pitch, Type B, After Pyrolysis at 748K for 2, 4 and 7 Hours.
Top at 3.4 MPa, Bottom at 0.5 MPa. (1.5X)



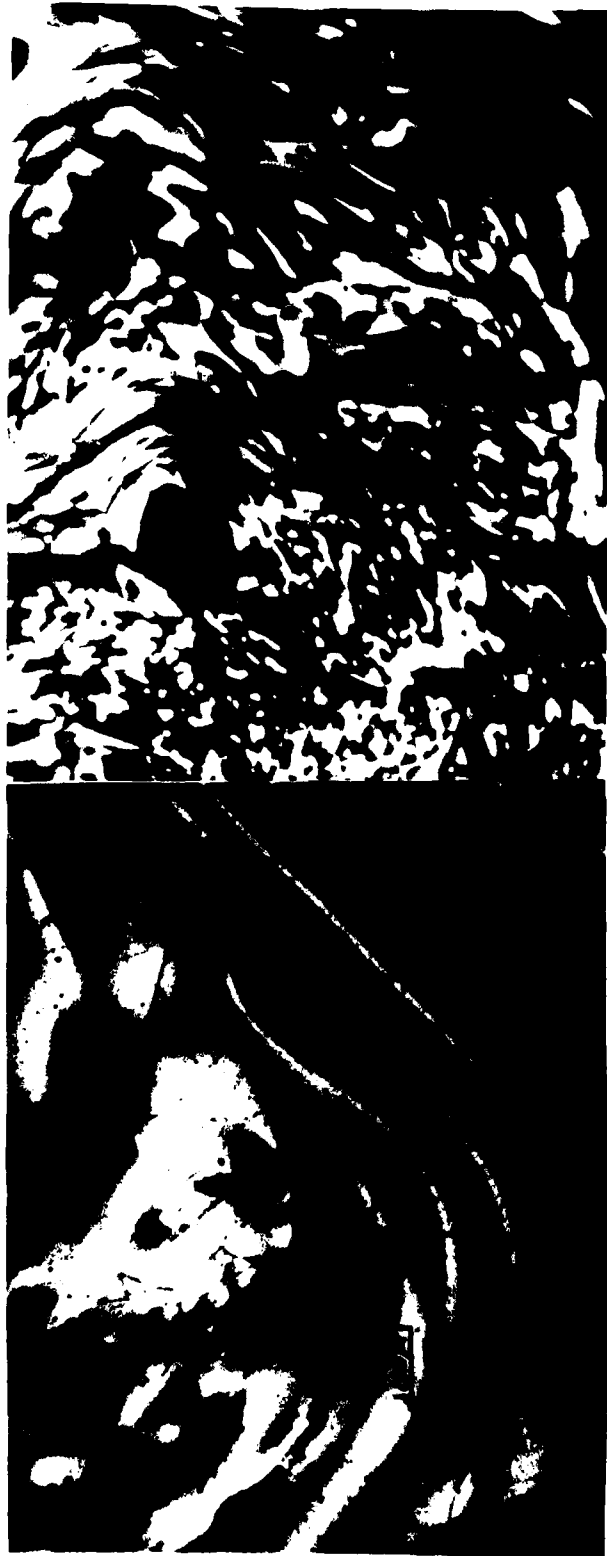
Figure 6. Allied 277 Pitch After Pyrolysis at 748K for 2, 4 and 7 Hours.
Top at 6.2 MPa, Bottom at 3.4 MPa. (1.5X)



Figure 7. Allied 277 Pitch After Pyrolysis at 748K for 2, 4 and 7 Hours at 0.5 MPa. (1.5X)



Figure 8. Coalesced Mesophase in Koppers Type A Pitch After Pyrolysis at 6.2 and 0.5 MPa, 7 Hours 748K Showing Effect of Pressure in Reducing Turbulence. (100X)



100 μm

Figure 9. Coalesced Mesophase in Koppers Type B Pitch After Pyrolysis for 7 Hours at 6.2 and 0.5 MPa, 748K (100X)



100 μm

200 μm

Figure 10. Coalesced Mesophase in Allied 277-15V Pitch After Pyrolysis at 6.2 and 0.5 MPa Showing Effect of Varying Turbulence. 100X, 50X.



200 μm

20 μm

Figure 11. Insoluble Particles Around Mesophase Droplets in Allied 277-15V Pitch. (500X, 50X)



Figure 12. Appearance of Immiscible Phase in Koppers Type B and Allied 277-15V Pitches, 50X.



Figure 13. Immiscible Phase in Coalesced Mesophase in Koppers Type B Pitch After Pyrolysis for 7 Hours at 6.2 and 0.5 MPa. (100X)



JAC/454

Figure 14. Immiscible Layers in Bubbles in Unconverted Pitch Regions. Type A Left and Center, 277 Right. 100X

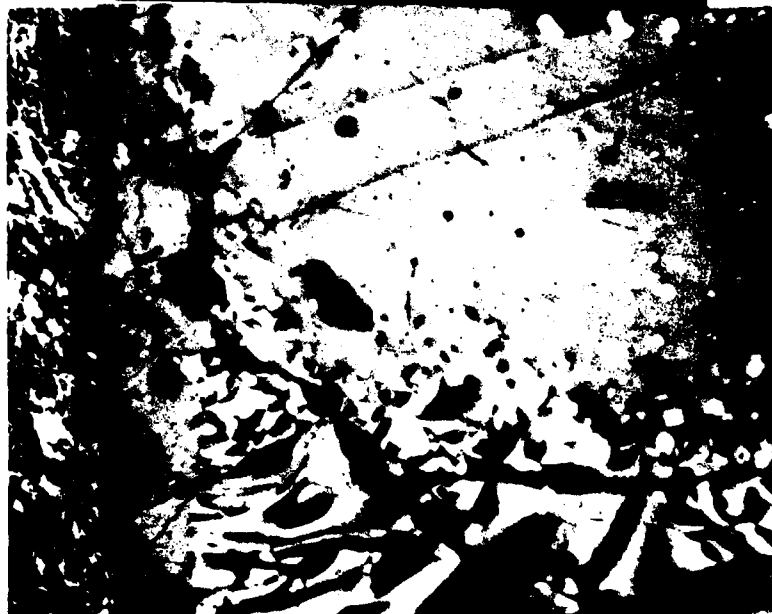


Figure 15. Connected Bubbles at Container Wall in Koppers Type A Pitch Pyrolyzed 7 Hours, 6.2 MPa (50X), Top; Large Mesophase Spheres Sinking to Interface of Unconverted and Coalesced Koppers Type B Pitch, During Pyrolysis at 6.2 MPa for 7 Hours (100X)

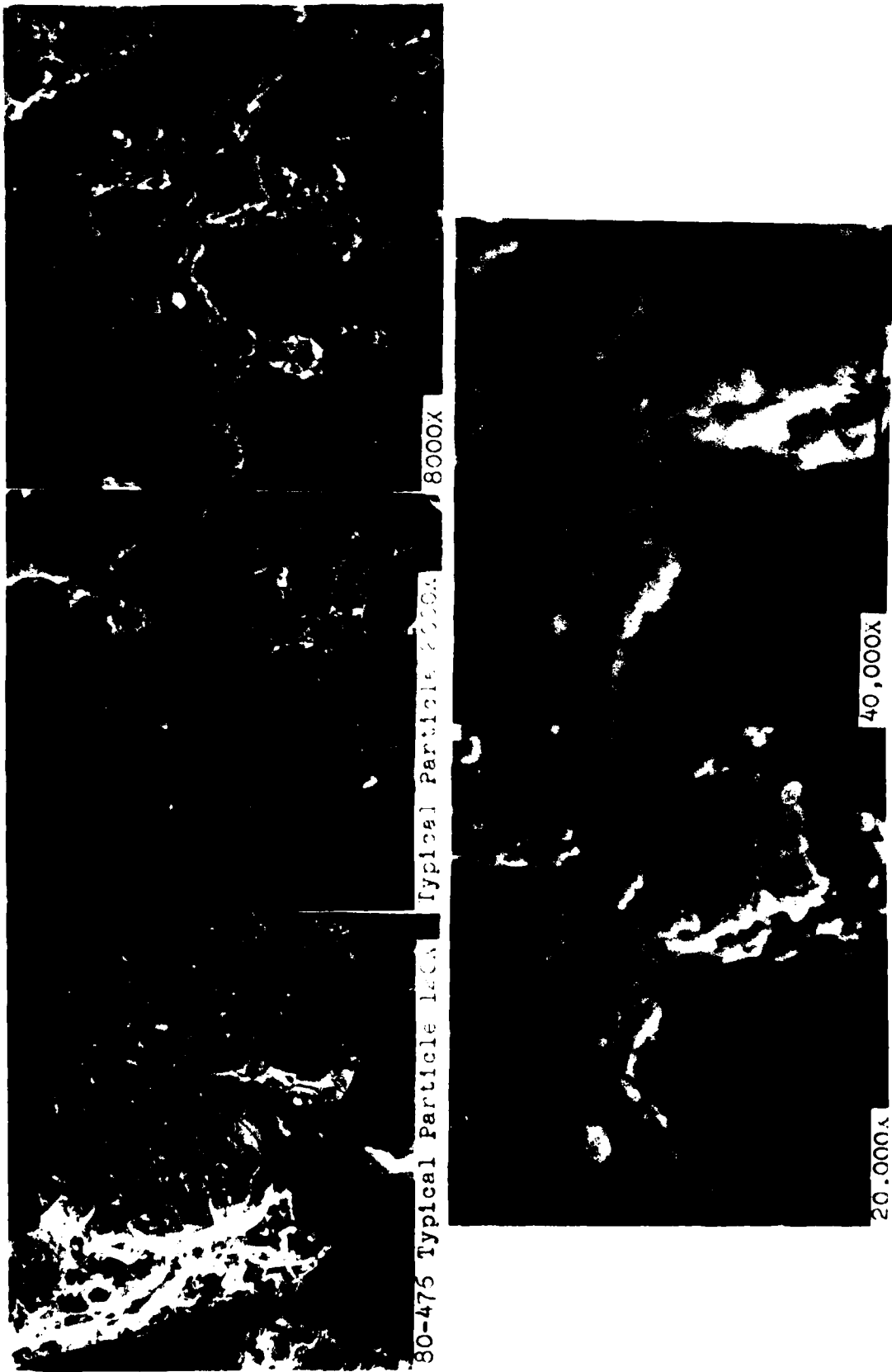
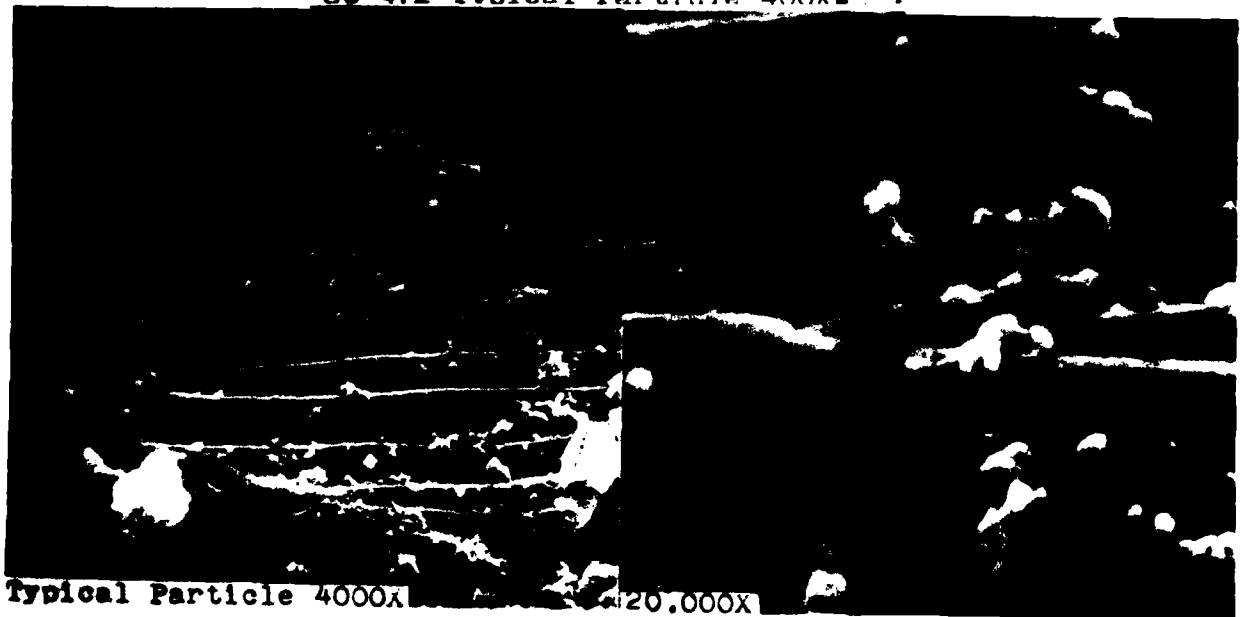


Figure 16. Surface Layers on Partially Pyrolyzed Koppers Type A Pitch - 3.4 MPa, 723K, 7 Hours



80-472 Typical Particle 400x



Typical Particle 4000x 20.000X

Figure 17. Surface Layers on Partially Pyrolyzed Koppers Type A Pitch - 6.2 MPa 748K, 7 Hours Showing Smooth Glassy-like Structure Beneath Surface Layer of Loose Particles.



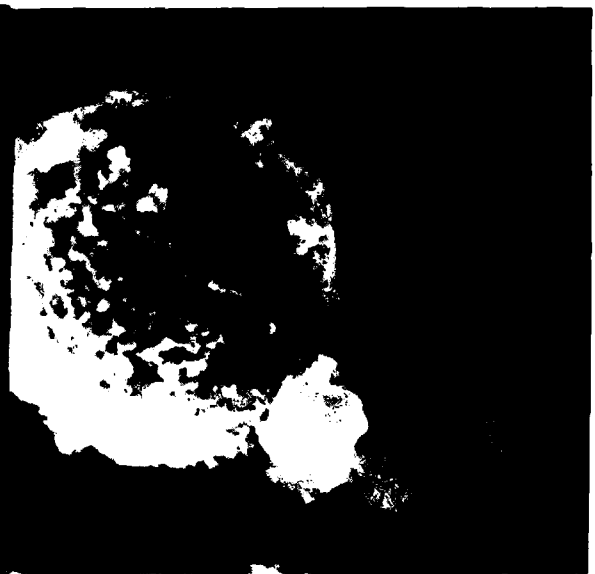
80-492 Possible Mesophase 2000X



Surface Detail of Mesophase 20,000



80-485 Typical Field 950X



80-485 Typical Field 2,400X

Figure 18. SEM Views of Larger Mesophase Droplets, Formed by Pyrolysis at 3.4 MPa, 7 Hours, 748K. Top Koppers Type A Exhibits Less Surface Debris Than 277-15 Pitch at Bottom.

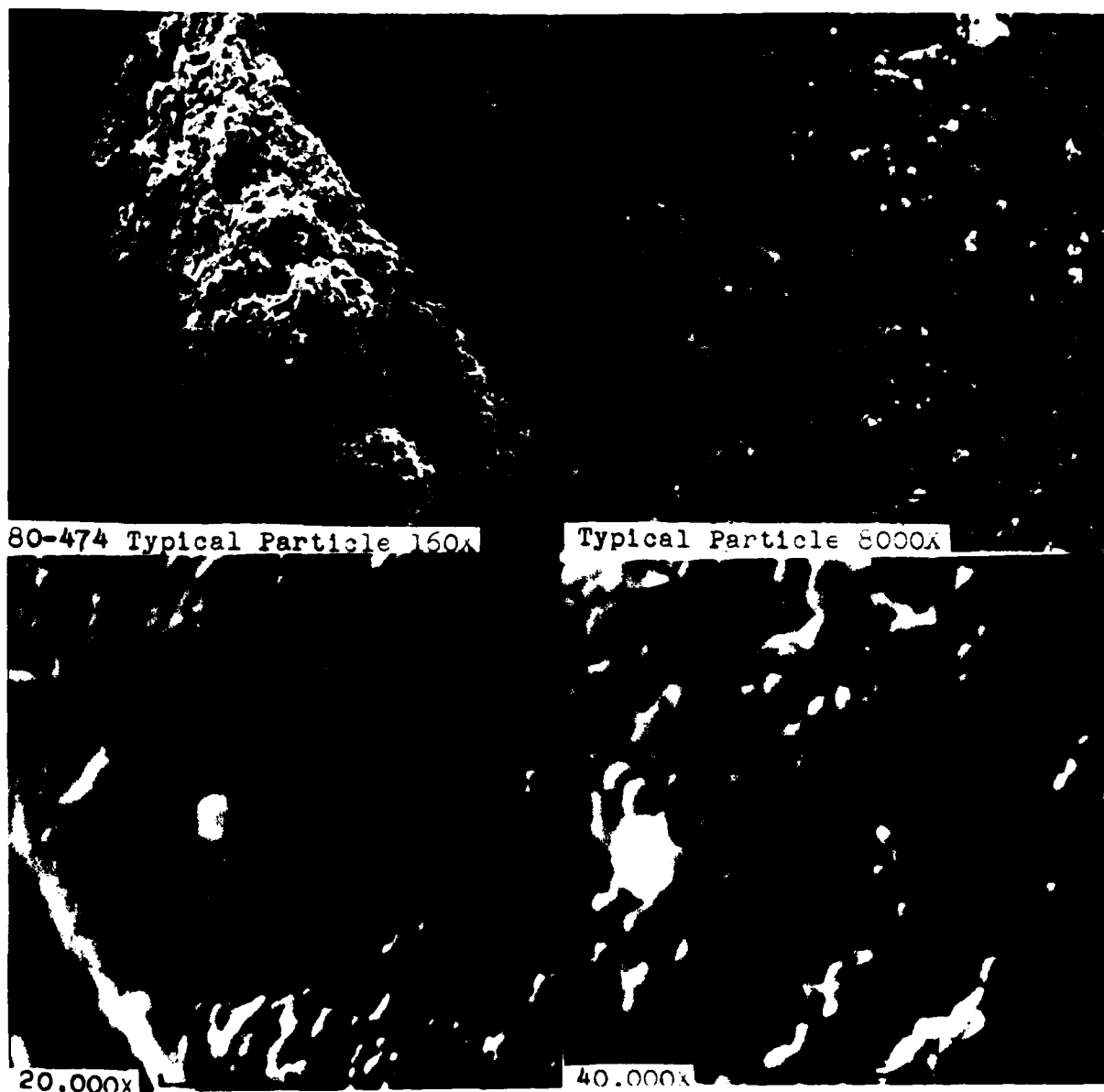
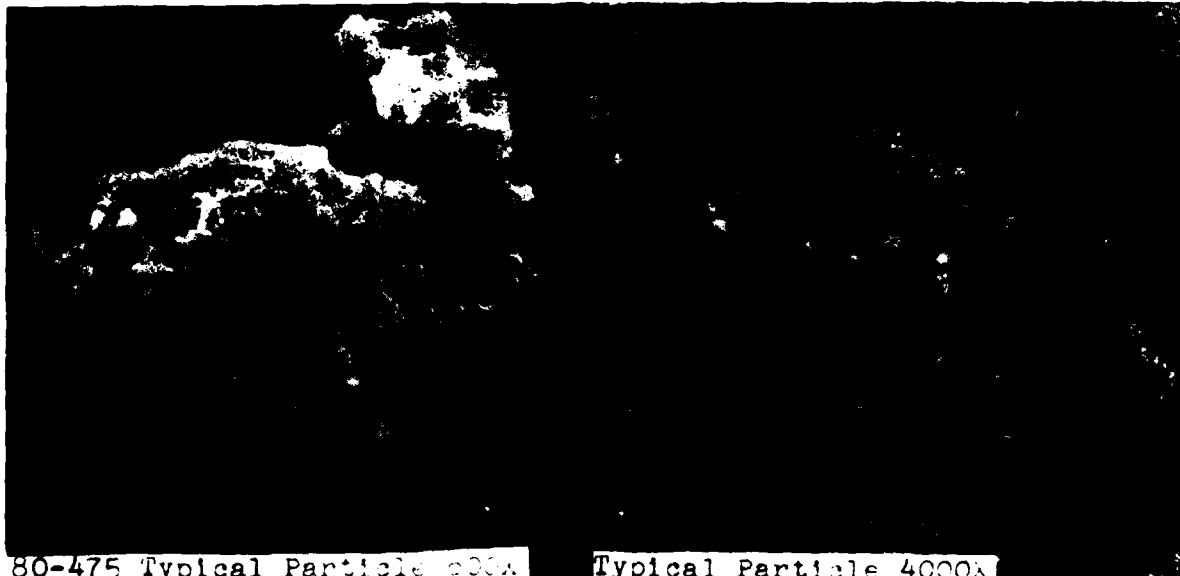


Figure 19. SEM Views of Koppers Type A Pitch After Pyrolysis for 2 Hours at 6.2 MPa and 748K - Note Small Spherical Particles on Particle Surface.



80-475 Typical Particle 2000x

Typical Particle 4000x



20,000x

Figure 20. SEM Views of Koppers Type A Pitch Pyrolyzed 7 Hours at 3.4 MPa and 748K.

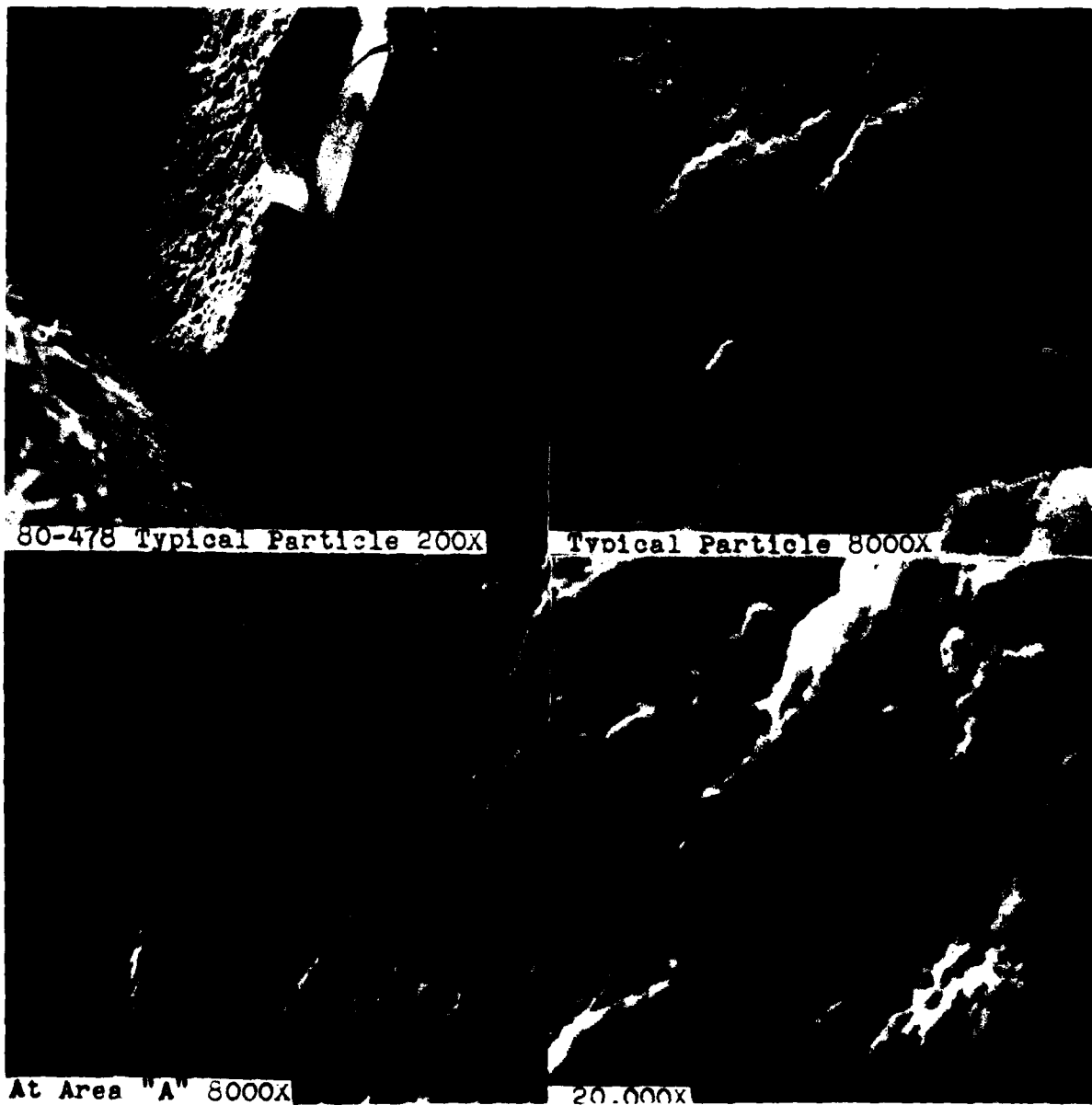


Figure 21. SEM Views of Koppers Type B Pitch After Pyrolysis for 4 Hours at 6.2 MPa and 748 - Fine Particles Appear to be More Coherent Than Those in Type A (Figure 19).

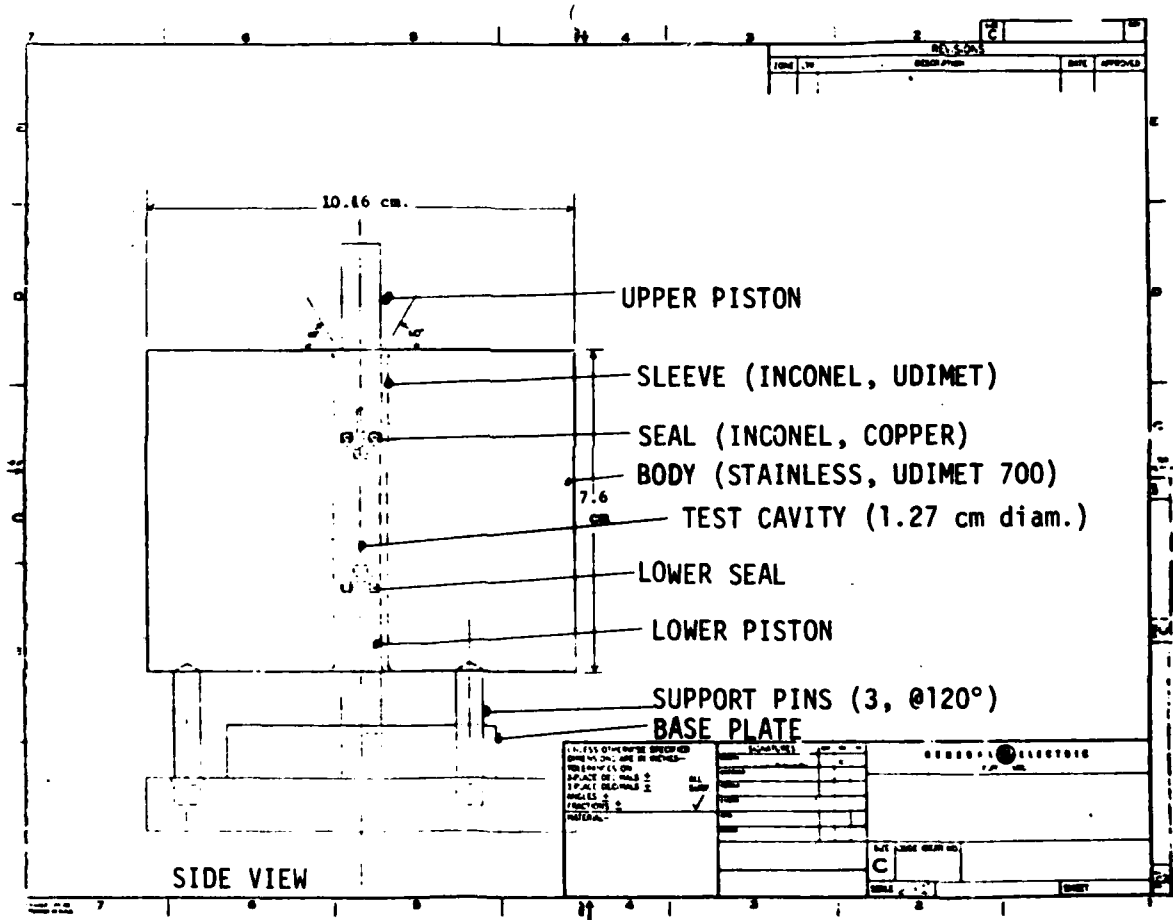


Figure 22. Schematic of High Pressure Sound Velocity Cell.

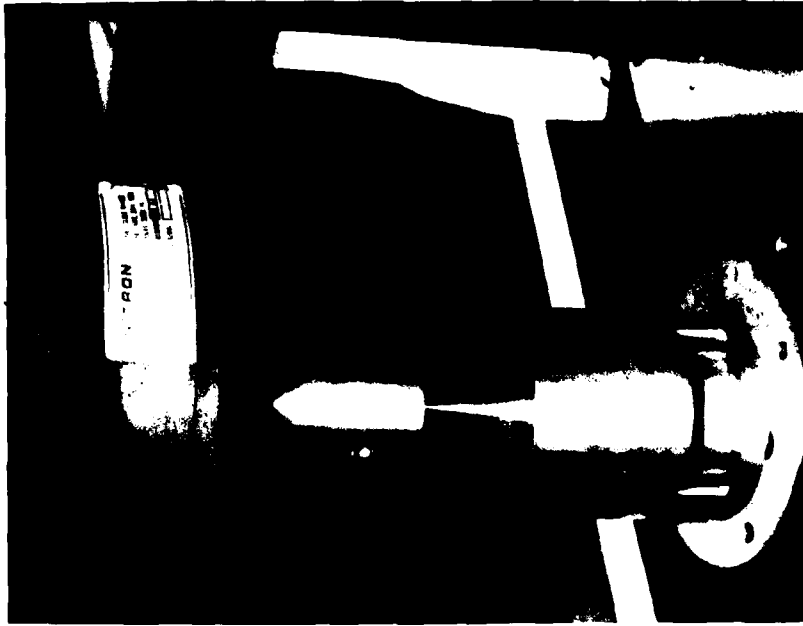


Figure 23. Exploded and Assembled Views of High Pressure Sound Velocity Cell.

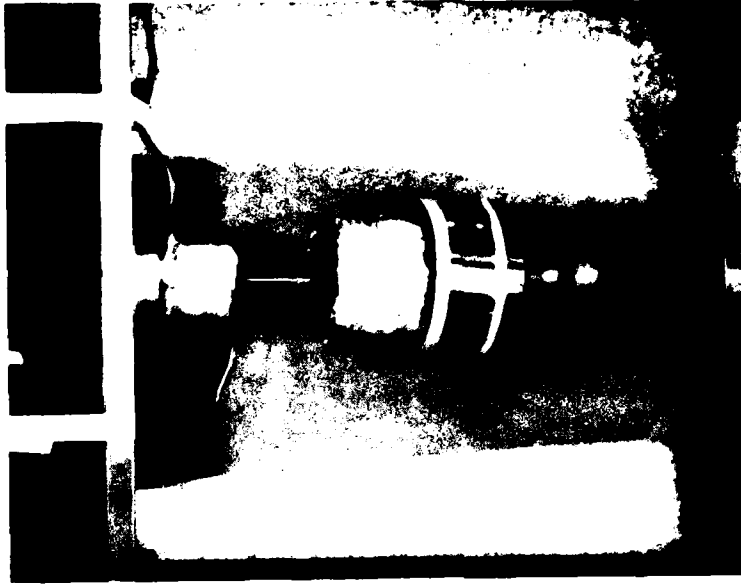
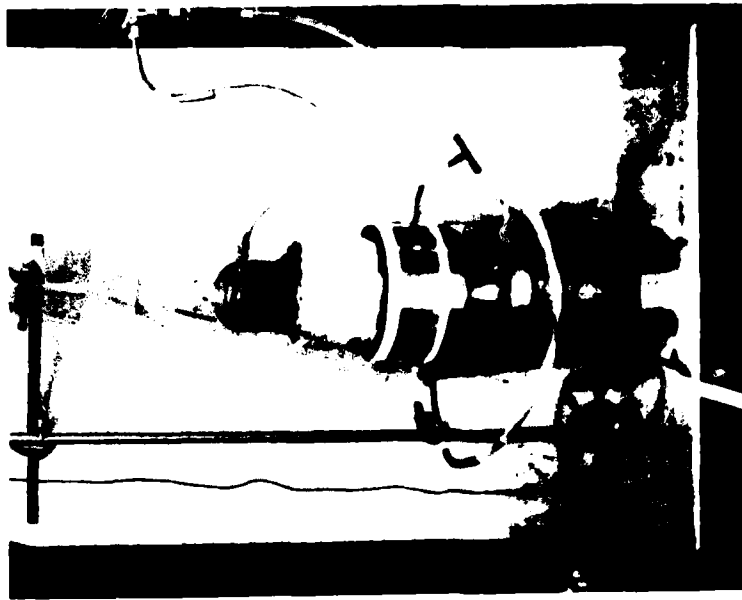


Figure 24. Operation of High Pressure Sound Velocity Cell.

Left: Loading Operation, Showing Vacuum-Inert Gas System for Preventing Oxidation.

Right: Cell in Position Between Load Cell and Platform. Cooling Line and Piezoelectric Crystal are Shown at Top.

Figure 25. Calibration Curve - Sound Velocity at 6.5 MHz in Water vs. Pressure at 303K (30°C). Solid Line from Data in Ref. 7.

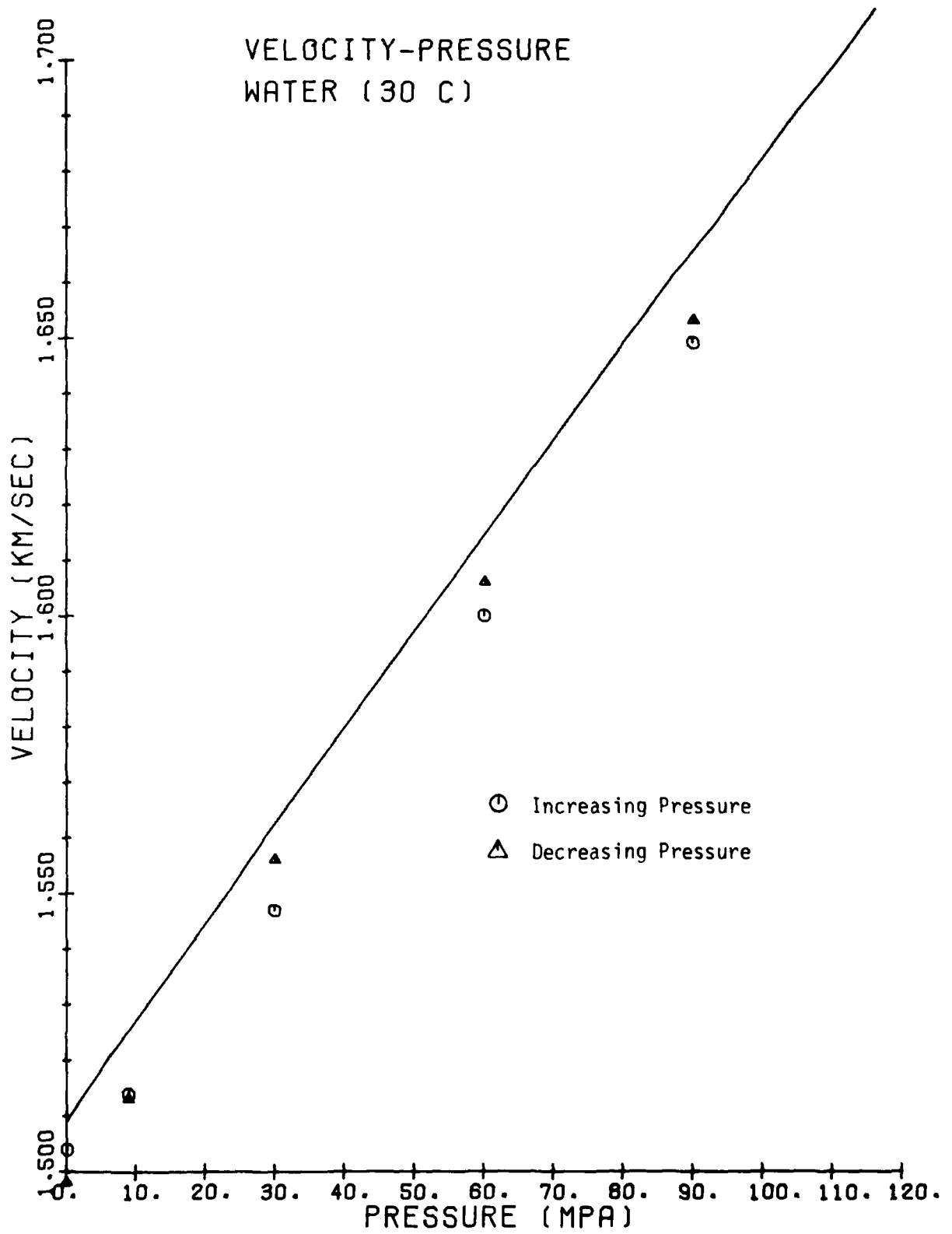


Figure 26. (Sound Velocity)³ at 6.5 MHz vs. Pressure in Phenanthrene at Various Temperatures.

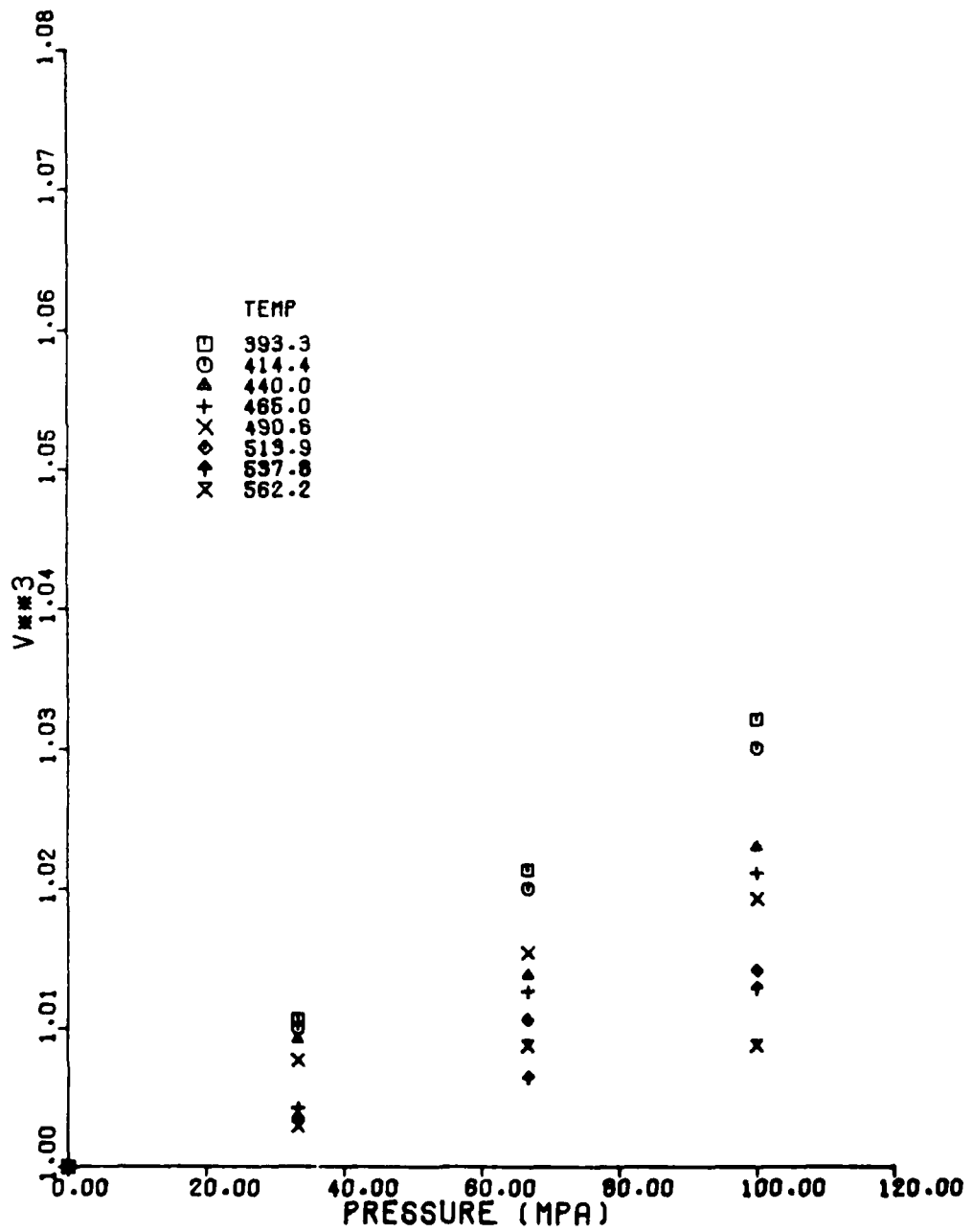


Figure 27. (Sound Velocity)³ at 6.5 MHz vs. Pressure in Phenanthrene at 393.3K (120°C).

TEMP= 393.3

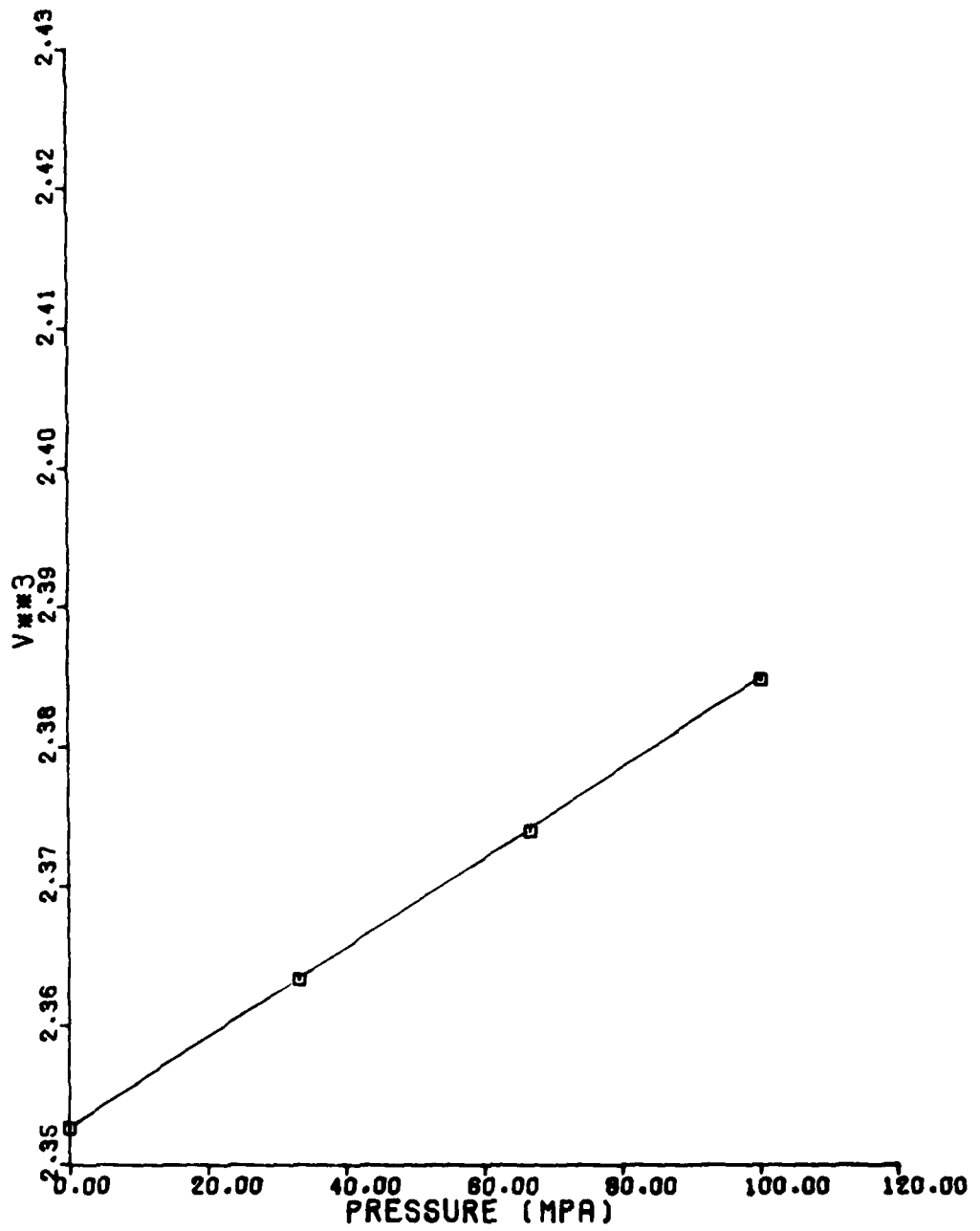


Figure 28. (Sound Velocity)³ at 6.5 MHz in Phenanthrene vs. Pressure at 414.4 K.

TEMP= 414.4

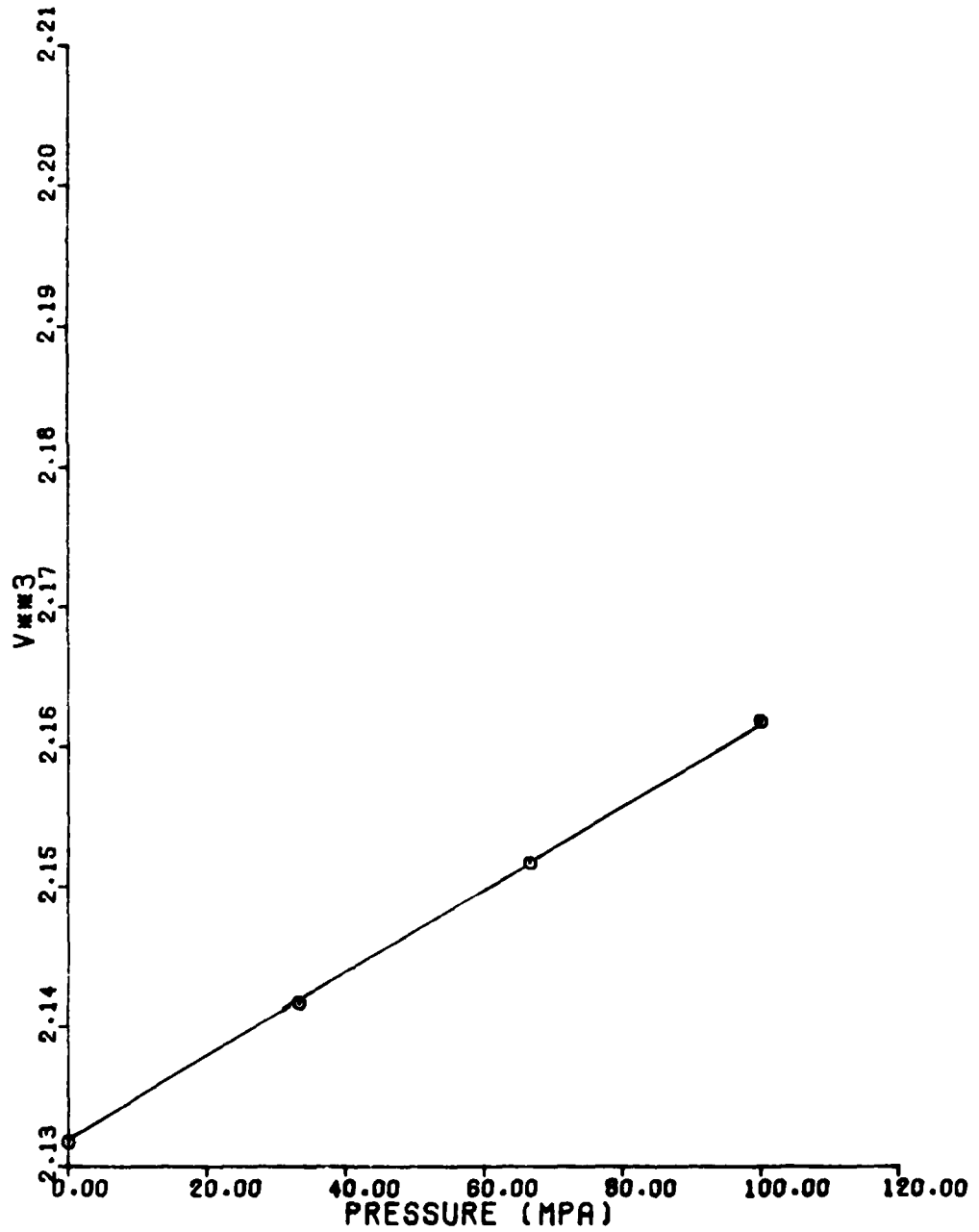


Figure 29. (Sound Velocity)³ at 6.5 MHz in Phenanthrene vs. Pressure at 440.0K.

TEMP= 440.0

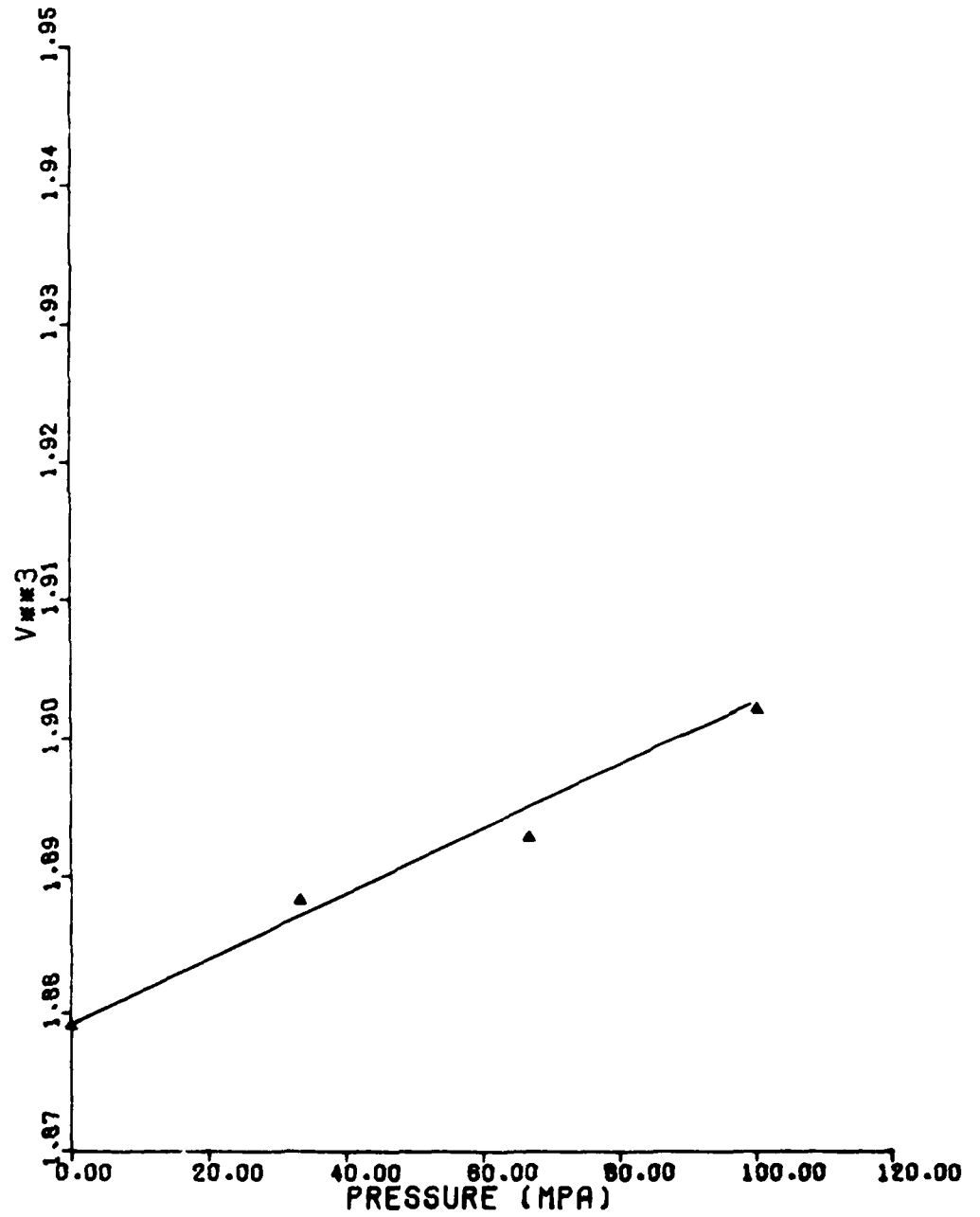


Figure 30. (Sound Velocity)³ at 6.5 MHz in Phenanthrene vs. Pressure at 465.0K.

TEMP= 465.0

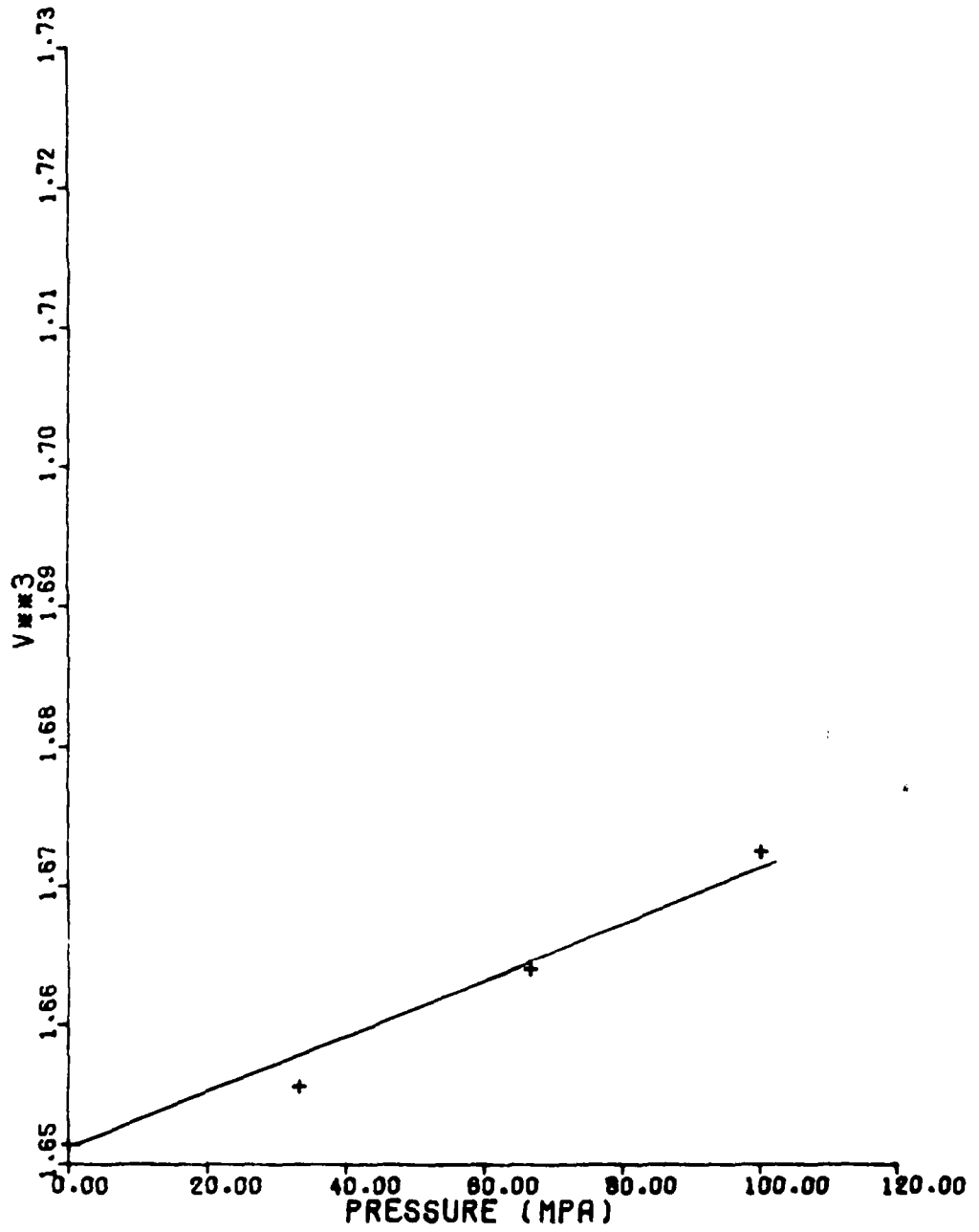


Figure 31. (Sound Velocity)³ at 6.5 MHz in Phenanthrene vs. Pressure at 490.6K.

TEMP = 490.6

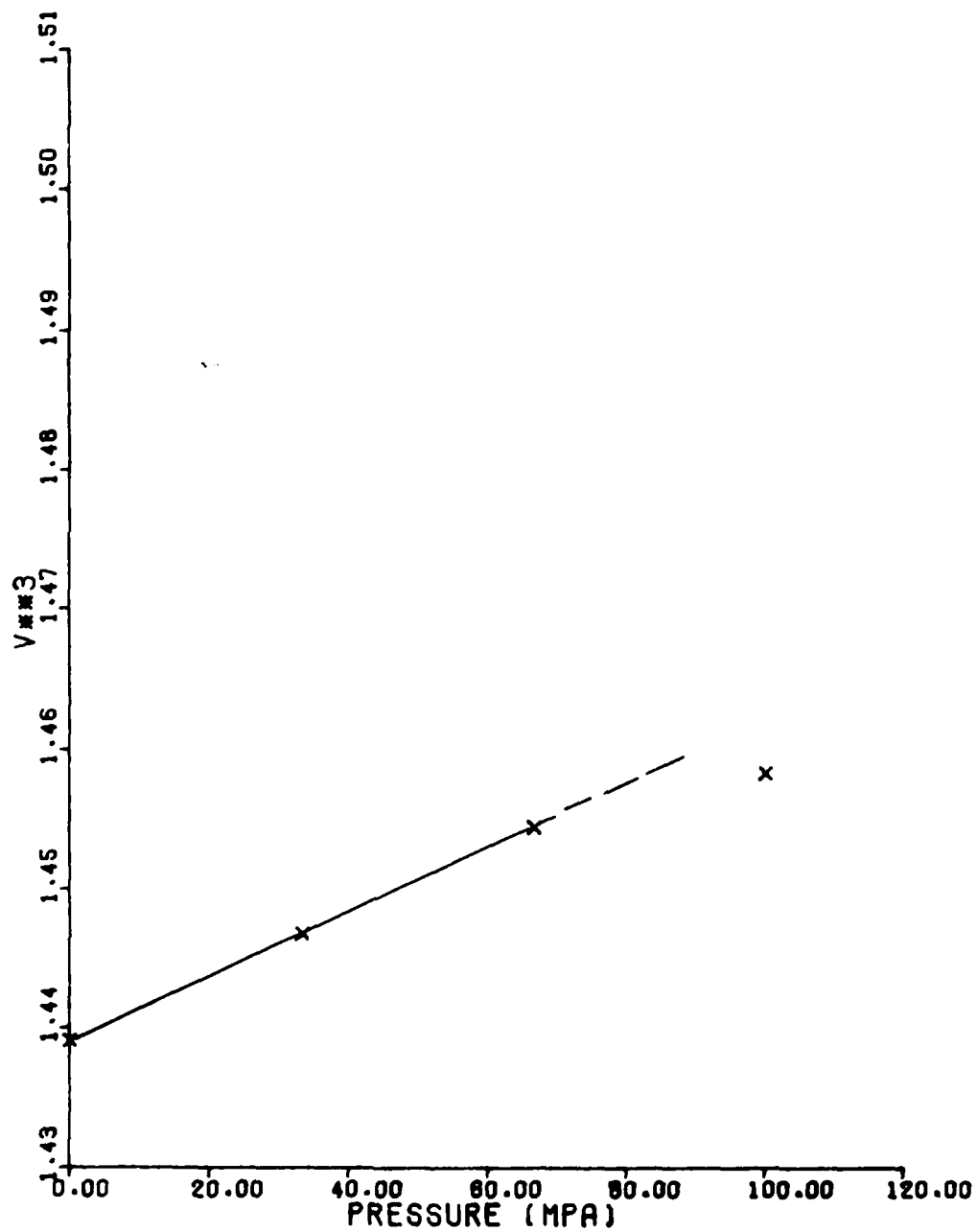


Figure 32 . (Sound Velocity)³ at 6.5 MHz in Phenanthrene vs. Pressure at 513.9K.

TEMP= 513.9

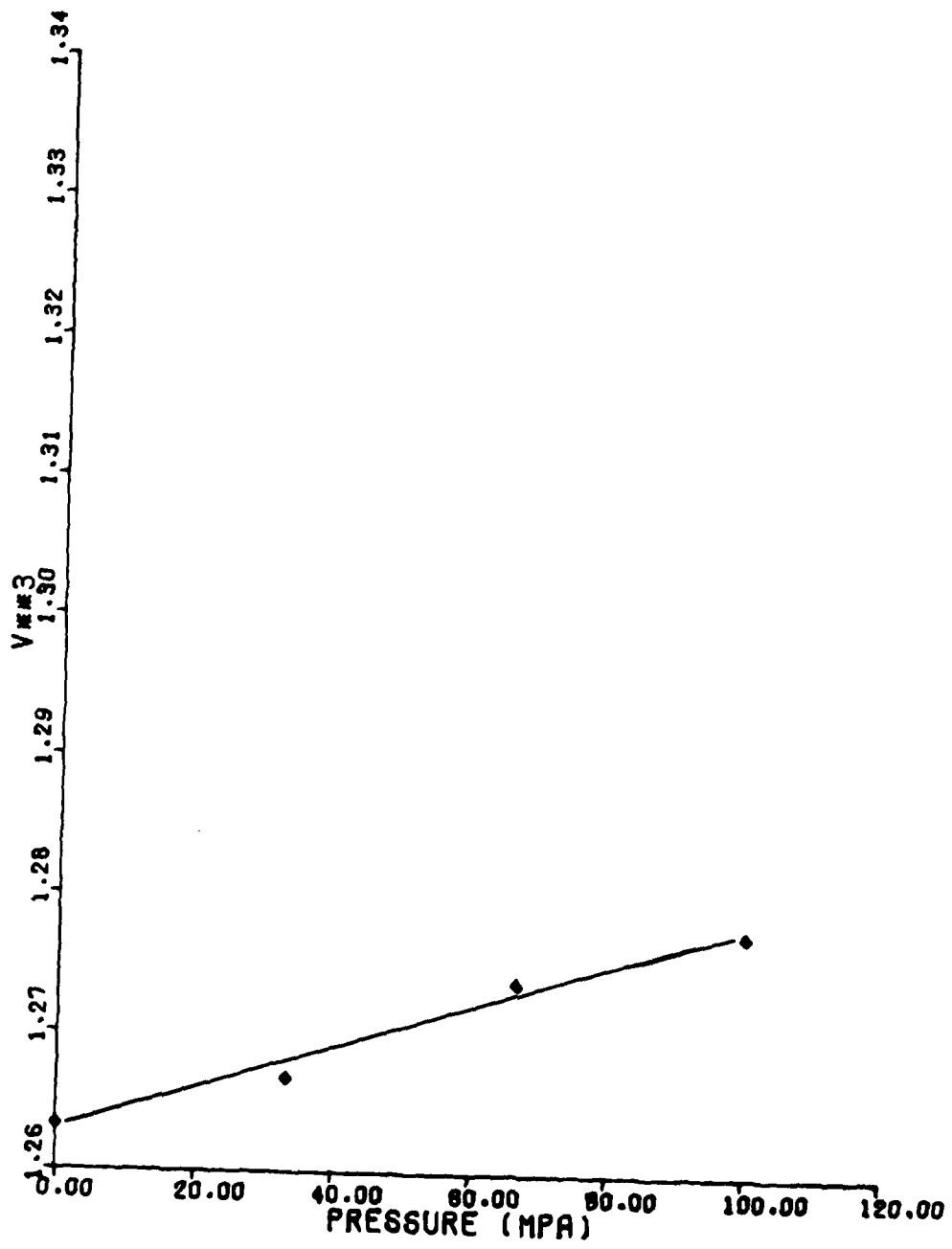


Figure 33. (Sound Velocity)³ at 6.5 MHz in Phenanthrene vs. Pressure at 537.8K.

TEMP = 537.8

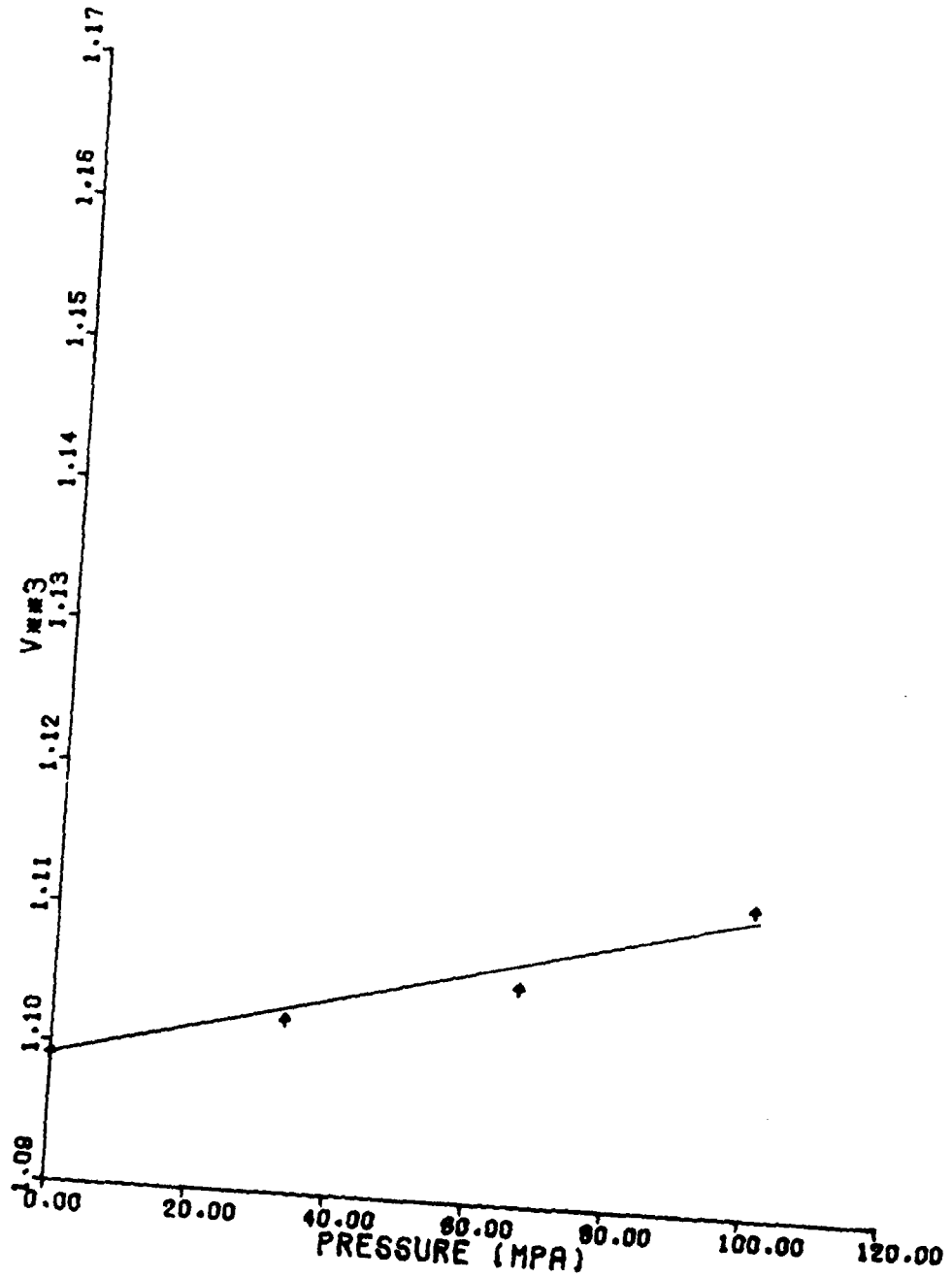


Figure 34. (Sound Velocity)³ at 6.5 MHz in Phenanthrene vs. Pressure at 562.2K.

TEMP= 562.2

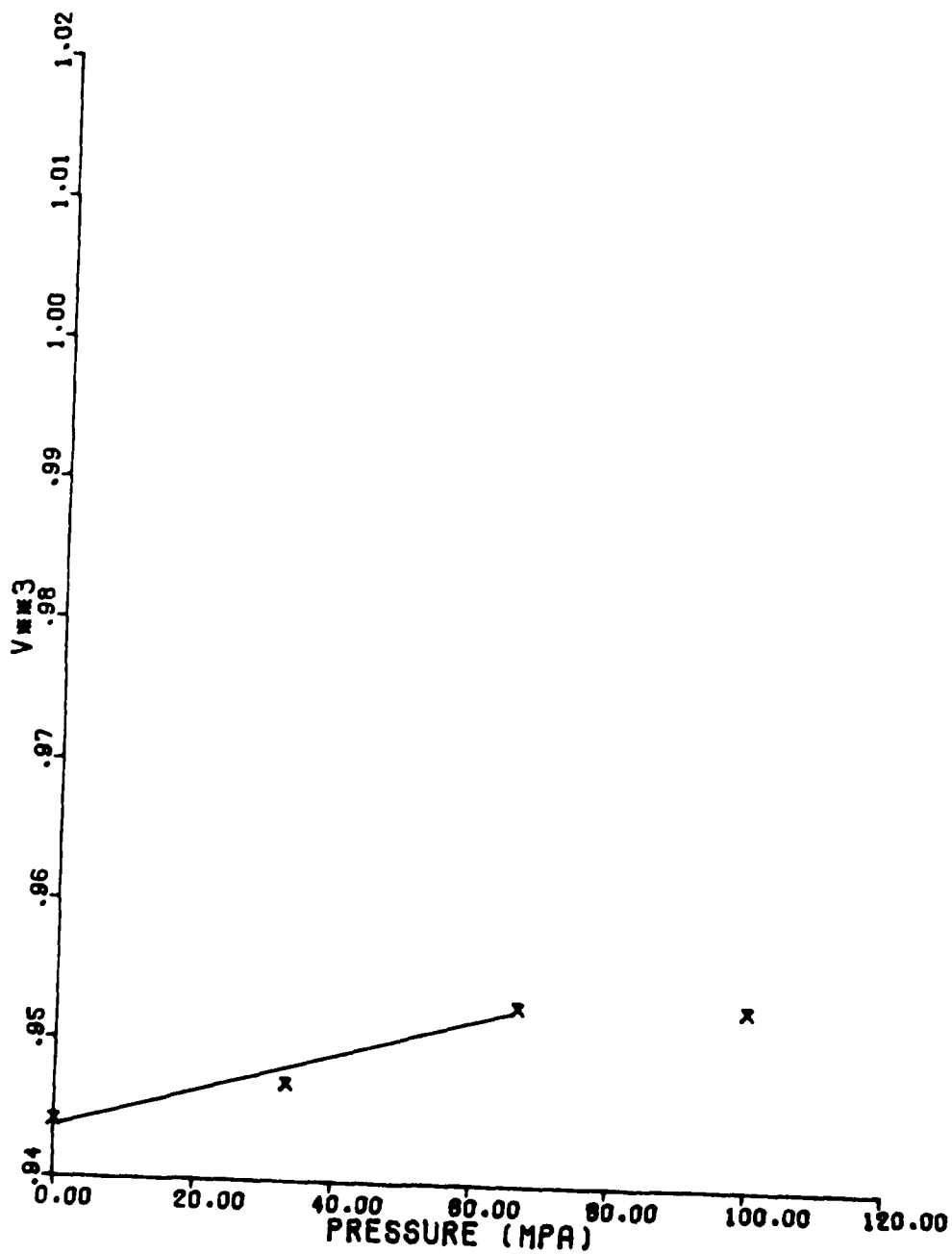


Figure 35. Sound Velocity in Phenanthrene and Allied 277 Pitch vs. Temperature

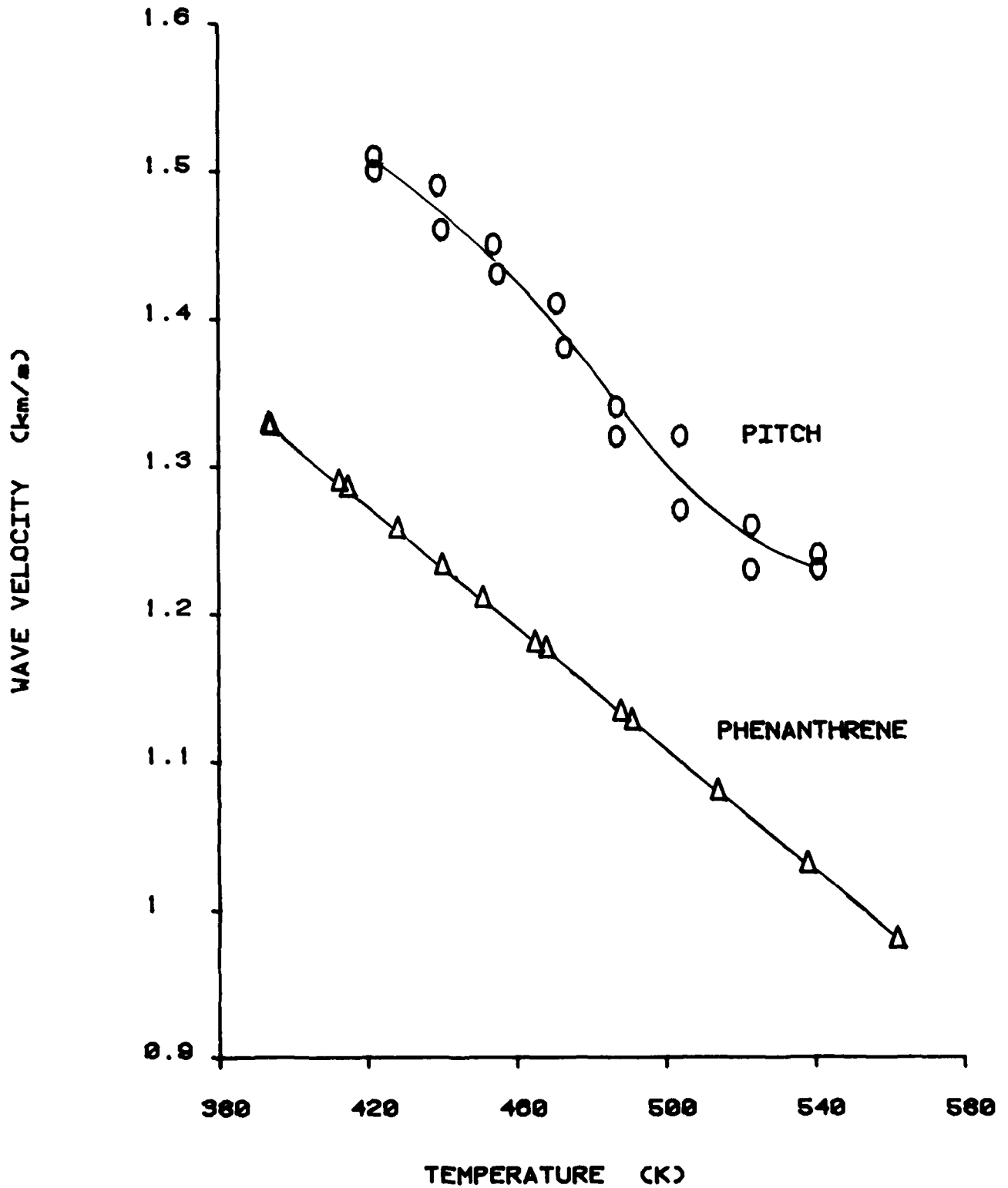
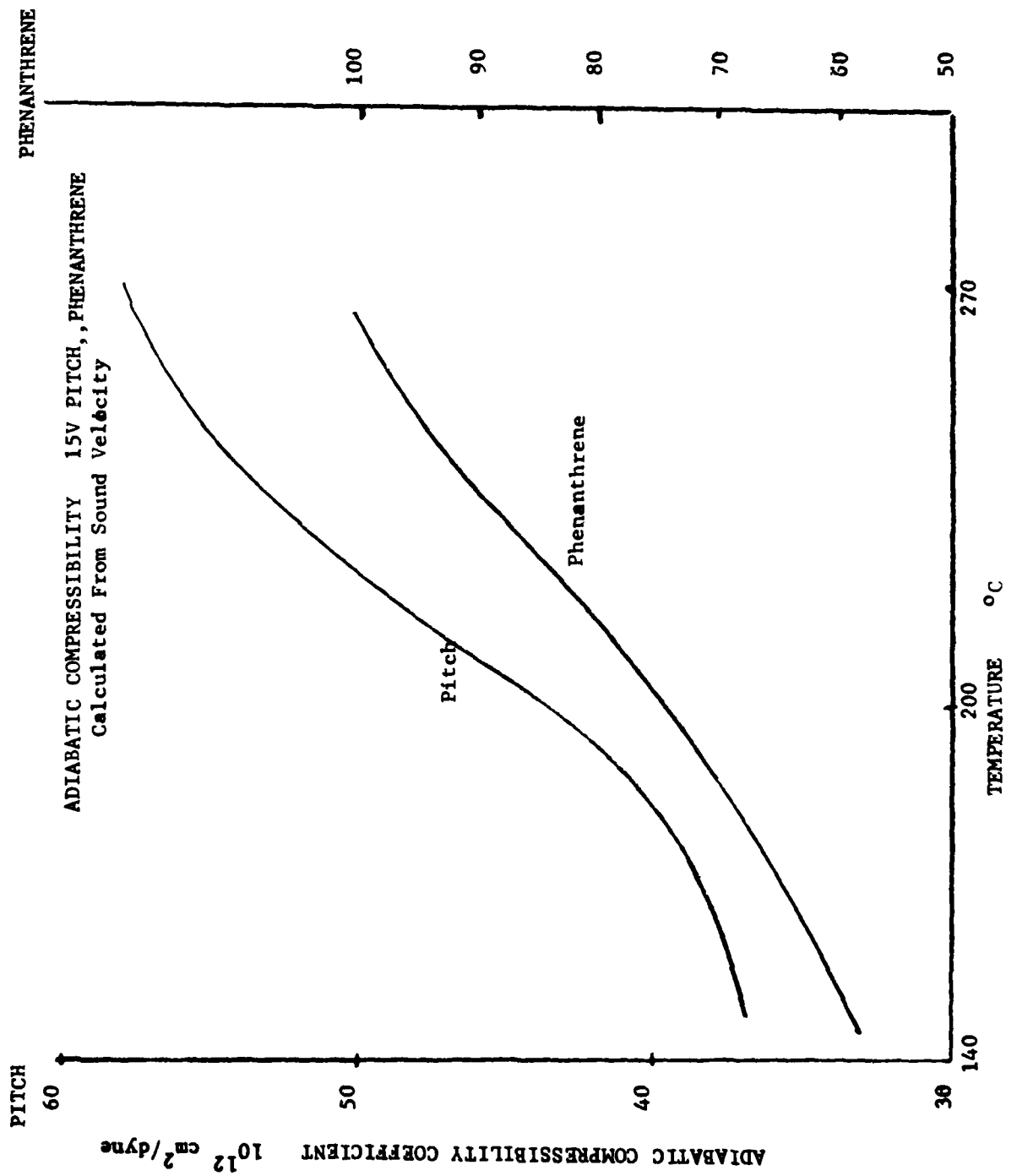


FIGURE 36



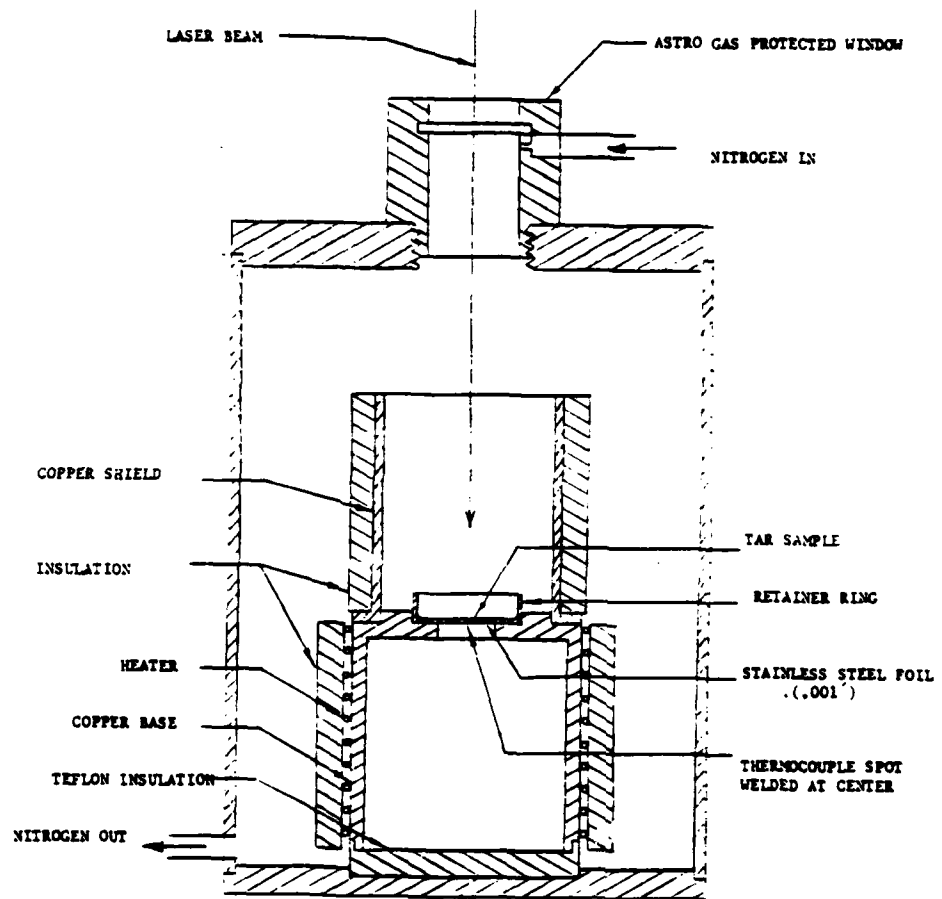
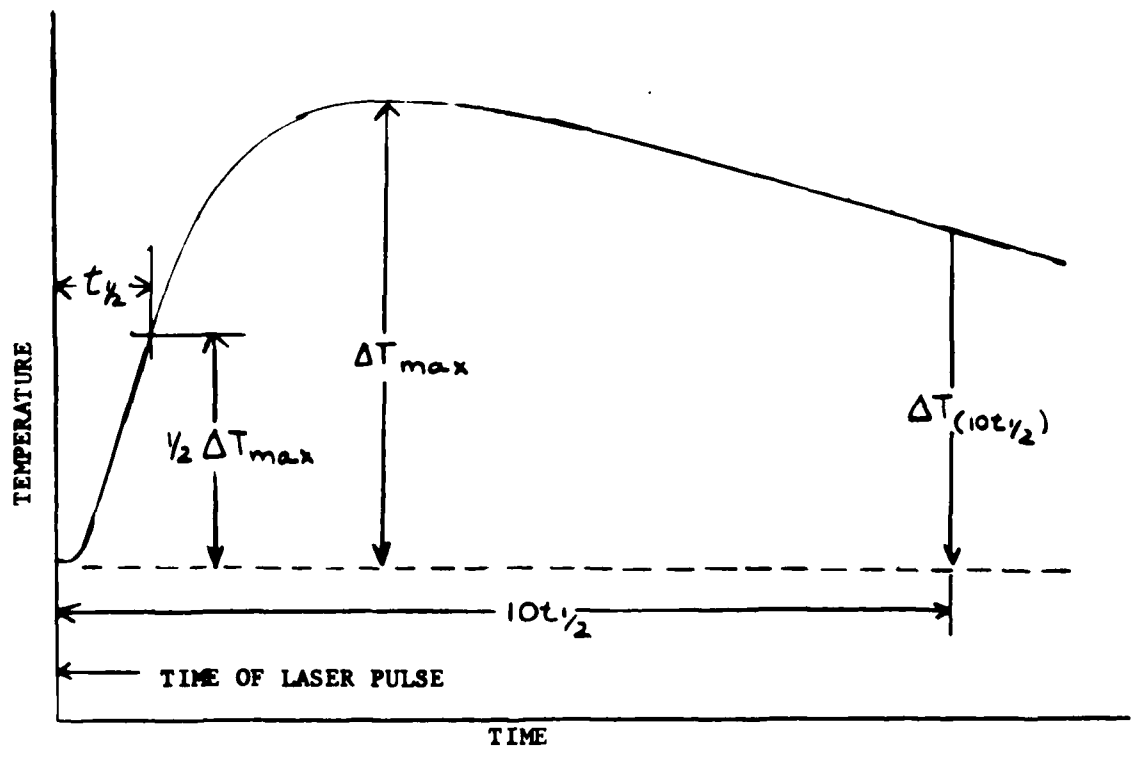


Figure 37. Apparatus for Measuring the Thermal Diffusivity of Tar Pitch as a Function of Temperature.

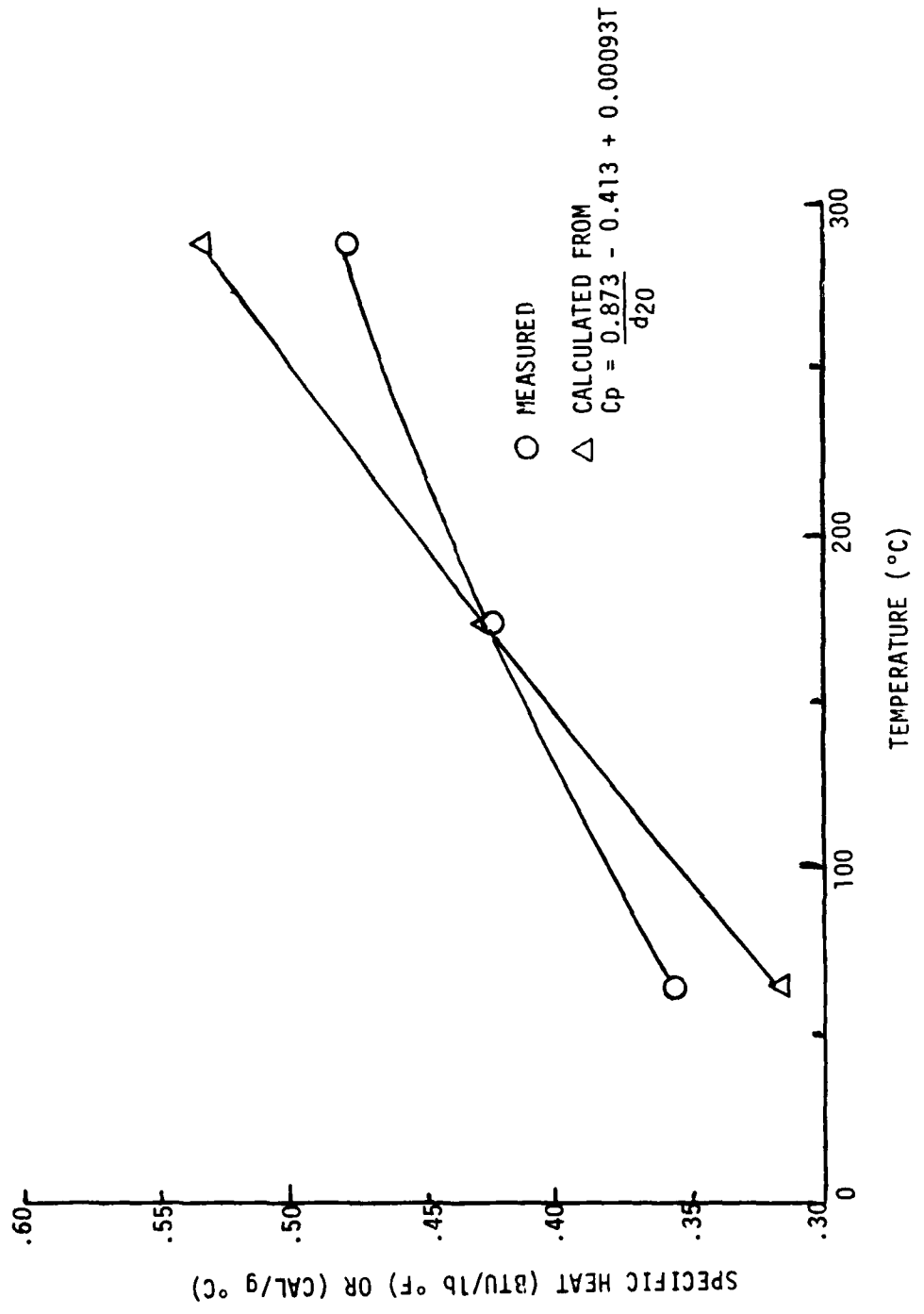


TRANSIENT THERMAL WAVEFORM AT THE BACK FACE OF THE SAMPLE
(WITH SIGNIFICANT HEAT LOSS)

FIGURE 38
LASER FLASH DIFFUSIVITY DATA FORM

FIGURE 39

MEASURED AND CALCULATED SPECIFIC HEATS OF COAL TAR PITCH 15V



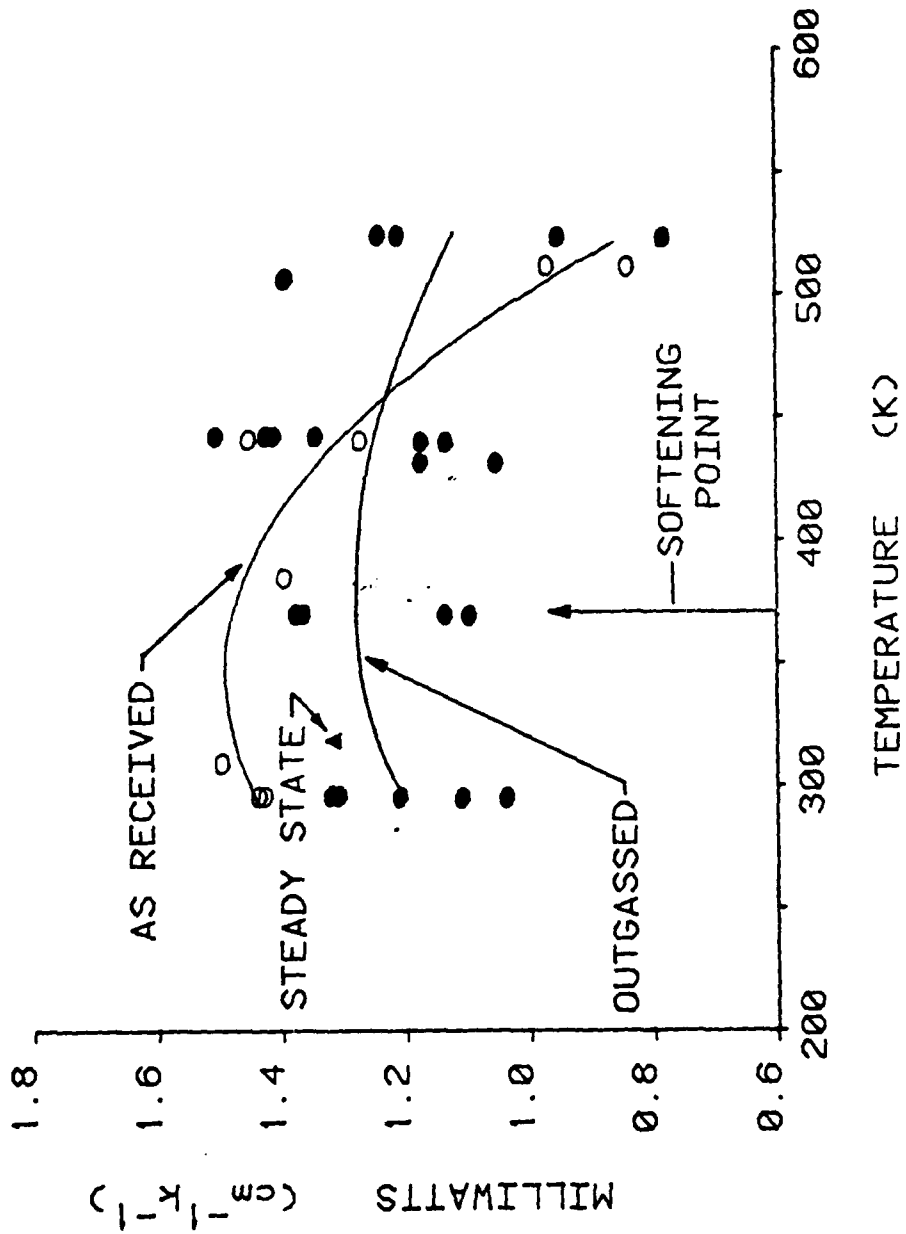


Figure 40. Thermal Conductivity of Allied 277-15V Pitch vs. Temperature

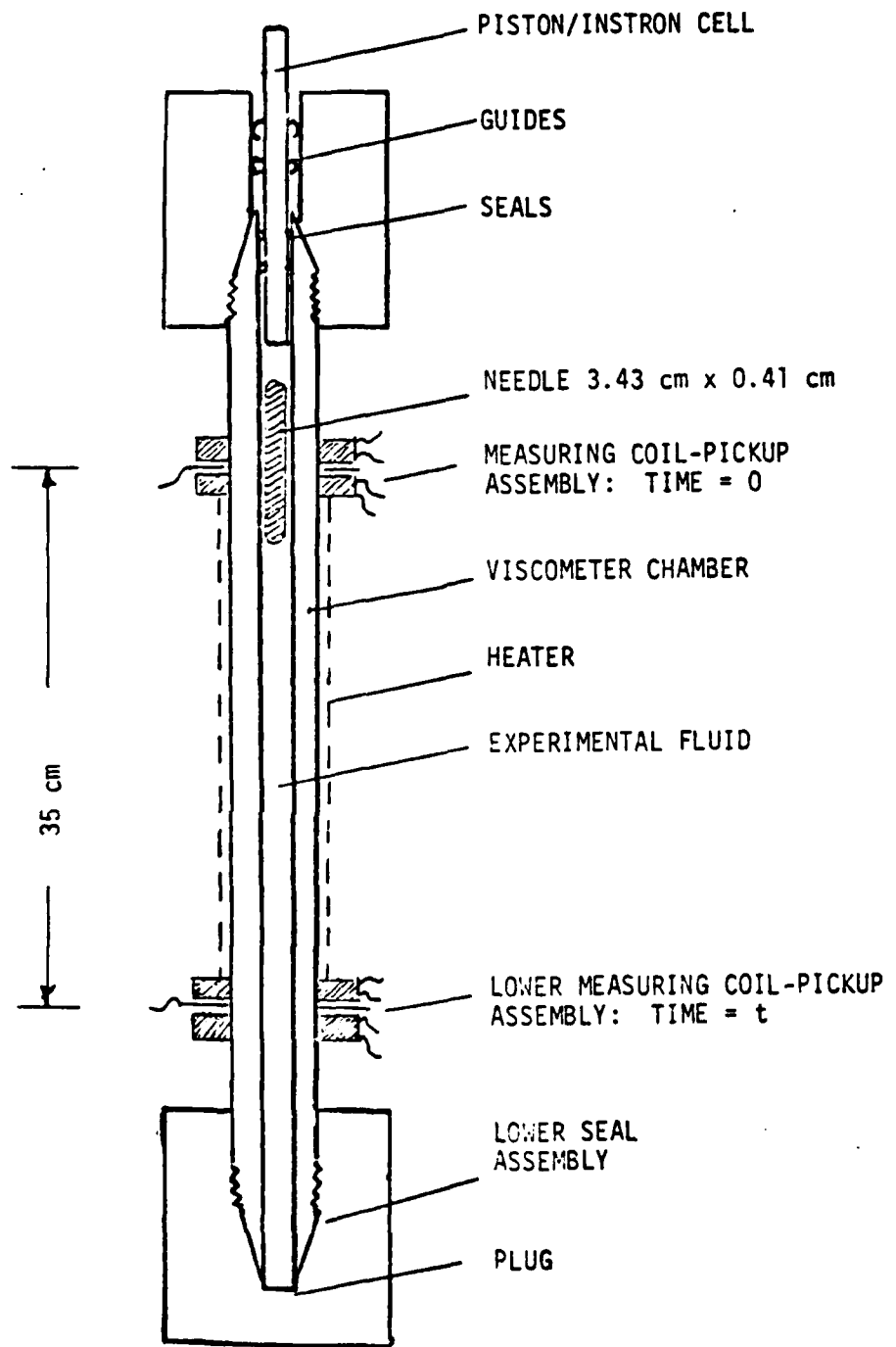


FIGURE 41
 SCHEMATIC OF HIGH PRESSURE VISCOMETER
 WITH FRICTION SEAL

Distance between sharp peaks indicates distance traveled by sinker in inches/second

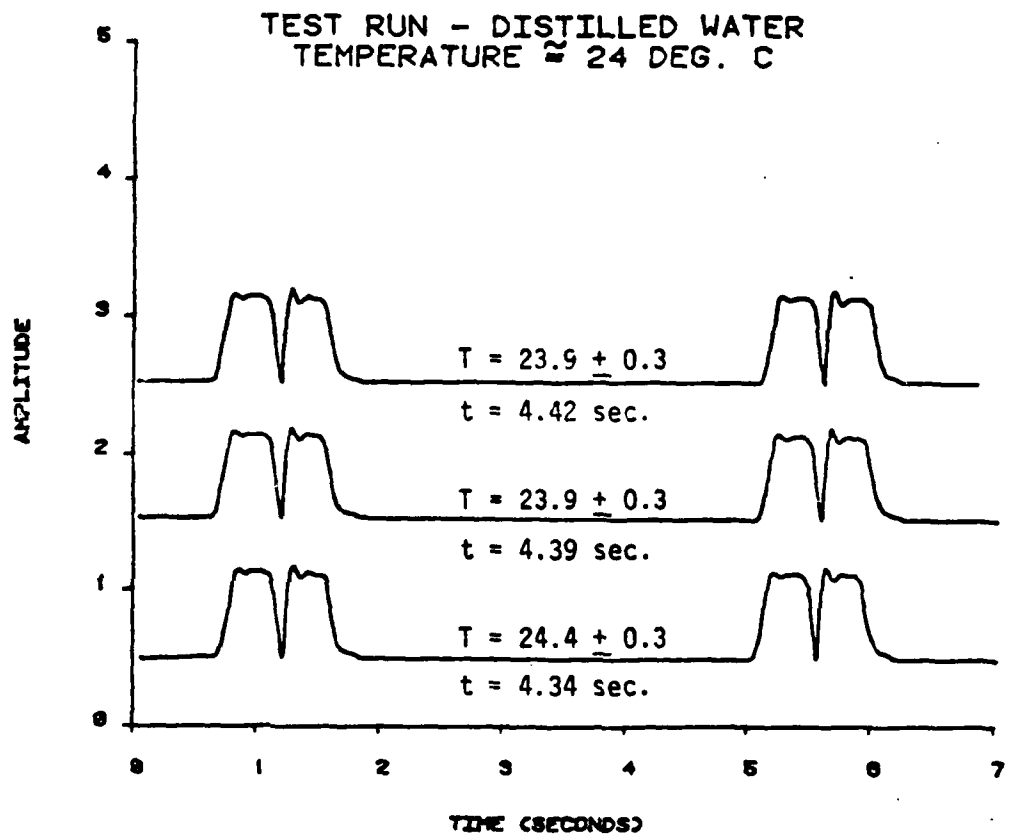


FIGURE 42
CALIBRATION OF HIGH PRESSURE VISCOMETER

FIGURE 43
VISCOMETER CALIBRATION
USING CASTOR OIL

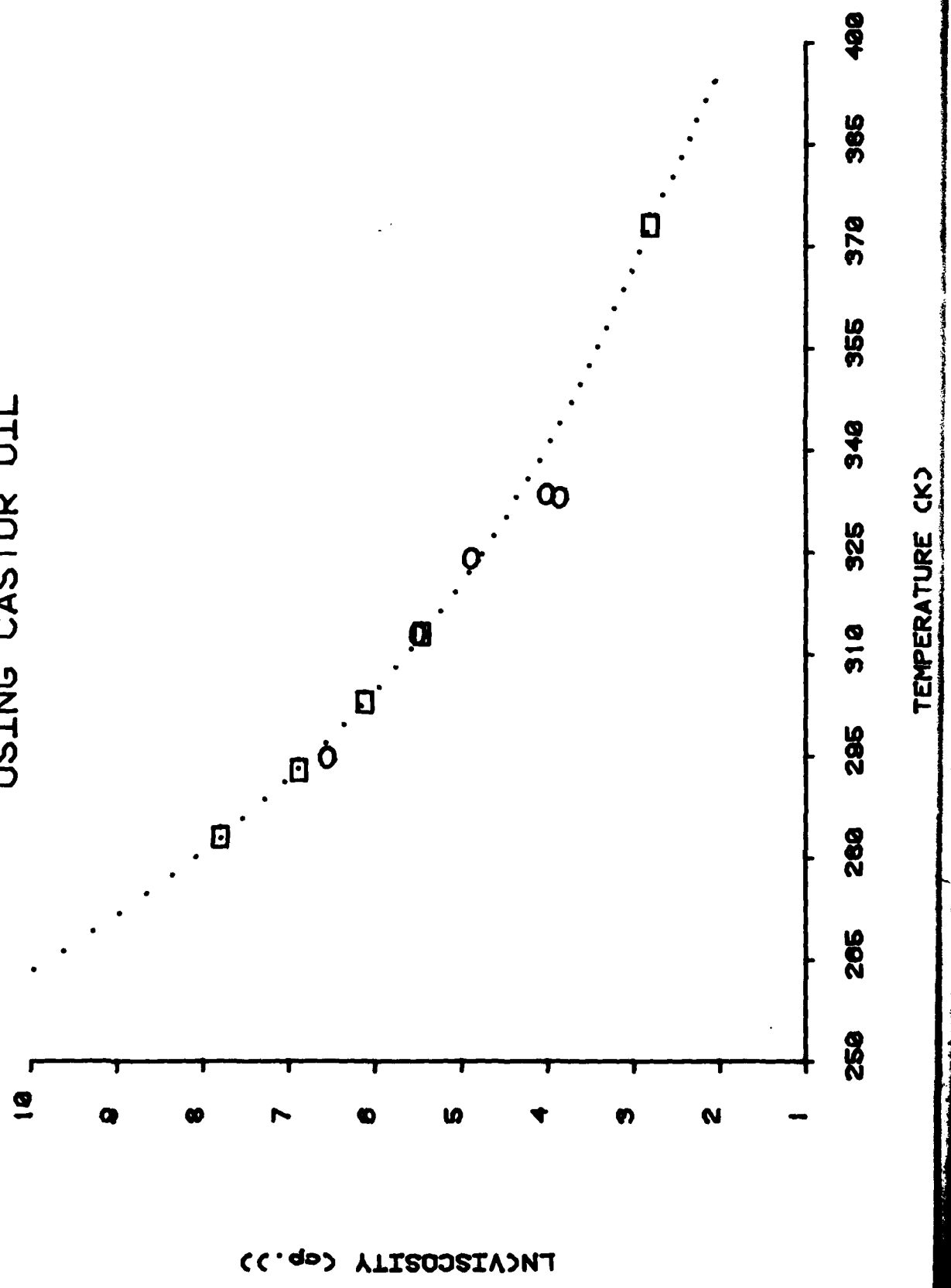




Figure 44. Modified High Pressure Viscometer with Seal-Bellows Attachment (Right) and Lower Seal and Support (Left).

FIGURE 45

PHENANTHRENE VISCOMETER DROP TIMES

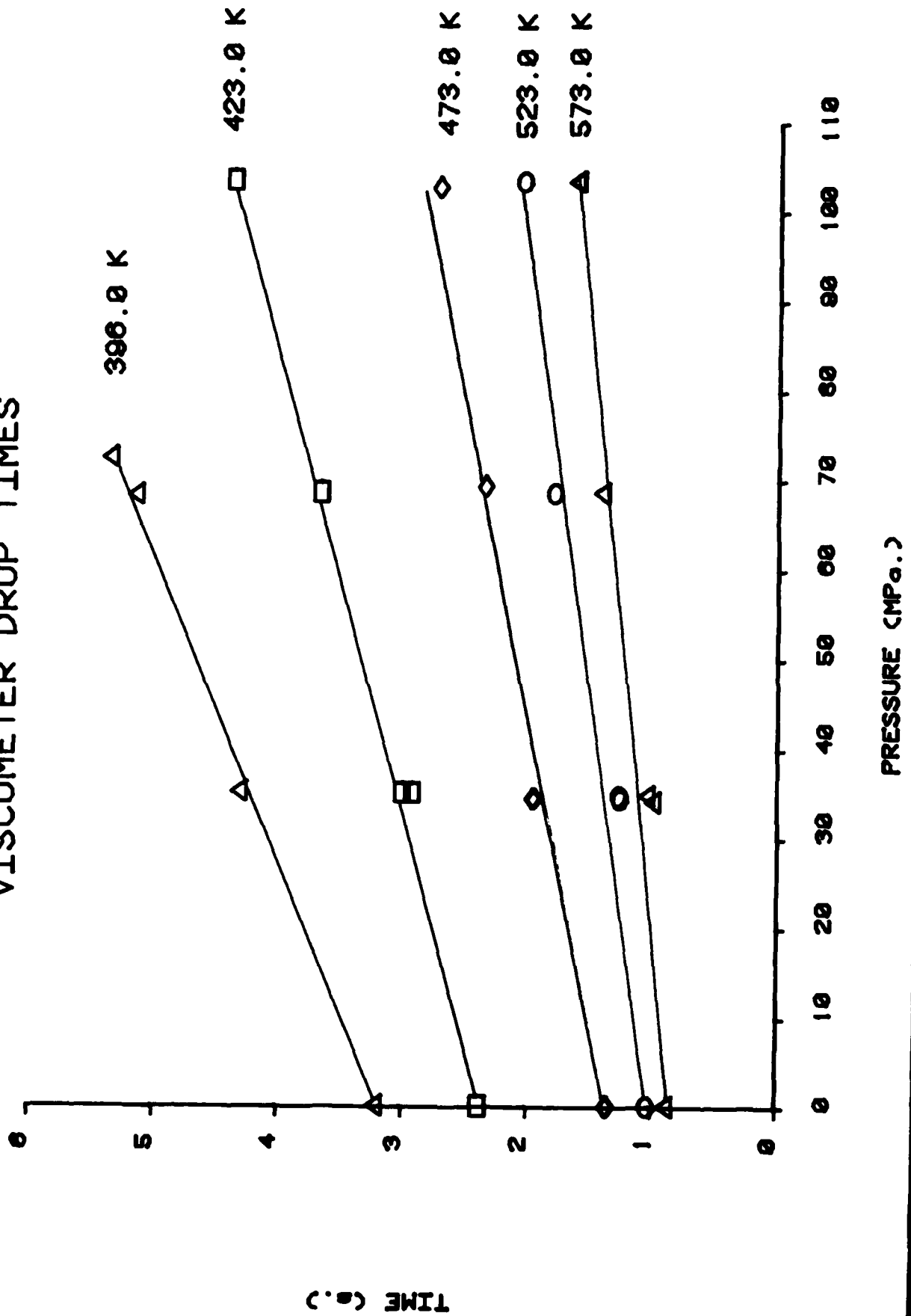


FIGURE 46

NAPHTHALENE -- EFFECT OF PRESSURE
ON THE MELTING POINT.

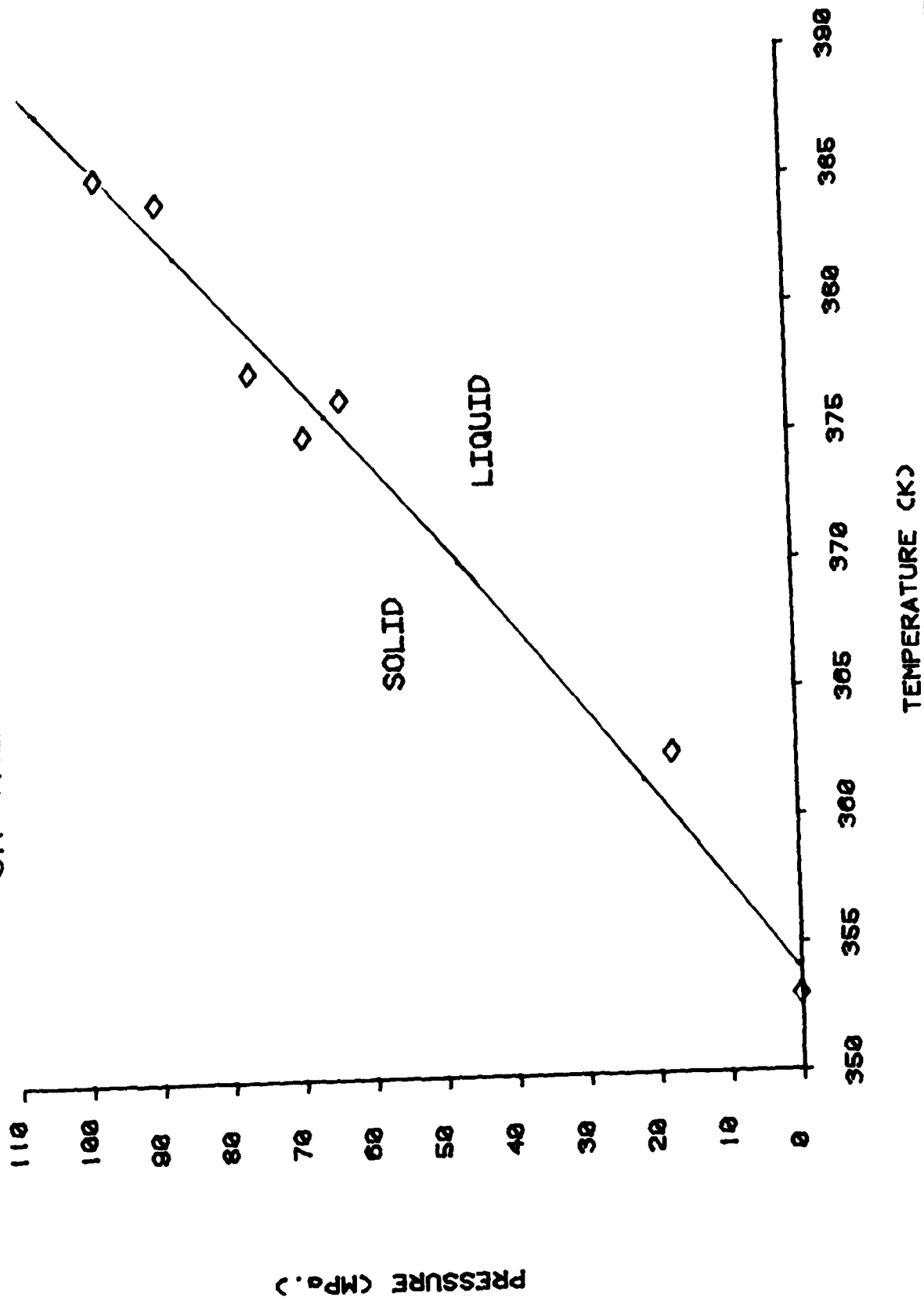


FIGURE 47

NAPHTHALENE VISCOMETER DROP TIMES

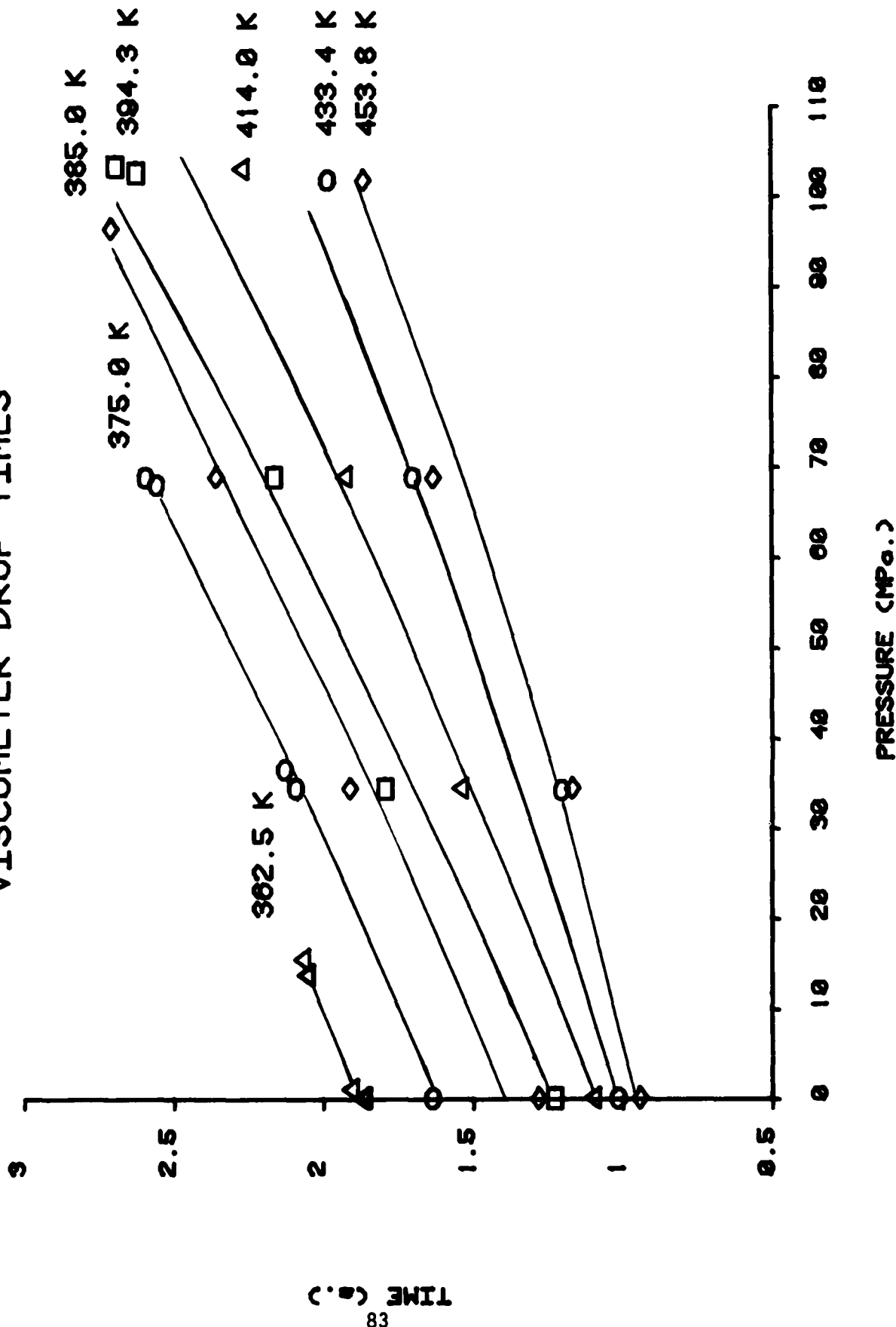


FIGURE 48

VISCOSITY OF NAPHTHALENE VS
TEMPERATURE AT 0.1 AND 101 MPa

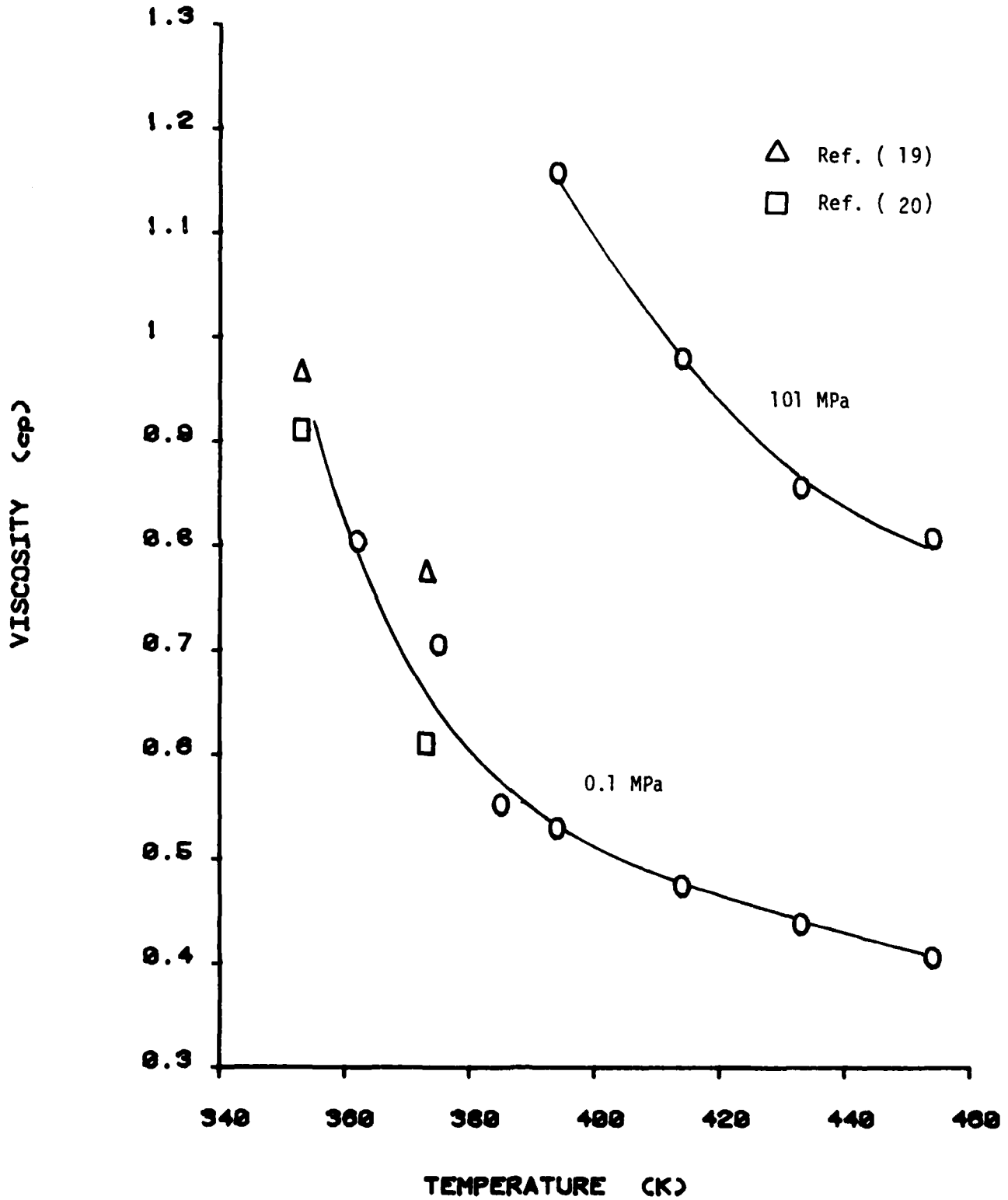
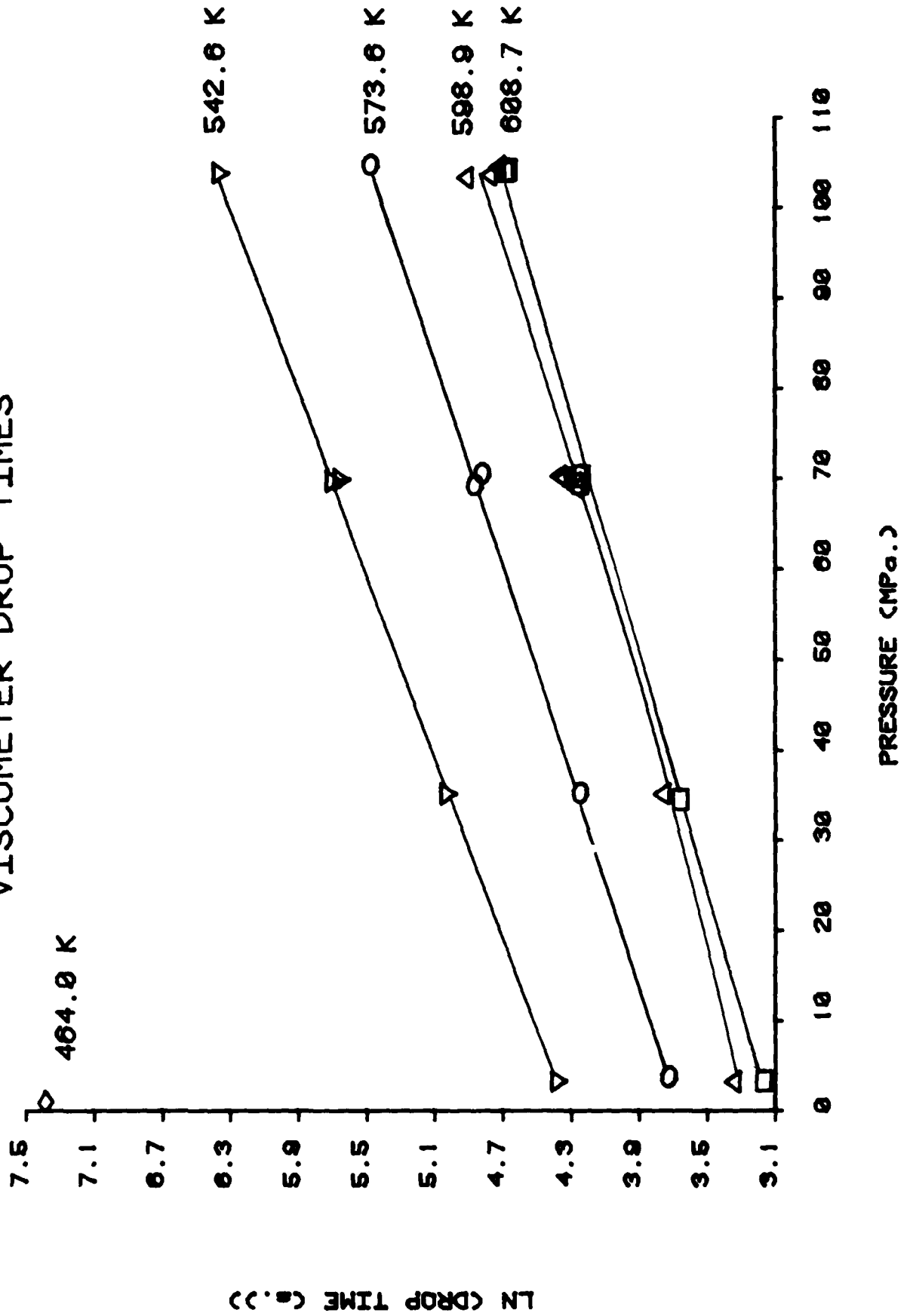




Figure 49. Positive Print of Radiograph Showing Needle (I) Within Viscometer. Lower Electromagnetic Coil is Shown at H. A Solid Brass Stop (J) was used to Prevent Needle from Falling Below Retrieval Point. Light Area Within Tube is Coal Tar Pitch. Needle is Cylindrical Above a Narrower Pointed Cylinder to Give a Hydrodynamically More Stable Leading Edge.

FIGURE 50

ALLIED 277-15V PITCH
VISCOMETER DROP TIMES



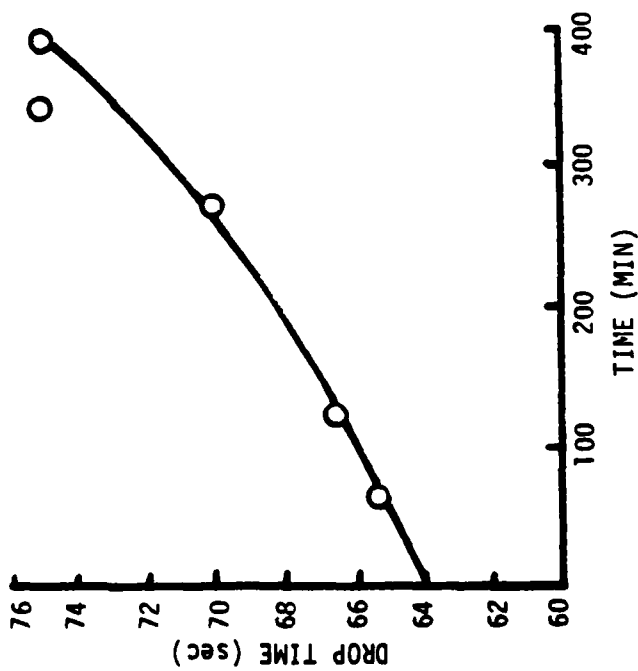
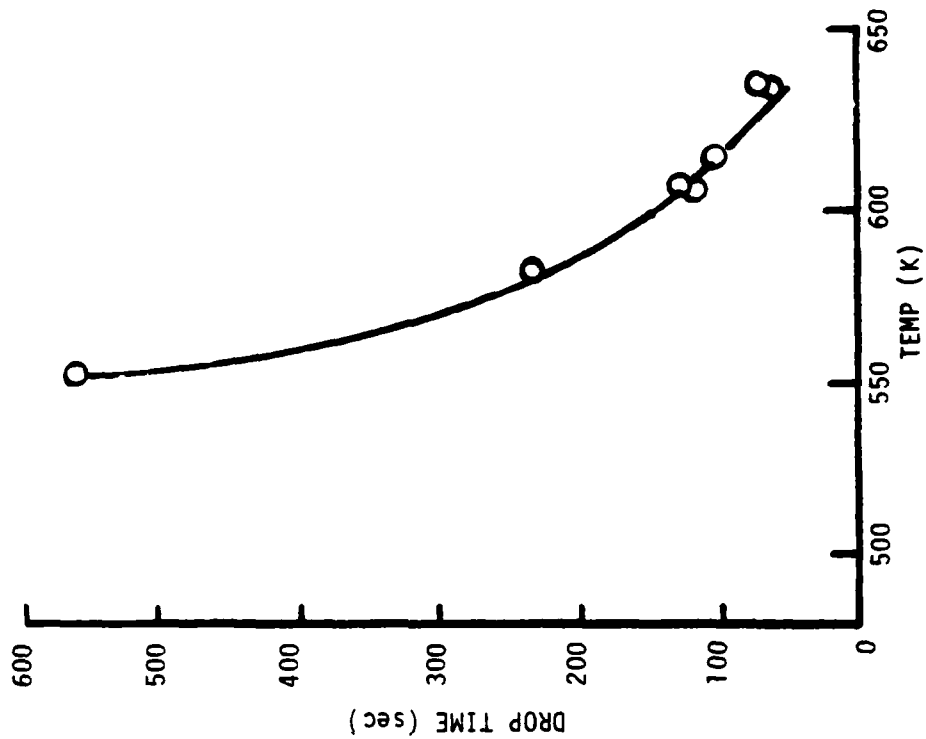


Figure 51. Drop Time in 277 Pitch vs Time at 101 MPa and 628.5 - 629.3K (left)
 Drop Time in 277 Pitch vs Temperature at 101 MPa (right)

TABLE 1
PROPERTIES OF PITCHES USED IN PYROLYSIS STUDIES

	KA	KB	277
Softening Point °C	152	128	95
Benzene Insol. %	-	-	16.6
Quinoline Insol. %	nil	0.9	6.0
Xylene Insol. %	33	25	
Coking Value %	64	57	46.2

TABLE 2

ANALYTICAL DATA ON PARTIALLY PYROLYZED PITCHES

A. T = 748K

P(MPa)	KA			KB			277			
	6.2	3.4	0.5	6.2	3.4	0.5	6.2	3.4	0.5	
<u>1. Quinoline Ins.</u>										
t hrs	7	73.5	80.4	79	54.8	58.1	40.2	63	59.4	72.8
	4	66.0	47.8	35.5	40.3	24.9	27.8	51.7	50.5	39.3
	2	15.3	13.7	36.1	13.2	11.0	17.9	30.5	23.3	24
	0	0	0	0	0.9	0.9	0.9	6.0	6.0	6.0
<u>2. % Wt. Loss</u>										
t hrs	7	8.6	8.1	8.2	12.6	9.0	4.6	14.2	12.7	21.6
	4	6.1	5.4	5.8	8.2	4.6	2.3	14.6	12.0	17.0
	2	7.8	3.9	3.9	7.5	0.7	5.2	13.8	9.4	12.7
<u>3. CVC %</u>										
t hrs	7	85.3	85.3	84.8	79.6	79.4	72.5	79.0	78.4	83.9
	4	81.7	78.6	75.7	74.7	70.4	70.9	75.9	75	73.6
	2	73.1	70.2	74.7	70.1	64.1	68.4	70.1	64.4	65.8
	0	64	64	64	57	57	57	46.2	46.2	46.2
<u>4. S.P. °C</u>										
t hrs	7	300+	300+	-	300+	300+	-	300+	-	-
	4	300+	-	-	225	-	-	300+	-	-
	2	177	-	-	187	143	-	-	140	-
	0	152	-	-	128	-	-	95	-	-

B. T = 723K t = 7 hrs. P = 3.4 MPa

	KA	KB	277
1. Q.I. %	16.1	22.6	22.2
2. % wt. loss	5.6	10.1	16.2
3. CVC %	71.2	71.1	68.1
4. S.P. °C	172	300	-

TABLE 3. COMPOSITION AS PER GPC FRACTIONS (%) AFTER PYROLYSIS AT 748K

FRACTION	Koppers KB Pitch						Koppers KB Pitch						Allied #277-15V Pitch					
	Virgin	#1	#2	#3	#6	#9	Virgin	#1	#2	#3	#6	#9	Virgin	#1	#2	#3	#6	#9
A	0.20	0.08	0.03	0.09	0.00	0.11	0.11	0.08	0.02	0.17	0.09	0.06	0.33	0.14	0.03	0.24	0.02	0.11
B	0.46	0.15	0.20	0.32	0.11	0.27	0.90	0.49	0.36	0.73	0.55	0.61	1.80	0.29	0.19	0.46	0.14	0.50
C	1.17	0.53	0.43	0.58	0.52	0.61	3.48	2.09	2.35	2.10	2.29	2.99	7.97	0.80	1.08	0.81	1.19	1.07
D	5.76	3.18	2.33	3.53	2.20	3.77	13.10	11.77	11.39	11.74	11.02	12.56	13.33	6.84	6.24	6.70	6.73	7.04
E	14.04	11.52	11.11	12.23	10.13	12.57	26.33	24.64	24.74	24.77	24.75	25.29	14.21	18.43	18.25	18.36	18.32	18.33
F	27.12	25.83	27.54	27.36	27.06	27.89	30.49	30.79	31.78	30.99	32.26	30.87	24.61	28.71	30.52	29.56	30.56	27.79
G	49.71	56.14	55.76	53.66	57.14	52.70	25.03	29.38	28.58	28.81	28.27	26.99	36.94	43.27	42.24	42.59	41.71	41.94
H	1.55	2.58	2.59	2.24	2.87	2.08	0.57	0.77	0.78	0.69	0.76	0.63	0.81	1.52	1.45	1.27	0.12	1.21
P (MPa) =	-	6.2	6.2	6.2	3.4	0.5	-	6.2	6.2	6.2	3.4	0.5	-	6.2	6.2	6.2	3.4	0.5
t (hrs) =	-	7	4	2	2	2	-	7	4	2	2	2	-	7	4	2	2	2
Wt. Avg. MW	247.8	242	242.5	246.2	240.8	245.8	279.8	278.1	276.1	278.8	275.7	278.3	297.2	259.8	261.1	260.6	261.2	261.2
Nb. Avg. MW	203.2	201.6	204.5	206.8	201.5	207.9	272.4	268.9	267.5	269.7	267.4	270.5	261	231.2	232.9	232.1	233.1	233.4
Dispersivity	1.22	1.2	1.185	1.19	1.195	1.18	1.027	1.034	1.032	1.034	1.031	1.029	1.139	1.124	1.121	1.122	1.12	1.119
Z-Avg. MW	268.9	260.5	259.3	264	257.9	263.1	282.8	282.7	280.3	283.4	279.9	282.4	313.1	272.2	273.6	273.5	273.8	274.3
Total Integrated Area	545	261	297	430	280	439	648	385	447	473	454	536	637	272	375	405	424	435
Area % of Total Area	--	47.9	54.5	78.9	51.4	80.5	--	59.4	69.0	73.0	70.1	82.7	--	42.7	58.9	63.6	66.6	68.3
% Chloroform Solubles (by weighing technique)	--	35.4	42.0	--	40.0	53.6	74.5	57.6	63.9	61.3	68.2	67.9	90.4	42.4	62.0	57.8	65.8	64.5

TABLE 4
 SOUND VELOCITY-PRESSURE DATA
 FOR WATER (30°C) AT 6 MHz

<u>Pressure</u>			<u>Velocity (Km/sec)</u>	
<u>Kg/cm²</u>	<u>MN/m²</u>	<u>psig</u>	<u>Increasing P</u>	<u>Decreasing P</u>
0	0.1	0	1.504	1.498
92	9.02	1310	1.514	1.513
307	30.1	4360	1.547	1.556
613	60.2	8730	1.600	1.606
920	90.2	13100	1.649	1.653

TABLE 5

SOUND VELOCITY IN PHENANTHRENE
(Km/sec)

<u>TEMPERATURE</u>		<u>PRESSURE MPa</u>				<u>△</u>
<u>K</u>	<u>°C</u>	<u>0.1</u>	<u>33.77</u>	<u>67.53</u>	<u>101.3</u>	
393.5	120.5	1.333	1.332	1.334	1.336	0.006
414.7	141.7	1.287	1.289	1.291	1.293	0.006
440.2	167.2	1.234	1.236	1.237	1.239	0.005
465	192.0	1.182	1.183	1.185	1.187	0.005
491	217.8	1.129	1.131	1.133	1.134	0.005
514	241.1	1.081	1.082	1.084	1.085	0.004
538	265	1.032	1.033	1.034	1.036	0.004
562	289	0.981	0.982	0.984	--	--

TABLE 6
 SOUND VELOCITY IN ALLIED 15 V PITCH
 AT ONE ATMOSPHERE

<u>TEMPERATURE</u>		<u>VELOCITY (km/s)</u>
<u>°C</u>	<u>K</u>	<u>AT 2 MHz</u>
149	422	1.51
149	422	1.50
165	439	1.49
167	440	1.46
181	454	1.45
182	455	1.43
198	471	1.41
200	473	1.38
214	487	1.32
214	487	1.34
231	504	1.32
231	504	1.27
250	523	1.23
250	523	1.26
268	541	1.24
268	541	1.23

TABLE 7

SPECIFIC HEAT OF 15V PITCH
EQUILIBRATED 15 MINUTES AT TEMPERATURE OF MEASUREMENT

<u>TEMPERATURE</u> <u>°C</u> <u>(°F)</u>	<u>MEASURED(a)</u> <u>BTU/lb °F</u>	<u>CALCULATED(b)</u> <u>BTU/lb °F</u>
65.6 (150)	0.353	0.316
176.7 (350)	0.424	0.428
287.8 (550)	0.477	0.532

(a)
Perkin-Elmer Differential Scanning Calorimeter

(b)
Encyclopedia of Chemical Technology, 19, p. 676. (Ref. 12)

$$C_p = \frac{0.873}{d_{20}} - 0.413 + 0.00093T$$

d_{20} = density at 20°C = 1.29 g/cm³

T = Temperature, °C

In Reference (7), the third term on the right appears as 0.0093T, evidently a misprint.

TABLE 8
THERMAL DIFFUSIVITY AND CONDUCTIVITY OF 277-15V PITCH

NOT OUTGASSED						OUTGASSED					
TEMP. K	THICK. (mm)	THERMAL DIFFUSIVITY (cm ² /sec x 10 ⁻⁴)	THERMAL CONDUCTIVITY watts/cm-K x 10 ⁻⁴	THERMAL CONDUCTIVITY (BTU/ft-sec-of x 10 ⁻⁵)	TEMP. K	THICK. (mm)	THERMAL DIFFUSIVITY (cm ² /sec x 10 ⁻⁴)	THERMAL CONDUCTIVITY watts/cm-K x 10 ⁻⁴	THERMAL CONDUCTIVITY (BTU/ft-sec-of x 10 ⁻⁵)		
307	.648	8.61	15.2	2.44	294.3	.381	7.00	12.1	1.95		
	.648	8.61	15.2	2.44		.381	7.53	13.2	2.12		
383.2	.610	6.81	13.4	2.16		.305	5.98	10.5	1.68		
	.610	6.81	13.4	2.16		.533	6.23	11.0	1.76		
438.8	.254	6.27	16.9	2.68		.533	7.58	13.1	2.10		
	.254	5.52	14.7	2.36	366.5	.533	6.85	13.7	2.20		
510.9	.229	3.47	10.4	1.68		.592	5.53	11.0	1.77		
	.229	4.02	12.1	1.94	368.8	.592	5.70	11.4	1.83		
294.9	.483	8.11	14.3	2.29	430.4	.366	4.79	10.6	1.70		
	.483	8.18	14.4	2.31		.366	5.36	11.8	1.90		
					437.6	.328	5.07	11.4	1.83		
						.328	5.28	11.8	1.90		
					444.3	.592	5.98	13.6	2.18		
						.592	5.31	14.3	2.29		
						.551	6.67	15.1	2.43		
						.551	6.33	14.3	2.30		
					504.3	.594	5.64	13.9	2.24		
						.594	5.64	13.9	2.24		
					522.1	.229	3.20	7.9	1.27		
						.229	3.91	4.6	1.54		
						.582	4.95	12.3	1.97		
						.582	5.03	12.5	2.00		

TABLE 9

THERMAL DIFFUSIVITIES OF THREE PARTIALLY PYROLYZED COAL TAR PITCHES

 α = DIFFUSIVITY cm^2/sec

t = THICKNESS, IN.

A. KOPPERS TYPE A (KA)											
6.2 MPa						0.5 MPa					
2 HRS		4 HRS		7 HRS		2 HRS		4 HRS		AS-RECEIVED	
$10^4 \alpha$	t	$10^4 \alpha$	t	$10^4 \alpha$	t	$10^4 \alpha$	t	$10^4 \alpha$	t	$10^4 \alpha$	t
6.10	.0118	8.38	.0182	9.34	.0204	6.09	.0151	7.30	.0172	6.13	.0106
6.95	.0121	6.00	.0131	6.96	.0157	5.80	.0164	6.62	.0138	5.73	.0121
7.26	.0161	4.92	.0103	8.29	.0186	6.09	.0157	5.90	.0147	5.26	.0128
8.25	.0164	6.88	.0152	7.05	.0176	7.43	.0153	6.50	.0142	5.77	.0134
AVG	7.14	6.54		7.91		6.35		6.58		5.72	
S.D.	0.89	1.46		1.13		0.73		0.57		0.36	

B. KOPPERS TYPE B (KB)											
6.2 MPa						0.5 MPa					
2 HRS		4 HRS		7 HRS		2 HRS		4 HRS		AS-RECEIVED	
$10^4 \alpha$	t	$10^4 \alpha$	t	$10^4 \alpha$	t	$10^4 \alpha$	t	$10^4 \alpha$	t	$10^4 \alpha$	t
6.34	.0126	5.94	.0142	7.04	.0165	6.43	.0124	6.79	.0181	6.60	.0171
5.37	.0116	7.05	.0188	6.66	.0155	5.37	.0117	7.42	.0187	6.43	.0141
5.87	.0137	6.50	.0143	5.60	.0144	6.14	.0134	6.79	.0166	5.95	.0120
6.94	.0123	5.79	.0125	6.29	.0156	5.47	.0117	6.00	.0109	6.75	.0141
AVG	6.13	6.32		6.39		5.85		6.75		6.43	
S.D.	0.67	0.57		0.61		0.51		0.58		0.35	

C. ALLIED 277-15V											
6.2 MPa						0.5 MPa					
2 HRS		4 HRS		7 HRS		2 HRS		4 HRS			
$10^4 \alpha$	t	$10^4 \alpha$	t	$10^4 \alpha$	t	$10^4 \alpha$	t	$10^4 \alpha$	t		
6.23	.0118	6.38	.0140	7.34	.0138	6.98	.0139	6.81	.0178		
6.16	.0100	6.84	.0117	8.41	.0168	5.93	.0153	8.46	.0106		
7.25	.0114	7.83	.0187	9.07	.0197	6.06	.0111	5.96	.0110		
6.49	.0127	7.56	.0150	7.69	.0172	6.83	.0157	7.75	.0112		
AVG	6.53	7.15		8.13		6.45		7.24			
S.D.	0.50	0.66		0.77		0.53		1.09			

TABLE 10. THERMAL CONDUCTIVITY OF THREE PARTIALLY PYROLYZED PITCHES

MATERIAL	PRESSURE PSI	TIME HRS	SAMPLE NUMBER	THERMAL DIFFUSIVITY cm ² /sec	SPECIFIC HEAT cal/g°C	DENSITY g/cm ³	THERMAL CONDUCTIVITY watts/cm-K	THERMAL CONDUCTIVITY BTU/ft. sec. OF
Koppers Type A	-	-	Virgin	5.72 x 10 ⁻⁴	.256	1.314	8.06 x 10 ⁻⁴	1.29 x 10 ⁻⁵
	900	7	1A	7.91 x 10 ⁻⁴	.246	1.136	9.25 x 10 ⁻⁴	1.48 x 10 ⁻⁵
	"	4	2A	6.54 x 10 ⁻⁴	.246	1.118	7.53 x 10 ⁻⁴	1.21 x 10 ⁻⁵
	"	2	3A	7.14 x 10 ⁻⁴	.240	1.149	8.24 x 10 ⁻⁴	1.32 x 10 ⁻⁵
	50	4	8A	6.58 x 10 ⁻⁴	.247	1.303	7.69 x 10 ⁻⁴	1.23 x 10 ⁻⁵
"	2	9A	6.35 x 10 ⁻⁴	.246	1.288	8.42 x 10 ⁻⁴	1.35 x 10 ⁻⁵	
Koppers Type B	-	-	Virgin	6.43 x 10 ⁻⁴	.258	1.281	8.90 x 10 ⁻⁴	1.43 x 10 ⁻⁵
	900	7	1B	6.39 x 10 ⁻⁴	.254	1.250	8.49 x 10 ⁻⁴	1.36 x 10 ⁻⁵
	"	4	2B	6.32 x 10 ⁻⁴	.252	1.258	8.39 x 10 ⁻⁴	1.35 x 10 ⁻⁵
	"	2	3B	6.13 x 10 ⁻⁴	.255	1.265	8.28 x 10 ⁻⁴	1.33 x 10 ⁻⁵
	50	4	8B	6.75 x 10 ⁻⁴	.254	1.293	9.28 x 10 ⁻⁴	1.49 x 10 ⁻⁵
"	2	9B	5.85 x 10 ⁻⁴	.255	1.291	8.06 x 10 ⁻⁴	1.29 x 10 ⁻⁵	
Allied 277-15V	-	-	Virgin	6.70 x 10 ⁻⁴	.277	1.238	9.62 x 10 ⁻⁴	1.54 x 10 ⁻⁵
	900	7	1C	8.13 x 10 ⁻⁴	.252	1.176	10.09 x 10 ⁻⁴	1.62 x 10 ⁻⁵
	"	4	2C	7.15 x 10 ⁻⁴	.264	1.218	9.63 x 10 ⁻⁴	1.55 x 10 ⁻⁵
	"	2	3C	6.53 x 10 ⁻⁴	.259	1.192	8.44 x 10 ⁻⁴	1.35 x 10 ⁻⁵
	50	4	8C	7.24 x 10 ⁻⁴	.254	1.274	9.81 x 10 ⁻⁴	1.57 x 10 ⁻⁵
"	2	9C	6.45 x 10 ⁻⁴	.257	1.260	8.75 x 10 ⁻⁴	1.40 x 10 ⁻⁵	

TABLE 11
CELL CONSTANT DETERMINATION

Needle Diam		Constant $C_0 \times 10^3$	
		In H ₂ O $\eta = .890$ cp	In Castor Oil $\eta = 986$ cp
(cm)	(in)		
0.3208	(0.1263)	2.65	7.07
0.3739	(0.1472)	1.53	2.53
0.4067	(0.1601)	0.804	0.808

TABLE 12
CASTOR OIL VISCOSITY

Temperature		Viscosity (cp)	
<u>K</u>	<u>°C</u>	Handbook	Measured
283	10	2420	-
293	20	986	-
294.7	21.7	-	700
303	30	451	-
313	40	231	245
324.1	51.1	-	134
333.	60	-	47.8
333.6	60.6	-	55.8
373	100	16.9	-

TABLE 13. VISCOMETER DATA FOR PHENANTHRENE

(DROP DISTANCE = ~~25.24~~ cm)
15.24

<u>TEMPERATURE</u> (K)	<u>PRESSURE</u> (MPa)	<u>DROP TIME</u> (seconds)
396	0.1	3.21
"	34.3	4.31
"	66.7	5.15
"	70.7	5.36
423	0.1	2.38
"	34.3	2.92
"	34.3	3.00
"	67.0	3.66
"	101.3	4.37
473	0.1	1.36
"	0.1	1.35
"	33.7	1.94
"	33.7	1.955
"	67.7	2.345
"	100.3	2.725
523	0.1	1.030
"	33.7	1.255
"	34.0	1.265
"	67.0	1.790
"	101.3	2.050
573	0.1	0.885
"	33.3	0.990
"	34.0	1.040
"	67.0	1.415
"	101.3	1.620
"	101.3	1.630

TABLE 14. VISCOMETER DATA FOR NAPHTHALENE

(DROP DISTANCE = ~~25.24~~ cm)
15.24

<u>RUN NO.</u>	<u>TEMPERATURE</u> (°C)	<u>PRESSURE</u> (psi)	<u>DROP TIME</u> (seconds)	η (cp) corr.	η (cp) no corr.
1	89.0	15	1.865	.803	.804
2	89.0	15	1.910	.819	.82
3	89.5	2000	2.060		
4	90.0	2000	2.055		
5	90.0	2250	2.070		
6	101.5	5000	2.090		
7	102.5	10000	2.592		
8	102.5	5300	2.125		
9	102.0	9875	2.555		
10	102.0	15	1.635	.705	.705
11	111.5	15	1.280	.553	.552
12	111.7	5000	1.908		
13	112.0	10000	2.355		
14	112.2	14000	2.705		
15	121.5	15	1.227	.531	.529
16	121.4	5000	1.790		
17	121.6	10000	2.160		
18	89.5	15	1.875		
19	121.0	14900	2.620		
20	121.1	15000	2.690	1.157	1.160
21	140.6	14950	2.270	.979	.979
22	140.7	10000	1.928		
23	141.2	5000	1.540		
24	141.2	15	1.100	.477	.474
25	160.4	15000	1.980	.856	.854
26	160.4	10000	1.700		
27	160.4	4975	1.202		
28	160.6	15	1.015	.442	.438
29	180.6	15000	1.860	.807	.802
30	181.0	10000	1.630		
31	180.8	5000	1.165		
32	180.8	15	0.942	.411	.406
33	100.0	5000	2.14		

TABLE 15. ALLIED 277-15V PITCH: VISCOMETER DATA

RUN #	TEMP. K	PRESSURE MPa	(DROP DISTANCE = 25.24 cm)	LOG t	η (a) cp
			15.24 DROP TIME (sec.)		
5	608.2	3.2	23.7	1.3747	10.0
6	609.2	33.7	38.7	1.5877	16.3
7	608.2	67.8	69.5	1.8420	29.3
10	609.2	68.7	68.9	1.8382	29.1
8	609.2	101.8	105.6	2.0237	44.5
9	609.2	101.7	107.3	2.0306	45.2
1	598.2	3.0	28.5	1.4548	12.0
2	598.2	34.2	43.2	1.6355	18.2
3	599.2	67.3	68.4	1.8551	28.8
11	600.2	68.3	77.4	1.8887	32.6
12	599.2	68.5	79.2	1.8987	33.4
4	599.2	102.0	113.0	2.0531	47.6
13	601.2	101.2	118.9	2.0752	50.1
14	597.2	100.8	136.7	2.1358	57.6
15	573.2	3.4	41.5	1.6180	17.5
16	574.2	34.2	69.7	1.8432	29.3
17	575.2	68.7	123.6	2.0920	52.0
18	573.2	67.3	129.3	2.1116	54.4
19	573.2	102.0	237.9	2.3764	100.1
21	543.2	2.7	79.1	1.8982	33.2
22	542.2	33.8	150.9	2.1787	63.4
23	541.2	67.7	296.1	2.4714	124.4
24	544.2	67.8	281.6	2.4496	118.3
25	543.2	101.3	573.0	2.7582	240.8
20	464.2	0.1	1607.4	3.206	672

(a) Calculated using densities corrected for temperature.

TABLE 16

DROP TIME IN ALLIED PITCH VS TIME AT TEMPERATURE AT 101 MPa

<u>t (min)</u>	<u>TEMP (K)</u>	<u>PRESSURE (MPa)</u>	<u>DROP TIME (SEC)</u>
0	627.6	3.36	-
30	611	99.7	-
53	628.8	101	65.3
120	629.3	101	66.5
274	629.3	101	70.1
344	628.5	101	74.8
392	629.3	101	74.9

REFERENCES

1. "Encyclopedia of Chemical Technology", R.E. Kirk and D.F. Othmer, Vol 4, pp 162 et seq.
2. Brooks, J.D. and Taylor, G.H., "Chemistry and Physics of Carbon" ed. P. L. Walker, Jr. Vol 4, 243, M. Dekker & Co., 1968.
3. White, J.L., "Formation of Microstructure in Graphitizable Carbons", Aerospace Corp., SAMS0-TR-74-93 (1974). AD 777-814; Marsh, H., and Cornford, C., "Petroleum Derived Carbons" ACS Symposium Series 21, pp 266-281 (1976).
4. Mantell, C.L., "Carbon and Graphite Handbook" J. Wiley & Co., (1968); "Industrial Graphite Engineering Handbook" Nat. Carbon Div of Union Carbide Co. (1965).
5. Yamada, Y. et al., Proc. 12th Int Conf on Carbon, Pittsburgh, PA, 1975, Extended Abstracts, pp 271-2; Honda, H. et al, J. Carbon, 8 181 (1970)
6. Huttinger, K.J. and Rosenblatt, U., 4th Int. Conf. on Carbon and Graphite, London 1974 Preprint No. 73; Inagaki, M., Ishihara, M., and Naka, S., High Temp-High Press., Vol 8, 1976, 279-291.
7. Holten, G., Hagelberg, M.P., Kas, S. and Johnson, W.H., Jr., J. Acoust. Soc. 43 (1) 102-67 (1968).
8. Mamedov, I.A., FazoolaeV, Z. and Aliev, A.A., Trans. of Petroleum and Gas Inst., #10, pp 65-68 (1973).
9. Batalin, G.E. and Mizernitskii, M.P., Zhur. Priklad. Khim., 42 (2) 363-368 (1969).
10. ASTM Standards, Part 15, ANSL/ASTM pp 706-7.
11. Cowan, R.D., J. Appl. Phys. 34 926 (1963)
12. Encyclopedia of Chemical Technology, 19 p. 676.
13. Boelhouwer, JWM and Toneman, L.H., Proc. Conf on Lubrication and Wear, Lond. Inst. of Mech. Eng., London 1957, pp 214-218.
14. Handbook of Chemistry and Physics, 40th Ed., Chemical Rubber Publishing Co., Cleveland, 1958-9.
15. P.W. Bridgman "The Physics of High Pressure", Dover Publ. Inc., N.Y. (1970)
16. Deffet, L., Bull Soc. Chim. Belg. 49 223 (1940)
17. Chem. Eng. Handbook, ed. by R. H. Perry, C. H. Chilton and S. D. Kirkpatrick, McGraw-Hill, 1963 p 3-213.
18. *ibid* p 3-216

REFERENCES (continued)

19. Handbook of Chemistry and Physics, 56th Ed., CRC Press, 1976 p C-375.
20. *ibid* p. F-54.
21. Ref. 17, p. 3-199, 200.
22. Huttinger, K.J. and Rosenblatt, U., Proc. 12th Biennial Conf. on Carbon, Pittsburgh, PA 1975 p 269-70, 4th London Conf. on Carbon and Graphite, 1974, Paper No. 73.
23. Fitzer, E. and Terwiesch, B., Carbon 11 570-74 (1973).
24. Bradshaw, W. and Mamone, V.P., Proc. 14th Biennial Conf. on Carbon, Penn State U., 1979 pp 403-404.
25. "Physicochemical Effects of Pressure", S.D. Hamann, Butterworths, London, 1957 pp 189-191.
26. Whang, P.W., Dachille, F. and Walker, P.L., Jr., Proc. 11th Biennial Conf. on Carbon, Gatlinburg, Tenn. 1973 pp 114-115.
27. White, J.L., in "Petroleum-Derived Carbons" 21 282-314, Amer. Chem. Soc. Symposium Series (1976).
28. Ref. 17 pp 3-213.

ACKNOWLEDGEMENTS

The efforts of J. A. Roetling, F. G. Rouse and J. O. Hanson of the Mechanical Physics Section in the design and performance of the thermophysical measurements are gratefully acknowledged. The cooperation of Koppers Co. personnel, specifically Messers. H. R. Sulkowski, J. Campbell and J. Bluhm, was invaluable, and their assistance in providing specimens, analytical data and technical discussions is deeply appreciated.